SAPIENZA

UNIVERSITA' DI ROMA

DOTTORATO DI RICERCA IN MEDICINA SPERIMENTALE
XXXIV CICLO

"miR-579-3p restrains tumor heterogeneity to overcome resistance to target therapies in metastatic melanoma"

DOTTORANDO

Domenico Liguoro

DOCENTE GUIDA

Prof.ssa Rita Mancini

COORDINATORE DEL DOTTORATO
Prof. Maurizio Sorice

ANNO ACCADEMICO 2020/2021

Ai miei genitori,

a mia sorella e mio fratello,

agli amici di una vita,

alle splendide persone che ho incontrato durante questo percorso.

ABSTRACT

My PhD thesis has been directed to the study of the mechanisms responsible for the development of drug resistance in melanoma. A large subset of melanoma patients harbors activating mutations in the BRAF oncogene at position V600. These mutations sensitize tumors to inhibition by inhibitors of BRAF in combination with inhibitors of the downstream kinase MEK. This has led in the past years to approval of combo therapies composed of a BRAF and a MEK inhibitor for these patients. These combo therapies give rise to strong objective responses and provide significant improvements in overall survival. However their duration in time is strongly limited by the development of drug resistance. While initial studies focused mainly in genetic mechanisms at the basis of de novo drug resistance, in recent years several groups, including my PhD supervisor, focused their attention of non genetic mechanisms and in particular to phenotypic changes underlying drug adaptation. In this context several microRNAs have been shown to play an important role, in particular miR-579-3p which was discovered some years ago as an oncosuppressor and antagonist of drug resistance in the lab of my supervisor.

In order to assess the role of this microRNA my PhD thesis has been directed initially to build and characterize a human melanoma cell line engineered to express miR-579-3p in a transcriptionally inducible manner. After the initial characterization the cell line has been subjected to a series of studies which have led to the demonstration that miR-579 is able to severely affect the development of drug resistance. A particular emphasis has been given to bulk RNA sequencing studies as well as to single cell mass cytometry which have shown that induction of expression of miR-579-3p is able to impair drug adaptive mechanism and to strongly diminish the degree of the heterogeneity in a isogenic cell population of melanoma cells when these cells are exposed to the selective pressure of BRAF and MEK inhibitors.

3.3 RNA extraction and real-time PCR analysis

3.4 Western blot analysis

3.5 Cell viability assay

3.6 In vitro colony formation assay

3.7 FACS analysis

3.8 Generation of inducible cell clones

3.9 Bulk RNA Sequencing

3.10 RNA data processing, identification of DEGs and pathway analysis

3.11 Single cell mass cytometry

1. INTRODUCTION

1.1 Melanoma: epidemiology, genetic classification and therapies

Cutaneous melanoma is one of the most lethal forms of skin cancers (1). Cutaneous melanomas derive from the malignant transformation of epidermal neural-crest derived melanocytes, i.e. the cells that are responsible for melanin synthesis (2-4). Worldwide, in year 2020, 324.635 (1.7%) cases of primary malignant cancers have been diagnosed as cutaneous melanoma with 56.047 deaths (5). Over the last decades, cutaneous melanoma's incident rate has increased especially in fair-skinned Caucasian populations as compared to any other type of cancer (6). The incident rate is dramatically high in countries as New-Zealand and Australia with 28,3 cases per 100.000 person-years (standardized to the world standard population) while the lowest rate is observed in Asia and Africa with 0.48 and 0.51 cases per 100.000 person-year, respectively (7). In Europe, cutaneous melanoma represents the 5th most common type of cancer with an estimate of 106.369 new cases (4% of all new cancer diagnoses) and 16.488 deaths (1.3% of all deaths due to cancer) in 2020 (8). The European Cancer Information System (ECIS) highlights that about half of new cases of cutaneous melanoma occur between 45-69 age group and the cumulative risk of developing melanoma by age 74 is 1.33% (1 in 75) in females and 1.51% in male (1 in 66) (8). The different proportion of incident rate across ethnic groups is probably due to the fact that eumelanin, highly expressed in dark-skinned people, is more protective to UV (9). In fact, one of well-established environmental risk factors for cutaneous melanoma is ultraviolet radiation following excessive sun exposure. Other risk factors for melanoma development are related to high number of widespread nevi on the body, fair complexion and family members affected by this disease (10-12).

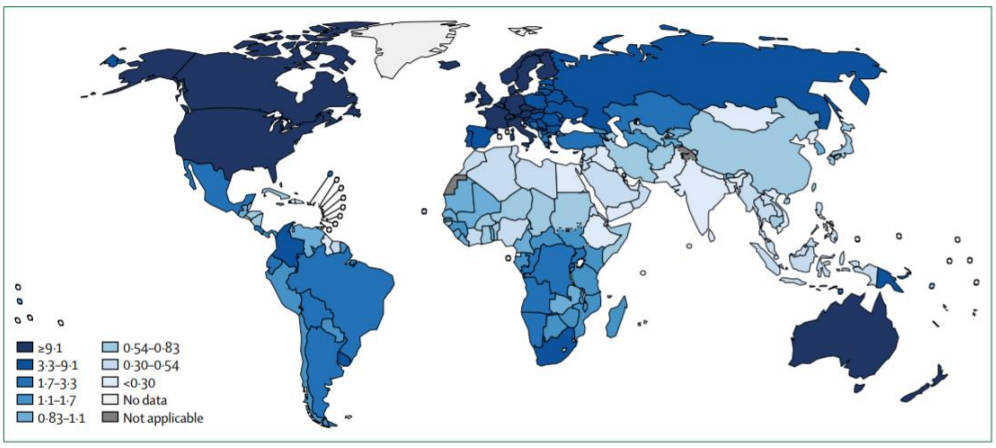

Figure 1. Estimated age-standardized worldwide incidence of cutaneous melanoma in both men and women in 2012 (Matthew et al, 2017).

Cutaneous melanoma is one of the most genetically unstable and highly mutated cancer (13,14). The Cancer Genome Atlas (TCGA) analysis highlighted the landscape of genomic alterations in cutaneous melanomas through DNA, RNA, and protein-based analysis from a large cohort of melanoma tissue samples (18). Based on different genomic alterations, cutaneous melanoma could be divided in four subgroups: BRAF-mutant melanomas, which represent roughly 50% of melanomas; RAS (N/H/R)-mutant melanomas, which occurs roughly in 25% of cases; NF1-mutant melanomas, which occur roughly in 15% of cases; and triple-wild-type melanomas, which occur roughly in 10% of cases (18). The malignant proliferation toward metastatic melanoma is generally accompanied by several additional genetic alterations involving genes such as CDKN2A, TP53 or PTEN and the acquisition of a high mutational tumor burden (15-17). Independently from the genetic subtypes, TCGA analysis highlighted immune signatures enriched for immune genes expression associated with lymphocyte infiltration, immune signaling molecules and -stimulatory and co-inhibitory immune checkpoint proteins (18).

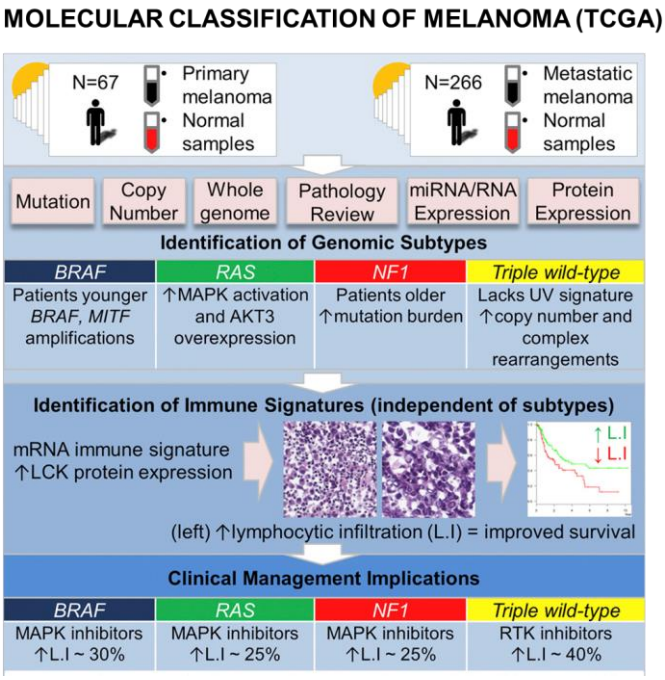

Figure 2. Landscape of genomic alterations in cutaneous melanomas. It is shown a scheme of genomic classification into one of four subtypes based on the pattern of the most prevalent significantly mutated genes: mutant BRAF, mutant RAS, mutant NF1, and Triple-WT (wild-type). Samples have been characterized for immune signature enriched in immune gene expression associated with lymphocyte infiltrate and high LCK protein expression (The Cancer Genome Atlas Network).

For patients with primary *in situ* melanomas (stage I-II), surgical removal of tumors represents the standard treatment and is associated with a 5-year survival rate above 95% (19-21). In contrast, the prognosis for metastatic stages (stage III-IV) remains exceedingly poor and the 5-year survival rate drops to 15-20% (22). Before 2011, the weapons to treat metastatic melanoma were only three Food and Drug Administration (FDA)-approved drugs: chemotherapy with Fotemustine or Dacarbazine or high-dose of Interleukin (IL)-2. However, they were able to achieve only modest response rates (up to 15%) with median progression free survival (PFS) of 1.7 months. In addition, only 25.5% of patients were still alive at 1 year (23).

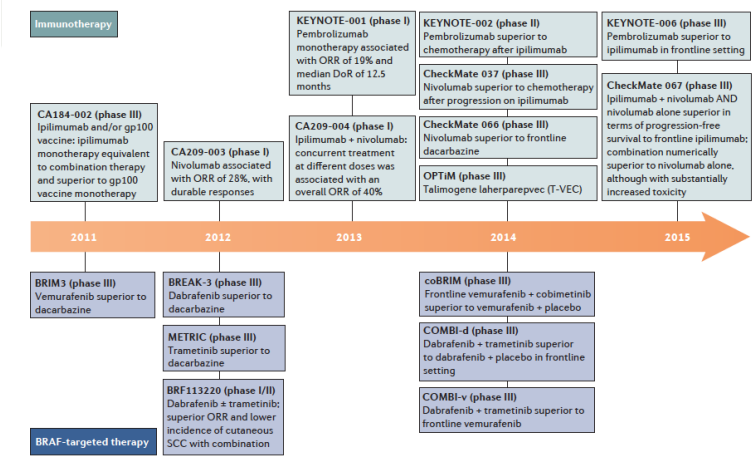

Figure 3. Chronology of the therapies (immunotherapy above the arrow and targeted therapy under the arrow) approved to treat metastatic melanoma (Luke et al, 2017).

The therapeutic landscape of metastatic melanoma has changed dramatically over the last 15 years thanks to the introduction of target therapy and of immunotherapy with immune checkpoint inhibitors. The discovery that roughly 50% of metastatic melanoma patients harbor hot-spot mutations in the B-Raf proto-oncogene serine/threonine kinase (BRAF), paved the way to the development of targeted therapies. Normally, this kinase exists as a monomer with the ability to activate *Mitogen-Activate Protein Kinase* (MAPK)-ERK downstream signaling only following its homo-dimerization or its hetero-dimerization with other RAF isoforms after cell exposure to external growth factors (24). The majority of BRAF activating gene mutations occur at the Val 600 position in the kinase catalytic domain, leading to a constitutively active monomeric protein which in turn promotes hyper-phosphorylation of MAPK-ERK signaling pathway and uncontrolled melanoma cell proliferation and survival (25, 26). As shown in the pie chart below, the most common mutation is a substitution of a valine to glutamic acid (BRAFV600E) and occurs in about 90% of cases, whereas in 5-6% V600K mutations have been found (valine changes into lysine) (26). BRAF mutations in which valine is substituted into arginine (V600R) are very rare (26).

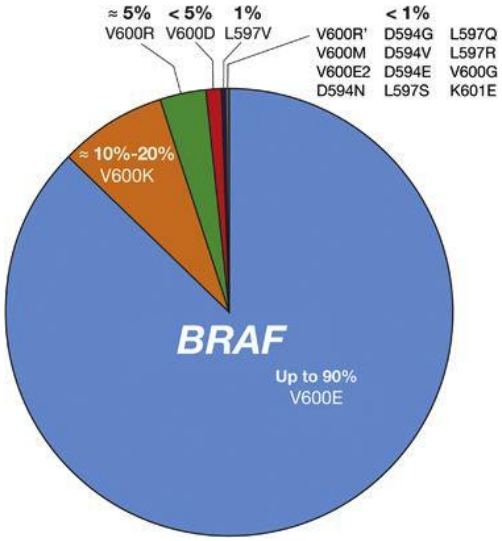

Figure 4. Pie chart showing the percentage distribution of BRAF oncogene mutations. (Cheng et al, 2018)

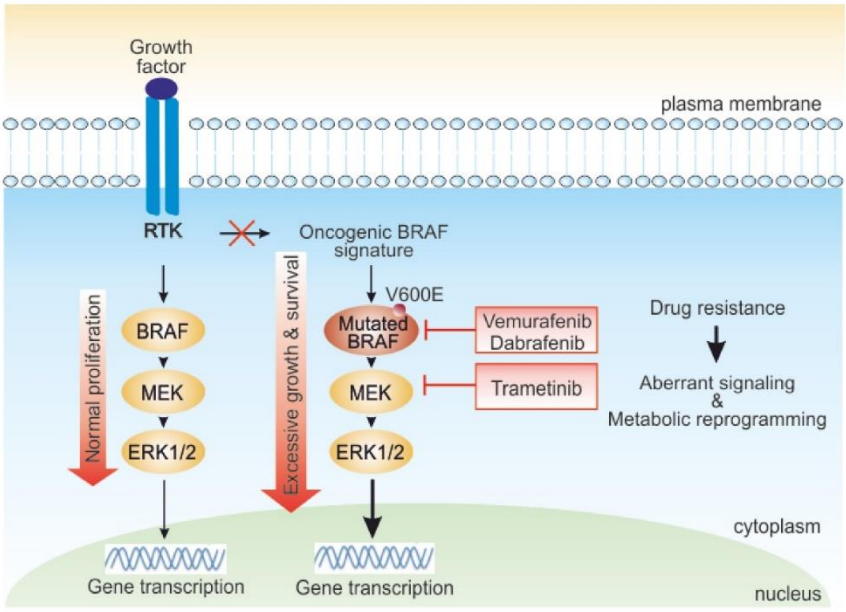

Figure 5. MAPK-ERK signaling pathway. ERK1/2 is the terminal kinase which translocates to the nucleus where activates transcriptional programs mediating growth, migration and differentiation. Normally, Receptor-Tyrosine Kinases activate the MAPK-ERK pathway upon exposure to external stimuli, i.e. presence of growth factors. Mutant BRAF acts as a monomer that could induce hyper-proliferation of MEK-ERK cascade. (Indini et al, 2021)

Starting from year 2011, FDA approved several oral small-molecules kinase inhibitors of the MAPK-ERK signaling. Vemurafenib (PLX4032) was the first clinically approved specific inhibitor of the mutated BRAF protein (27). This drug binds to the ATP pocket of the BRAFV600E catalytic domain, acting as a competitor for the ATP molecule and inhibiting its abnormal function (27). In randomized phase 3 trial, Vemurafenib monotherapy was able to improve Overall Survival (OS), Progression-Free Survival (PFS) and Objective Response

Rate (ORR) compared to Dacarbazine (28). Subsequently, another BRAF inhibitor, namely Dabrafenib, was developed showing superior clinical benefits as compared to Dacarbazine in BRAF-mutated V600E melanoma patients (29).

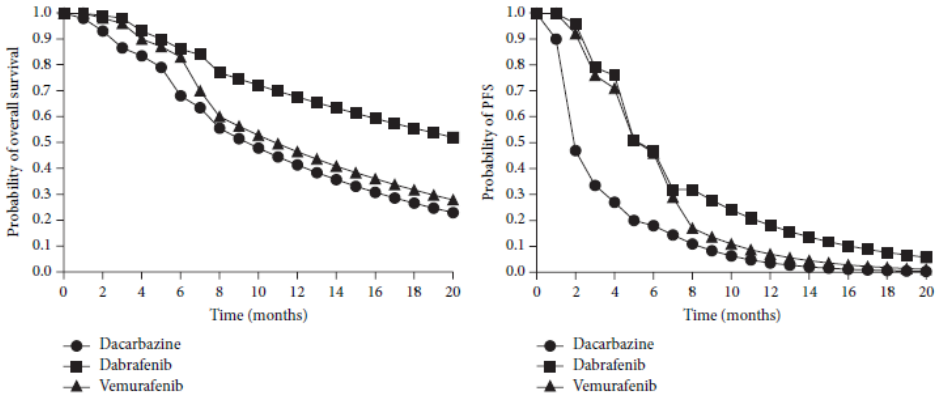

Figure 6. Kaplan-Meier Overall Survival Curve (A). Kaplan-Meier Progression-Free Survival Curve(B). Vemurafenib and dabrafenib improved Overall Survival and Progression Free Survival as compared with dacarbazine. (Shin V. et al, 2015)

In 2018, a third BRAF inhibitor, Encorafenib (LGX818), was also approved. This is a second generation BRAF inhibitor with pharmacological properties resulting in higher affinity to the BRAF protein's catalytic domain (30). Although monotherapy with BRAF inhibitors provides a clear clinical benefit, re-activation of the oncogenic MAPK-ERK pathway through *Mitogen-Activated Protein Kinase* MEK 1/2 aberrant activation, generally occurs after short time (31-33). In order to overcome this issue, non-ATP competitive allosteric inhibitors of the downstream kinases MEK1 and MEK2, namely Trametinib, Cobimetinib and Binimetinib were clinically developed in combination with BRAF inhibitors, resulting in superior efficacy and more durable clinical impact. Combo-therapy with BRAF and MEK inhibitors has, therefore, become the standard of care because of its capacity to combine rapidity of beneficial effects with unprecedented and more durable clinical benefit (34). Three BRAF-MEK inhibitor combinations are now currently used in clinical practice: Vemurafenib plus Cobimetinib; Dabrafenib plus Trametinib; Encorafenib plus Binimetinib. During last years several clinical trials have provided evidence that the use of combo-therapy has a superior efficacy as compared to mono-therapy. The last report of the randomized phase III coBRIM study (NCT01689519) demonstrated improvement of

Progression-Free Survival (PFS) and overall survival (OS) in Cobimetinib plus Vemurafenib-treated patients compared to Vemurafenib alone (35). In addition, in randomized phase 3 trials COMBI-d and COMBI-v (NCT01584648 and NCT01597908 respectively), Dabrafenib plus Trametinib combination increases both PFS rates and OS rates at 19% and 34% at 5 years, respectively (36). As shown in figure 7, an update of COLUMBUS clinical trial (NCT01909453) demonstrated that combo-therapy of Encorafenib plus Binimetinib improves clinical benefit and progression-free survival compared to mono-therapy with Vemurafenib (37).

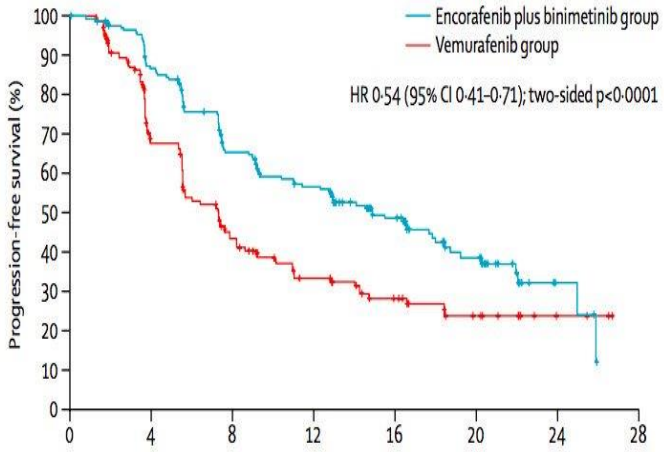

Figure 7. The combination of Encorafenib and Binimetinib significantly prolonged progression-free survival as compared to monotherapy with Vemurafenib (Dummer R et al, 2018).

For BRAF-wild type melanoma patients, targeted therapies show poor clinical benefits. For example, in the NEMO clinical trial (NCT01763164), the MEK inhibitor Binimetinib administered to N-RAS mutated melanoma patients showed a median PFS of only 2.8 months (38). Hence BRAF mutated melanomas still remain the only melanoma subtype where target therapy has demonstrated a clinical benefit.

The other recent approach with demonstrated clinical efficacy against metastatic melanoma is represented by immunotherapy.

It is well-known that metastatic melanoma is a highly immunogenic type of cancer capable to activate the host immune system to control cell growth and proliferation (39,40). Nevertheless, melanoma cells are able to avoid immunosurveillance through a series of

cancer cell intrinsic mechanisms such as for example downregulation of tumor-associated antigens expression or of MHC class I (41). Furthermore, an additional mechanism of immune escape is the suppression of T-cell effector activities through the activation of immune-check points such as PD-1 and CTLA-4 (42,43). PD-1 and CTL-4 are transmembrane molecules expressed on T cell surface which normally act as controllers of immune-tolerance during inflammation to avoid autoimmune reactions. CTLA-4 blocks the initial stage of T cells activation, by sequestering co-stimulatory ligands CD80/86 expressed on antigens presenting cell (APC) from the activation of the co-stimulatory receptor CD28. This interaction occurs mainly but not exclusively in lymph-nodes because T-cells expressing CTLA-4 can accumulate also within the tumor microenvironment (43). On the other side, PD-1 negatively affects later stages of T cells response, trough the binding with PDL-1 and PDL-2 which are expressed on many types of cell tissues as well as by different types of tumors. Cancer cells exploit these mechanisms in order to avoid immunosurveillance, e.g. up-regulation of PDL-1 to shut down T cells response (44). The purpose of immunotherapy with checkpoint inhibitors is to remove the "molecular axes" that blunt the immune response.

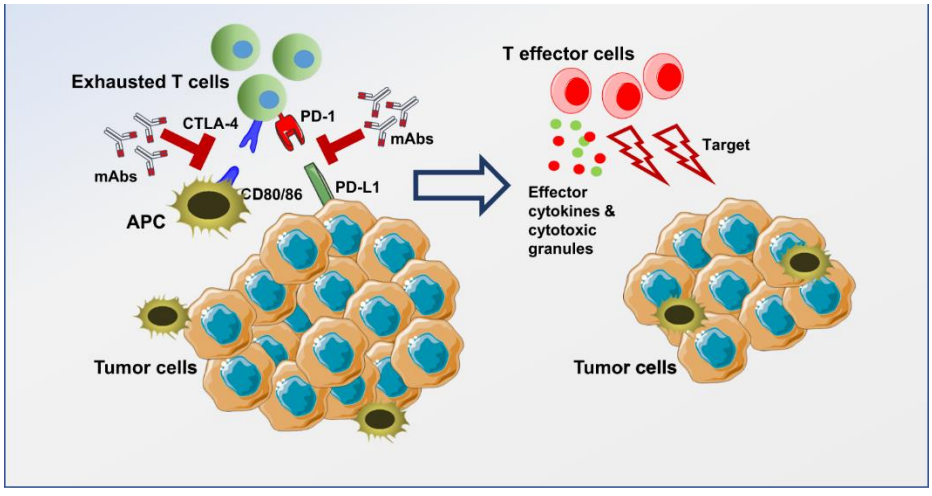

Figure 8. PD-1 and CTLA-4 are expressed on activated T cells .CD80/86 are expressed on antigens presenting cells (APC) while PDL-1 on tumor cells. Inhibitory effects due to CTLA-4-CD80/86 and PD-1-PDL-1 links can be blocked using specific monoclonal antibodies, leading to the activation of T cells which in turn hit tumor cells through the release of effector cytokines and cytotoxic granules (Darvin et al, 2018).

The first Immune-Checkpoint Inhibitor (ICI) approved by FDA was the monoclonal antibody Ipilimumab (anti-CTLA-4) (45). Ipilimumab binds the extracellular domain of CTLA-4 making it inaccessible for interaction with CD80/86. Clinical trials with Ipilimumab in metastatic melanoma resulted in durable clinical responses and a significant improvement of the overall survival. The clinical success of anti-CTLA-4 paved the way to the development of monoclonal antibodies against PD-1, namely Nivolumab and Pembrolizumab, which act by blocking interaction with its ligand PD-L1. Both drugs given as monotherapy provide superior clinical efficacy as compared to ipilimumab alone. Subsequently, based on the non-overlapping mechanisms of action of CTLA-4 and PD-1 the combination of Ipilimumab plus Nivolumab was clinically developed. Pleasingly, the phase 3 Checkmate-067 study (NCT01844505), showed the superiority of the Ipilimumab plus Nivolumab combination compared to either Ipilimumab or Nivolumab monotherapy both for response rate, duration of response and overall survival (OS at 3 years of 58% for Ipi+Nivo, vs 52% for Nivo, vs 34% for Ipi)(46).

In conclusion the introduction of both target therapy for BRAF mutated melanomas as well as immunotherapy with ICI for all metastatic melanoma patients has modified the clinical history of this disease with a significant increase in life expectancy at 5 years. Nevertheless, a major limitation is represented for both types of therapies by the occurrence of drug resistance. My PhD thesis work has been directed to the study of the mechanisms underlying the development of drug resistance against target therapy.

1.2 Resistance to target therapies is driven by both genetic and non-genetic mechanisms

As reported in the previous section combo therapy with a BRAF and a MEK inhibitor has become standard-of-care for melanoma patients harboring BRAF V600 mutations. From the clinical standpoint three different patterns of response are observed:1) Approximately 20% of patients initially undergo a complete response, but a large proportion of them experience disease relapse over time; 2) 50% undergo only partial responses with disease rapidly recurring; 3) the remaining 20–25% do not respond at all (47).

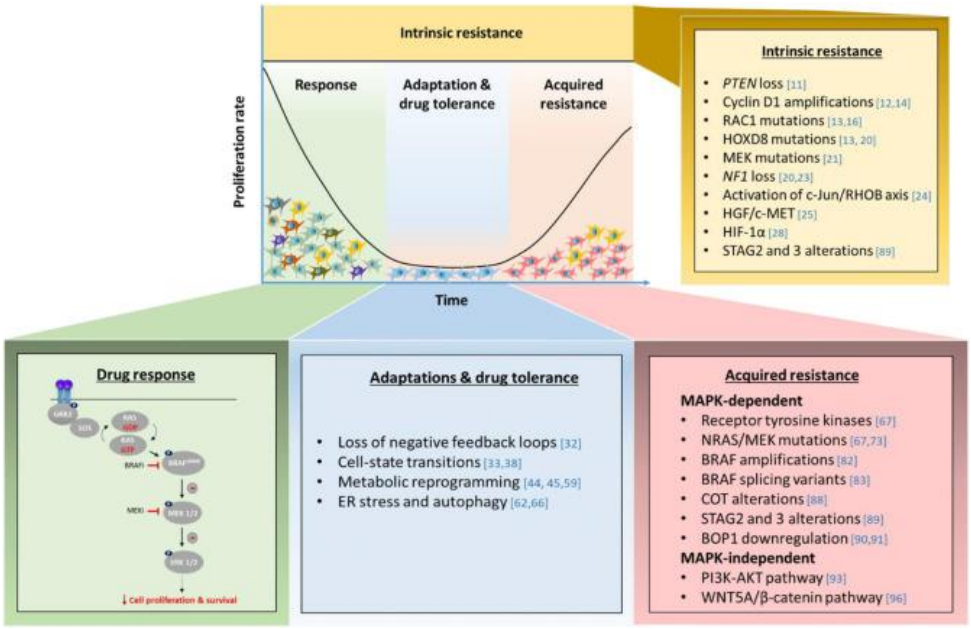

Figure 9. Mechanisms conferring intrinsic, adaptive and acquired resistance in BRAF-mutant melanomas (Tangella et al, 2020).

In the first two case we talk about acquired resistance, in the last case of intrinsic resistance. Over the last ten years drug resistance has been the object of intensive studies, which have provided evidence for the involvement of both genetic and non-genetic alterations. Figure 9 (top right) shows that the absence of *ab initio* clinical responses could be explained by several intrinsic resistance mechanisms which I am not going to review here.

On the other hand, acquired resistance was originally described as the accumulation of new mutational events occurring in BRAF mutated melanoma cell lines rendered resistant to

BRAF and MEK inhibitors as well as in patients' tissues upon disease progression.

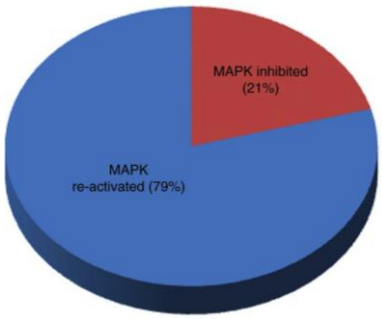

Figure 10. Gene Set Enrichment Analysis (GSEA) data demonstrated that 79% of the tumor progression is due to the de-novo activation of the MAPK pathway (Rizos et al, 2014).

Approximately 80% of de-novo mutations are responsible for the re-activation of MAPK signaling. For this reason, acquired resistance mechanisms are divided into MAPK-dependent (re-activated) or independent events (figure 10) (48). MAPK-dependent mechanisms include BRAF allele amplification, BRAF alternative splicing or additional mutations that by-pass the effect of RAF inhibition such as MEK 1/2 or N-K-RAS genes mutations resulting in the aberrant reactivation of MAPK-ERK pathway (49,50). Re-activation of MAPK signaling represents the rationale for the use of combinations of BRAF+MEK inhibitors as described above. This scenario is further complicated by mutations leading to the activation of alternative oncogenic signaling pathways such as PI3K/AKT, which are observed in approximately 22% of cases (51). Among them loss of PTEN gene has a crucial role in the hyper-activation of PI3K/AKT signaling during acquired resistance.

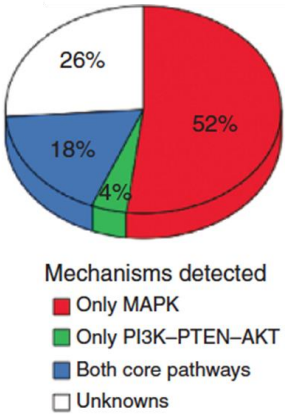

Figure 11. Percentage of mechanisms involved in adaptive resistance to Target Therapy (Shi et al,2014)

However, as can be observed in figure 11 roughly 26% of drug-resistant tumors, when subjected to deep sequencing, did not show the presence of bypass reactivating mutations (52).

This initial evidence was the first indication, albeit indirect, that non-mutational, phenotypic changes strongly contribute to acquired resistance and opened up to a wealth of investigations leading in recent years to the demonstration that drug adaptation even more than the selection of mutated new clones bearing bypass mutations plays a major role in the development of de novo drug resistance. It can be anticipated here that drug adaptation due to cancer cell plasticity are tightly linked to the co-existence in the tumor mass of cell populations with different transcriptional and post-transcriptional trajectories interchangeable with each other, i.e. namely with the concept of intratumor heterogeneity which will be treated more extensively in a following paragraph.

Several studies showed that non-mutational events take place early after drug exposure and involve a plethora of post-transcriptional, post-translational mechanisms as well as epigenetic changes which, again, converge in the re-activation of proliferation and survival pathways such as MAPK , PI3K/AKT as well as others which, all together, end up in therapeutic failures (53). Among them, for example the laboratory of Prof. Mancini in collaboration with Prof. Ciliberto discovered some years ago the rapid activation of an autocrine loop involving upregulation of neuregulin 1 with its receptor ErbB3 leading to

activation of the PI3K/AKT axis as an adaptive response of melanoma cells after exposure to BRAF and MEK inhibitors (54).

Non-genetic adaptative mechanisms have been shown to be responsible for the survival of a small fraction of tumor cells, whereas the majority are initially killed after drug exposure (55). The population of remaining cells, namely Drug-Tolerant Persister cells (DTPs), are a slow cycling population of cells that are able to survive to the presence of drugs and represent the *seed* for the development of resistant tumor cells. Drug-tolerant cells are characterized by rewiring epigenomic, transcriptomic and metabolomic pathways, such as for example the previously described Neuregulin1/ErBB3/P13K/Akt axis. To be mentioned in particular the robust evidence of the switch toward oxidative phosphorylation (OXPHOS) in order to increase ATP production as source of energy promoting survival even in the presence of drugs (56). In this regard it is important to point out that the OXPHOS phenotype is associated with a slow-cycling state (57).

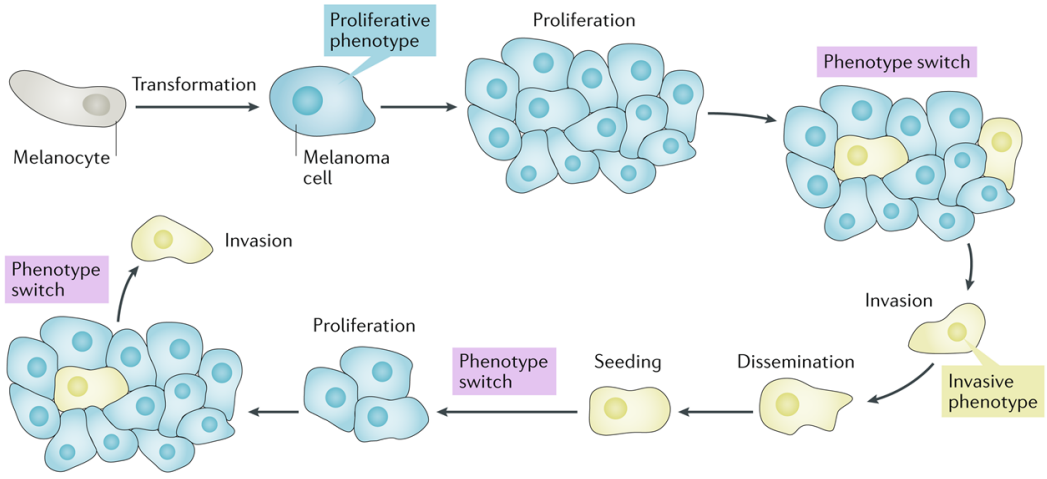

Figure 12. Switching phenotype model from proliferative to invasive state upon drugs exposure. This transitory model allow to switch back to the proliferative phenotype in order to promote growth at metastatic site (Arozerena et al, 2019).

Drug-adaptation is also characterized by "switching phenotype" model, a typical prerequisite of drug-tolerant cells. As described in figure 12, melanoma cells have a predisposition to switch their transcriptional programs from a proliferative/drug sensitivity phenotype to an invasive/drug-tolerant phenotype, in order to bypass the efficacy of drug treatments (58,59). Several studies have highlighted distinct molecular signatures belonging

to drug-sensitive or drug-tolerant phenotypes respectively both in in-vitro cultures and in sample biopsies. The drug-sensitive phenotype is associated with high levels of SOX10, MITF and MLANA genes whereas the drug-tolerant phenotype with TGFβ, SOX9 and AXL Tyrosine-kinase receptor expression (60, 61). Single-cell RNA Sequencing allowed to decipher different transcriptomic states which co-exist in a dynamic equilibrium and which dictate the degree of response to target therapies. These evidences led to conceptualize a model for which resistance to BRAF-MEK inhibitors derives from the switch from MITF high/AXL low to MITF low/ AXL high transcriptional programs (62). Moreover, a recent study on BRAF-mutated melanoma cell lines highlighted how the simultaneous existence of different transcriptional states could predict response to treatments (63). Finally, Neural-Grow Factor Receptor (NGFR) has been recently described as a marker of invasiveness and of stem cell like features (64). In *in vivo* models, high expression of NGFR is linked to epithelial to mesenchymal transition phenotype (65).

In conclusion drug-adaptation causes the loss of efficacy of target therapy with BRAF and MEK inhibitors. In order to identify new master regulatory networks involved in drug-adaptation our group started to study some years ago the involvement of microRNAs, a class of non-coding RNAs which act as important post-transcriptional modulators of gene expression in eukaryotic cells and which have been widely described as one of the hallmarks of cancer development and progression.

1.3 MicroRNAs orchestrate non-mutational mechanisms involved in drug-resistance in melanoma: focus on mir-579-3p

MicroRNAs (miRNAs) are small single-stranded non-coding RNAs, with average length of 22 nucleotides (66). Many miRNAs are highly conserved across species and are present in plants, animal and in some viruses. Actually, 2588 microRNAs are annotated in human genome (67). These small molecules act as key modulators of post-transcriptional gene expression by inhibition of specific mRNAs. Indeed, microRNAs action mechanism is based on perfect or imperfect pairing to the 3' UTR of the mRNAs through a 5' domain of the same micro-RNA defined as "seed region" that includes a number of 2-8 nucleotides (68). miRNAs characterized by the same "seed region" belong to the same family. In particular, a perfect binding induces the degradation of the messenger RNA, through the recruitment of deadenylase complexes such as CCR4-NOT and PAN2-PAN3 or the recruitment of decapping enzymes such as DCP1-DCP2. On the other hand, an imperfect binding leads to steric hindrance which in turn obstructs ribosome sliding on messenger RNA inhibiting translation mechanism (69).

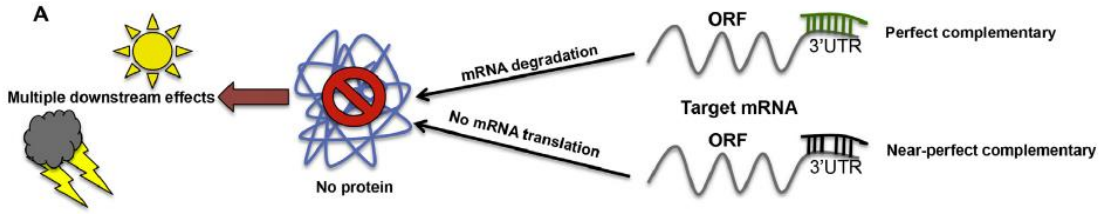

Figure 13. MicroRNAs mechanism of action. Perfect or near-perfect complementary on mRNAs target induce mRNA degradation or mRNAs non-translation as a consequence of translation block (Fattore et al, 2017).

Since microRNAs are essential elements in the maintenance of cellular and tissue homeostasis, their de-regulation alters normal biological functions triggering a whole series of human pathologies, including the development of cancer (70). miRNAs are key regulators of cell transcriptome because of their pleiotropic behavior, whereby a single molecule can inhibit the expression of several messenger RNAs, influencing multiple

cellular pathways simultaneously. Coherently, the same mRNA may be targeted by different micro-RNAs (70). The effects on cancer cell behavior allow to divide microRNAs into two categories: miRNAs with onco-suppressor properties by targeting onco-mRNAs (tumor suppressor miRNAs) or with oncogenic capacity by targeting mRNA-coding tumor suppressors (oncomiRs) (70).

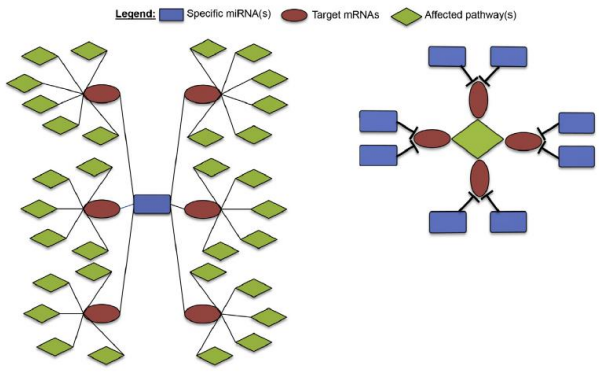

Figure 14. miRNAs control the expression levels of various mRNAs thus controlling multiple molecular pathways. In particular the figure shows how a single miRNA is able to target several mRNA targets (left drawing) or the same molecular pathway can be affected by multiple miRNAs (right drawing) (Fattore et al, 2018).

Due to well-known mode of action, several studies have highlighted how microRNAs are key players regulating non-mutational mechanisms involved in the establishment of adaptive drug-resistant states to target therapies in metastatic melanoma (71). In this context, microRNAs can act as "facilitators" or "antagonists" of resistance. As example of "antagonist" of resistance, the group of Prof. Mancini discovered some years ago miR-579-3p as a key regulator of melanoma progression and drug resistance (72). The expression of miR-579-3p drastically decreases in stage III and stage IV compared to normal melanocyte where the endogenous levels are higher. Moreover, low levels are associated with poor clinical outcomes. miR-579-3p acts as onco-suppressor since it inhibits specific oncogenes involved in proliferation and cell survival. Specifically, miR-579-3p has different consensus binding sites within the 3' UTR region of both BRAF and MDM2 oncogenes. Indeed, miR-579-3p enforced expression strongly reduces cell proliferation, exhibiting its onco-suppressive force. As mentioned in the previous paragraph, BRAF mutations are a principal

mechanism of activation of the MAPK proliferative pathway and its inhibition affects cell proliferation. On the other hand, MDM2 is a negative regulator of p53 and p21 genes that are two known onco-suppressor genes involved in DNA repair, apoptosis and cell cycle. Furthermore, miR-579-3p is able to potentiate the inhibition of proliferation induced by BRAF+MEK inhibitors in parental BRAF-mutated melanoma cell lines suggesting the use of this molecule in clinical practice. miR-579-3p levels are strongly down-regulated both in *in vitro* resistant melanoma cell lines and in tumor biopsies of melanoma patients after disease recurrence.

Subsequently, the laboratory of Prof. Mancini in collaboration with Prof. Ciliberto focused on the temporal evolution of global microRNAs changes (miRNAome) after treatment with BRAF+MEK inhibitors, both in vitro and in vivo (73). These studies led to demonstrate that changes in the expression of specific microRNAs corresponds to the deregulation of molecular pathways associated with melanoma progression and resistance to MAPK inhibitors such as resistance to apoptosis, activation of pro-oncogenic pathways or also modulation of angiogenesis. For instance, it was shown that miR-204-5p and miR-199-5p are down-regulated during the development of drug resistance and act as "antagonists" of resistance because they target oncogenic genes such as BCL-2 and VEGF respectively. On the other hand, up-regulated miR-4443 and miR-4488 are considered "facilitators" of resistance because of their targeting of PTPN14 , a negative regulators of the YAP/TAZ signaling pathway (73).

In conclusion, when I started my PhD thesis work the laboratory of Prof. Mancini had provided robust evidence as to the involvement of microRNAs in adaptive non genetic resistance of melanoma to target therapy and had discovered a set of interesting miRNAs among which in particular the newly discovered oncosuppressor miR-579-3p.

Given the pleiotropic effects of miR-579-3p, it was plausible at the time of beginning of my PhD thesis work to speculate that, enforcing its expression, would be able to affect simultaneously multiple cellular pathways and, therefore, could interfere heavily with drug adaptation mechanisms and, as discussed above, this would result in impairing the

establishment of drug resistance. As mentioned above, drug adaptation is due to cell plasticity and this in turn is linked to intratumor heterogeneity. Hence, it is necessary to introduce here the concept of tumor heterogeneity and briefly describe the single-cell technologies to study this phenomenon.

1.4 Tumor heterogeneity as fueling force driving resistance to target therapies

Tumor heterogeneity refers to the existence of different tumor cells that do not share the same genetic and phenotypic profiles such as proliferation-driving mutation, metabolism, motility, and metastatic potential (74-78). In cancer biology, tumor heterogeneity can be distinguished in two main types: inter-tumor and intratumor heterogeneity (79). Inter-tumor heterogeneity refers to different spectrum of molecular alterations among cancer patients. It has been long recognized that inter-tumor heterogeneity results from patient-specific factors including germline genetic variations, differences in the somatic mutation profile, and environmental factors. For example, melanomas are one of the most heterogeneous cancer and histological samples of this tumor showed molecular differences among patients, i.e. specific oncogenic mutations driving melanoma progression (79).

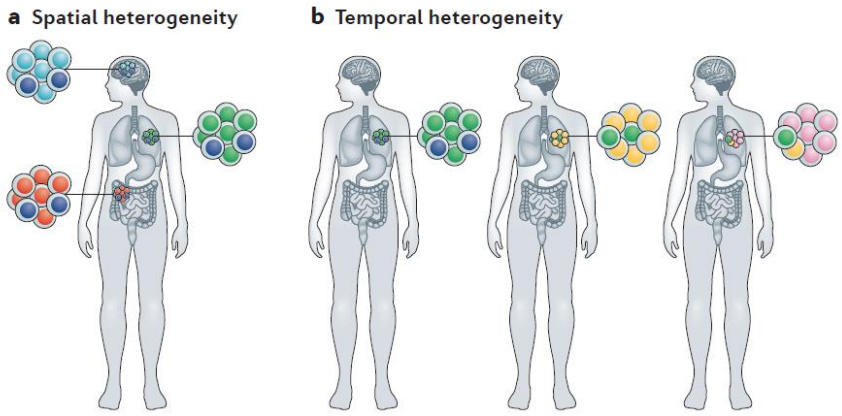

Figure 15. Spatial (a) and temporal (b) heterogeneity. Spatial heterogeneity reflects unequal distribution of cells with

genetic and phenotypic differences within same tumor lesion. Temporal heterogeneity arises as molecular changes upon the selective pressure of external perturbation such as therapies (Dagogo-Jack, 2017).

Intratumor heterogeneity refers to the co-existence within the same tumor of different cell sub-populations characterized by specific genomic, transcriptomic, epigenomic alterations (86). As described in figure 15, intratumor heterogeneity can be distinguished in two types: spatial and temporal. Temporal heterogeneity refers mainly to the molecular reprogramming of cancer cell composition over time triggered in response to external perturbations, such as anti-cancer therapies (80). Spatial heterogeneity consists in the uneven distribution of malignant cell subpopulations across different regions of the primary tumor and/or metastatic sites (80). In recent years the study of intratumor heterogeneity has been given an unprecedented impulse thanks to the development of several single cell technologies, in particular single cell RNA seq but also single cell proteomic approaches such as mass cytometry (81, 82).

In this regard it is important to point out that single cell RNA Seq studies demonstrated that BRAF-mutated drug-naïve melanoma cells are composed of cells with two distinct phenotypes characterized by high or low levels of MITF and its downstream target genes respectively (83). These cell populations are in equilibrium with each other. After short-term drugs exposure, the MITF high -derived subpopulation showed up-regulation of PKM2, LDH2 and SLUG oncogenes whereas MITF low-derived subpopulation was characterized by dominant expression of TNFR, N-cadherin and p-NFkB-p65. These findings support the notion that, in order to block the development of a drug tolerant state it is necessary to intervene pharmacologically on parallel transcriptional trajectories.

In conclusion, selective pressure imposed by target therapies induces a series of non genetic changes fueling spatial and temporal heterogeneity. Based on this concept, our group hypothesized that the previously identified miR-579-3p might exert its inhibitory effects on the development of drug resistance thanks to its capacity to inhibit simultaneously several cellular pathways. This could ultimately results in a reduction of cellular heterogeneity in response to drug treatment. In order to test this hypothesis we decided to use single cell

mass cytometry as technology to study temporal evolution of cell heterogeneity in a simplified system constituted by a genetically homogeneous population of melanoma cells where mir-579-3p expression can be turned on or off.

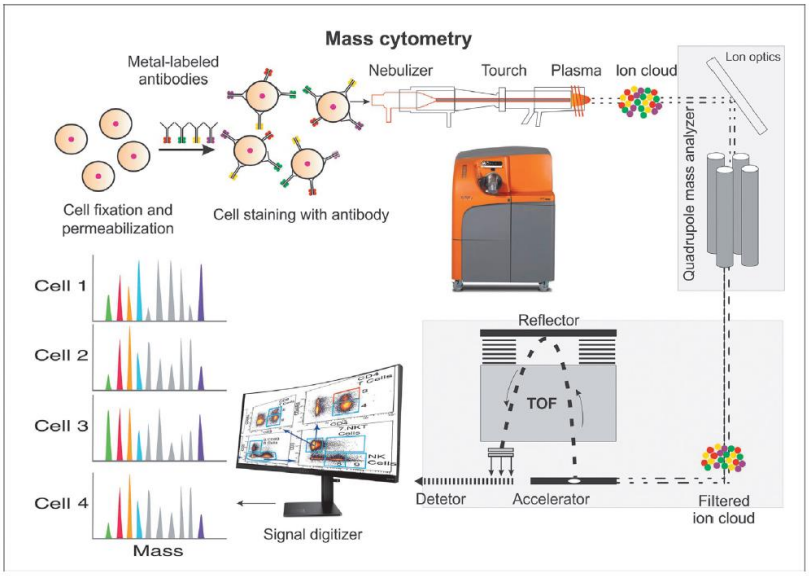

Figure 16. Single-cell proteomics by mass cytometry (Minakshi et al, 2021).

Single-Cell Mass Cytometry (CyTOF) is a highly-multiparametric technology that employs heavy metal-isotope coupled antibodies for surface and intracellular antigens. Isotope of the same metal differ by mass unit which do not cause overlapping signals, resulting in greater specificity and sensibility. Hence, it is possible to use more than 40 antibodies simultaneously. As shown in figure above, mass cytometry takes advantage of mass spectroscopy technology. After cell staining with antibodies cocktail, single cell are vaporized and atomized resulting a ion cloud of antibodies coupled with specific antigens. Ionized components are quantified using a time-of-flight (TOF) mass spectrometer as the isotope signal from individual cellular antigens arrives at the detector (figure 16).

2. AIMS OF THE THESIS

My PhD thesis work is directed to contribute to a better understanding of the mechanisms at the basis of the development of acquired resistance to target therapy in metastatic melanoma, and to try to identify approaches to inhibit them. In the last years growing evidence has been accumulating that in a population of BRAF-mutated melanoma cells exposed to BRAF and or MEK inhibitors non-mutational adaptative changes take place which allow the survival of a small subpopulation of tumor cells under this drug selective pressure. The subsequent development of acquired resistance and of overt tumor re-growth strictly depends upon events occurring in this surviving population. Therefore, a better understanding of the molecular mechanisms underlying drug-adaptation could allow to identify new vulnerabilities to reduce the risk of relapse and potentially to eradicate cancer. In this context, based on previous studies conducted in the laboratory of my PhD Thesis supervisor it was possible to speculate that microRNAs, given their role as pleiotropic controllers of several cell survival and oncogenic pathways, may be involved in cell adaptation through modulation of their expression. Hence the underlying rationale behind my PhD thesis work is that changes in microRNA expression contribute to drug adaptation and that reinstalling their correct expression is able to counteract drug adaptive changes and, as a consequence, to block the development of drug resistance. In order to test this hypothesis I chose to study the effect of modulating miR-579-3p expression. This miRNA was discovered a few years ago in the laboratory of Prof. Mancini in collaboration with Prof. Ciliberto to act as an oncosuppressor in drug resistant melanoma cells. As model system I decided to use one of the most widely used metastatic human melanoma cell lines, namely A375.

Based on the previous assumptions, the aims of my thesis have been:

- To engineering and phenotypically characterize BRAF-mutated A375 melanoma clones with transcriptionally inducible expression of miR-579-3p.

- To assess whether the inducible expression of miR-579-3p alone or in combination with exposure to BRAF-MEK inhibitors is able to reduce or delay the establishment of drug-tolerant state to target therapies over time and to impair long term tumor growth.
- To identify, through RNA-Sequencing, the main transcriptional pathways modulated by miR-579-3p alone or in combination with BRAF and MEK inhibitors which might be involved in the establishment of drug-tolerance
- To assess whether inducible expression of miR-579-3p alone or in combination with BRAF and MEK inhibitors is able to affect the degree of cell heterogeneity in a genetically homogeneous cell population, measured using mass cytometry (CyTOF)

3. MATERIALS AND METHODS

3.1 Cell lines and treatments

Human melanoma cell line A375 ($BRAF^{V600E}$) was purchased from American Type Culture Collection (ATCC®). HEK-293TN (LV900A-1-GVO-SBI) was purchased from System Biosciences (SBI). Drug resistant A375 melanoma cells were selected by treating drug sensitive cells for about two months with increasing drug concentrations every two weeks (from 50 nM to 2 μM). A375-CymR cell line was generated after lentiviral transduction with CymR repressor plasmid (see below). A375-miR579IndEx clones were generated after lentiviral transduction of A375-CymR with plasmid carrying miR-579-3p, followed by limiting dilution (see below). All human melanoma cell lines used in the present work were cultured in RPMI supplemented with 10% (vol/vol) FBS; HEK-293TN cells were cultured in DMEM supplemented with 10% (vol/vol) FBS. For short-term and long-term drug-treatments, BRAF inhibitor (Dabrafenib) and MEK inhibitor (Trametinib) were used at IC50 concentration for A375 melanoma cell line (84). For dose-response experiments, 11 scaled dose concentration (1:3) of Dabrafenib and Trametinib were used, starting from 1uM. As datasheet reported, 100 μg/ml of Cumate was used to induce the expression of miR-579-3p.

3.2 Antibodies and reagents

Antibodies against BRAF and GAPDH were obtained from Santa-Cruz Biotechnology. Phospho-ERK 1/2 was purchased from Cell Signaling Technology. TaqMan probes for U6 and miR-579-3p were purchased from Applied Biosystem. Forward and Reverse primers relative to H3 and CymR have been used in the work (85). Dabrafenib and Trametinib were obtained from Novartis Pharma S.p.A.

3.3 RNA extraction and real-time PCR analysis

RNA was extracted using TRIzol method (Invitrogen) according to manufacturer's instruction and eluted with 0,1% diethylpyrocarbonate (DEPC)- treated water. Total RNA

was quantitated by the Qubit 2.0 fluorometer (Thermo fisher) using the appropriate Qubit RNA BR (Broad Range) and HS (High Sensitivity) kits, containing a highly selective fluorescent molecule for binding with RNA molecules. 1μg of total RNA was treated with DNAse I (Thermo fisher), to eliminate the DNA contamination, and subsequently retrotranscribed using the kit Super Script First-Strand Synthesis System (Thermo fisher), according to the manufacturer's instructions. The cDNAs obtained, were adequately diluted in DEPC-H20. Subsequently 10 ng or 200 ng of cDNA were used to quantize the expression of miRNAs or genes respectively through Real-time PCR, using the TaqManW (Applied Biosystem) assay. Each targeted transcript was validated using the comparative Ct method for relative quantification (ΔΔCt). GADPH was used as a normalizer for genes while U6 was used as a normalizer for miRNAs and the relative expression of each gene was determined using method 2 (-ΔΔCT).

3.4 Western blot analysis

Cells were lysed with RIPA buffer; 50 μg of total protein were resolved under reducing conditions by 8% SDS-PAGE and transferred to reinforced nitrocellulose (BA-S 83, Schleider and Schuell, Keene, NH, USA). The membranes were blocked with 5% non fat dry milk in PBS 0.1% Tween 20, and incubated with the different primary antibodies. The membranes were rehydrated and probed again with anti-GAPDH, to estimate the protein equal loading. Densitometric analysis was performed using Quantity One Program (Bio-Rad Laboratories GmbH) and results were expressed as mean values from three independent experiments.

3.5 Cell viability assays

The number of viable melanoma cells was measured by quantification of the ATP present according to Cell Titer-Glo® Luminescent Cell Viability assay protocol and colony formation assays were performed as described in this work (84).

3.6 In vitro colony formation assays

Cells viability was determined by crystal violet staining. Briefly, the cells were stained for 20 min at room temperature with staining solution (0,5% crystal violet in 30% methanol), washed four times with water and then dried. Cells were then dissolved in acetic acid (CH3COOH) solution and the absorbance (595 nm) was read using a microplate ELISA reader.

3.7 FACS analysis

The expression of Green Fluorescence Protein (GFP) was evaluated by FACS analysis. A total of 1×10^5 cells were resuspended in 500 μL of 2 mM EDTA and 2% BSA in 1X PBS and run to a flow cytometer. Non-GFP cells were used as control. For cell cycle analysis, cells were pelleted and 250 μl PBS (Sigma-Aldrich) and 10 μl RNase-A (Sigma-Aldrich) were added to the pellet. Cells were incubated at 37 °C for 30 min. Then propidium iodide (Sigma-Aldrich) was added (1 mg/ml) and cells were incubated at room temperature, in the dark, for 5 min. Approximately 10,000 events per sample were acquired with a CytoFLEX (Beckman Coulter, Milan, Italy) instrument equipped with three lasers (488 nm, 405 nm and 638 nm) and 9 detectors. Quality control of the cytometer was assessed daily using CytoFLEX Daily QC Fluorospheres (Beckman Coulter #B53230). Data were collected by CytExpert 2.2 version (Beckman Coulter) software. If needed, a compensation matrix was calculated using a VersaComp Antibody Capture Kit (Beckman Coulter #B22804) according to the manufacturer's instructions. FCS files were analyzed using CytExpert version 2.2 software.

3.8 Generation of inducible cell clones

Human melanoma A375 cell line was used to generate inducible cell line expressing miR-579-3p. The construction of this new model is based on two subsequently lentiviral transductions. SparQ Cumate Switch protocol, Cat. #QMXXX Series from System

Biosciences S.p.A. was used.

- First Infection With The Lentivirus Containing Cymr Repressor

A375-CymR stable cell line was generated by infection with lentivirus containing CymR repressor and resistance to Puromycin as selection marker (QM200VA-1; *pCDH-EF1-CymR-T2A-Puro*). A375 cells were cultured in 24 well plates at a concentration of 20.000 cells per well and incubated overnight. For lentivirus infection, 10%-30% of cell confluence was required. A mix containing RPMI, Polybrene (1:1000) and 20 MOI (multiplicity of infections) of lentiviral particles were added to cells. Polybrene is a highly efficient infection reagent used to introduce lentiviral vectors into mammalian cells. Puromycin (500 μg/ml) was added to the culture medium 48 h after the transfection to select a pool of Puromycin-resistant cells (A375-CymR).

- Second Infection With Lentivirus Containing mir-579-3p Plasmid

Differently from generation of A375-CymR, second infection consist in two steps: 1) production of pseudoviral particle containing miR-579-3p plasmid; 2) Lentiviral transduction on A375-CymR. To this purpose, *pCDH-CuO-MCS-EF1-copGFP* (QM511B-1) plasmid containing miR-579-3p/green fluorescence protein (GFP) and pPACKH1 Packaging Plasmid Mix were purchased from System Biosciences (SBI). pPACKH1 Packaging Plasmid Mix contains the structural (gag), and replication (pol) genes which code for some of the proteins required to produce the lentivirus. To obtain pseudoviral particle, HEK293TN were plated at 10%-30% of confluence and subjected to co-transfection with 45 μl of Packaging Plasmid Mix together with 3 μg of plasmid containing miR-579-3p and GFP expression. 48h after co-transfection, HEK293TN will release in culture medium new pseudoviral particles containing *pCDH-CuO-MCS-EF1-copGFP* plasmid. Hence, culture medium were centrifuged at 3000 x g for 15 minutes at room temperature to pellet cell debris. Supernatant was resuspended wit 1X PBS and stored at -80°C.

Subsequently, A375-CymR were plated at 10%-30% of confluence and subjected to infection with mix containing 5 μl of lentiviral particles, RPMI and Polybrene (1:1000). After 72h of

lentiviral infection, individual clones were isolated from this pool by the method of limiting dilution and characterized by homogenous expression of GFP with FACS analysis and the capability to induce miR-579-3p after adding 100 μgr/ml of Cumate.

3.9 Bulk RNA Sequencing

Total RNA was extracted from matched PBMC and PEMC of 5 LUAD patients and from PBMC of 4 HDs, using Qiazol (Qiagen, Hilden, Germany), purified from DNA contamination through a DNase I (Qiagen) digestion step, and further enriched by Qiagen miRNeasy columns profiling (Qiagen). Quantity and integrity of the extracted RNA were assessed by Nanodrop Spectrophotometer (Nanodrop Technologies LCC, Thermo fisher, Waltham, MA, USA) and by Agilent 2100 Bioanalyzer (Agilent Technologies, Santa Clara, CA, USA), respectively. RNA libraries for sequencing were generated using the TruSeq RNA Exome kit (Illumina, San Diego, CA, USA). The procedure consists of two steps, the first one is a general whole transcriptome strand specific library preparation followed by a specific exon targeting enrichment. The quality of the resulting libraries was assessed via Bioanalyzer (High Sensitivity DNA Kit). The intermediate library, before exon enrichment, was quantified by Qubit, the final library by qPCR. Samples were sequenced in paired-end mode, sequencing 76 bp from each side, with NextSeq 500 System (Illumina).

3.10 RNA data processing, identification of DEGs and pathway analysis

RNA-seq raw data were processed thanks to the nf-core/rna-seq pipeline (v 2.4) (86), which carries out the primary analysis of the mapping onto the reference genome (GRCh37) providing Quality Control metrics of the analysed samples. Both the raw counts (Feature Counts) and the TPM (Transcript Per Million) normalized pseudo counts from the Salmon tool were obtained from the pipeline. For DEG identification, genes with Log2Fold Change> 0.15 and adjusted p-value <0.05 were considered as statistically significant. The biological function of DEGs was identified by Gene Ontology (GO) analysis using the R package (87). A Gene Set Enrichment Analysis (GSEA software; https://www.gsea-msigdb.

org/gsea/index.jsp) was conducted by using the curated gene sets of the Molecular Signature Database (MSigDB) derived from KEGG, Hallmark, Reactome, and Biocarta collections. GSEA was run in pre ranked mode using classic as metric and 1000 permutations (FDR<0.1, p-value<0.05).

3.11 Single-cell mass cytometry

For single-cell analysis via CyTOF2, 3×10^6 cells from each condition were used. Cells were centrifuged at 600× g for 5 min and washed in D-PBS w/o calcium and magnesium (BioWest, Milan, Italy). To minimize inter sample staining variation, we applied mass-tag barcoding protocol on fixed cells. Cells were fixed with 1 mL Fix I buffer and incubated for 10 min at RT. The fixation was quenched with Barcode Perm Buffer (Fluidigm, CA, USA). The samples from the different conditions were barcoded by individually incubating cells with the appropriate combination of palladium isotopes from the Cell-IDTM 20-Plex Pd Barcoding Kit in Barcode Perm Buffer for 30 min at RT. The staining was quenched with MaxPar Cell Staining Buffer (Fluidigm, CA, USA). The antibody staining with metal-tagged antibodies against surface and intracellular antigens was performed on pooled samples after mass-tag cellular barcoding. Samples were collected into one unique tube, and the surface antibody-staining protocol was performed according to the manufacturer's instructions for 30 min at RT. Surface-stained cells were then washed twice with MaxPar Cell Staining Buffer and permeabilized with ice-cold methanol on ice for 10 min. Membrane-permeabilized cells were washed twice with MaxPar Cell Staining Buffer and incubated with antibodies against intracellular antigens for 30 min at RT according to the manufacturer's instructions.

The full list of antigens is provided in Table 1.

ANTIGENS	**METALS**
CD63	150ND

CD47	209BI
CD147	156GD
CD90	161DY
CD271	149SM
CD274	159TB
CD273	172TB
CD56	163DY
NOTCH2	165HO
NG2	174YB
MART1	155GD
AXL	169TM
pNFKB	163ER
MITF	170ER
BETA-CATENIN	147SM
pERK 1/2	167ER
pAKT	152SM

pCREB	176YB
NESTINA	151EU
pSTAT3	158GD

After intracellular antibody staining, cells were washed twice with MaxPar Cell Staining Buffer and stained for 1 h at RT with an intercalation solution composed of Cell-ID Intercalator-Ir (191Ir and 193 Ir) (Fluidigm, CA, USA) into MaxPar Fix and Perm Buffer at a final concentration of 125 nM. Cells were washed twice with MaxPar Cell Staining Buffer and MaxPar Water supplemented with 0.1% Tween, respectively. For mass-cytometry acquisition, cells were resuspended at the final concentration of 2.5×10^5 cells per ml in ddH2O containing 10% of EQTM Four Element Calibration Beads and filtered through a 30-μm filter-cap FACS tube. All the reagents and antibodies for mass cytometry experiments were purchased from Fluidigm Corporation (Fluidigm, CA, USA). Samples were kept on ice prior to acquisition by using the mass-cytometry platform CyTOF2 (Fluidigm, CA, USA); data were collected as .fcs files.

3.12 CyTOF data processing

Following data acquisition, channel intensity was normalized using calibration beads and files were debarcoded by using the Debarcoder software (Fluidigm). Data were gated using Cytobank (Beckman Coulter, Milan, Italy) (88). Cells were identified by the incorporation of two iridium isotopes, 191Ir (DNA1) and 193Ir (DNA2). Next, singlets were discriminated from doublets using the event length parameter and analyzed using the tSNE and FlowSOM alghoritms. The t-SNE maps were generated by the t-SNE algorithm with the following

settings: 350,000 events using a proportional event sampling; 1000 iterations; perplexity 30; seed 641220519.

3.13 Statistical analysis

Experiments were replicated at least three times and the data were expressed as average ±SD or ±SE of the mean (SEM). Differences between groups were analyzed with a two-tailed paired or unpaired Student's t-test and were considered statistically significant for p-value <0.05.

4. RESULTS

4.1 Generation of a cell clone with transcriptionally inducible expression of miR-579-3p

miR-579-3p has been previously identified by the laboratory of my PhD thesis supervisor as a tumor suppressor microRNA whose down-regulation occurs during tumor progression. This microRNA was shown to have pleiotropic functions on cell proliferation, cell cycle progression, cell migration, and apoptosis. They are in part explained by its ability to target directly two oncogenes, namely BRAF and MDM2. miR-579-3p acts as antagonist of drug resistance to target therapies in BRAF-mutated melanomas in long term clonogenic assays (72). In order to study the influence of miR-579-3p on drug adaptation, i.e. in the very early response of BRAF mutated cells after drug exposure, we decided to build a stable cell line bearing a transcriptionally inducible construct coding for this microRNA. In order to achieve this goal we decided to use the Cumate Switch OFF/ON system which exploits the repressor from the bacterial operon CymR to regulate the desired target gene. As reported in the model in figure 17, in the OFF configuration the CymR Repressor binds to its operator which is cloned between a eukaryotic promoters (such as for example CMV) at the transcriptional start site of the target gene. This binding blocks gene expression. In the ON configuration, in the presence of the drug Cumate which binds the CymR Repressor, the repressor is released from the operator upon an allosteric conformational change of the protein and gene expression of the downstream gene can occur. Cumate causes a change in conformation of CymR repressor so that it cannot bind CuO site and CMV5 promote will be active.

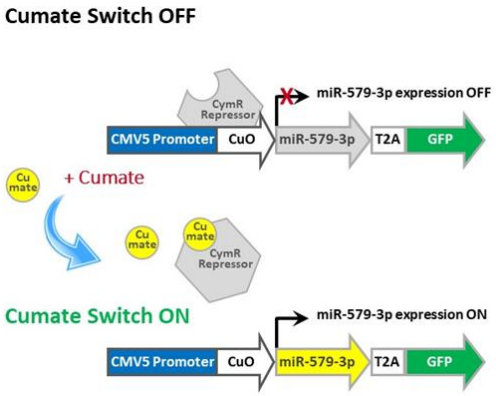

Figure 17. Molecular model of inducible system allowing switch on/off miR-579-3p expression (from Manual of SparQ™ Lentiviral Cumate Switch Inducible system) .

The construction of this system is based on two subsequent lentiviral transductions consisting first in the selection of a stable clone carrying the CymR repressor by plasmid *(pCDH-EF1-CymR-T2A-Puro)*. Subsequently these cells are lentivirally transduced with a second construct carrying the target gene under control of the Cumate operator followed by the *green fluorescent protein* (GFP) gene under control of a constitutively active EF1 promoter *(pCDH-CuO-MCS-EF1-copGFP)* (see materials and methods). We decided to use as cell system A375 a well-known and widely used BRAF mutated melanoma cell line of human origin (89). Firstly, A375 were subjected to lentiviral transduction with plasmid containing CymR repressor (figure 18 A). As shown, this plasmid contains the Puromycin resistance marker which allowed to select cells stably overexpressing the construct adding this antibiotic in culture medium. These cells were subjected to quantitative Real time-PCR in order to evaluate the expression of CymR repressor (figure 18 B). Results show that CymR repressor was highly expressed after lentiviral transduction. This new cell line, namely A375-CymR, was used for the second lentiviral transduction using the Cumate Switch Inducible system described in figure 18 C.

As shown in figure 18 D, a large proportion of lentiviral vector exposed cells showed expression of GFP as a control of efficient transduction. This cell population was subjected to serial limiting dilution in order to obtain individual clones starting from single cells.

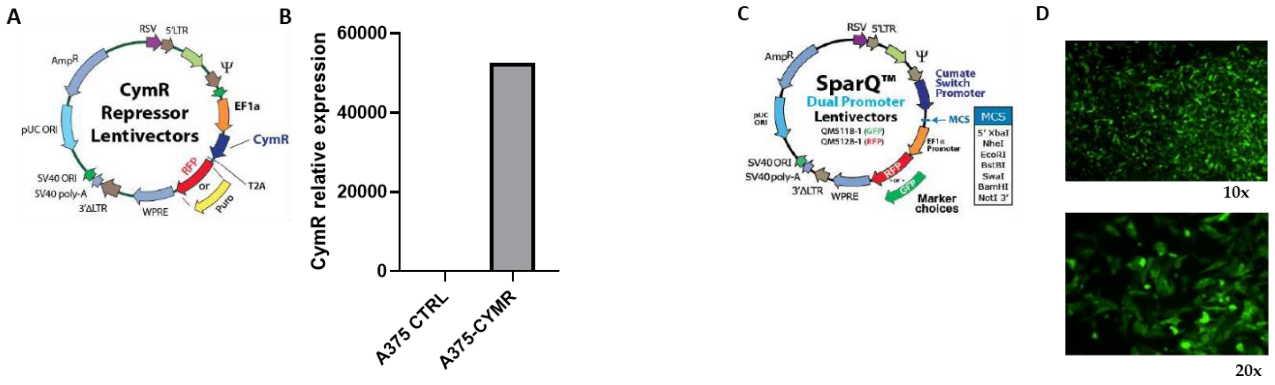

Figure 18. Steps to obtain clonal population containing "Cumate Switch" Inducible System. (A) Genetic map of plasmid containing CymR repressor. (B) CymR repressor was evaluated by RT-PCR. (C) Genetic map of construct carrying miR-579-3p. (D) The expression of green-fluorescent protein (GFP) by fluorescence microscope indicates that the insertion of lentiviral vectors into genome was successful (10x and 20x magnification).

Three different clonal populations were obtained after limiting dilution, which were characterized by the expression of miR-579-3p by adding Cumate to culture medium. As shown in figure 19, the different clones showed a different degree of up-regulation of microRNA expression. Clone n°1 showed the lowest increase of miR-579-3p; clone n°2 intermediate levels, clone n°3 the highest expression of miR-579-3p.

Based on these results clone n°3 has been chosen for further analyses.

Figure 19. Three different clones were obtained by limiting dilution. Levels of miR-579-3p were evaluated by RT-PCR after 72h upon Cumate adding.

The name given to this new cell population is A375-miR579IndEx (inducible expression). To better characterize clone n°3, FACS analyses were performed. Figure 20 shows the differences in GFP expression before (left panel) and after (right panel) limiting dilution. In detail, FACS results demonstrated that before limiting dilution transduced A375 were characterized by a heterogeneous GFP expression (left panel). In contrast clone n°3 is characterized by a higher intensity and a unique peak of GFP positivity (right panel). These results confirmed the purity of our clonal selection.

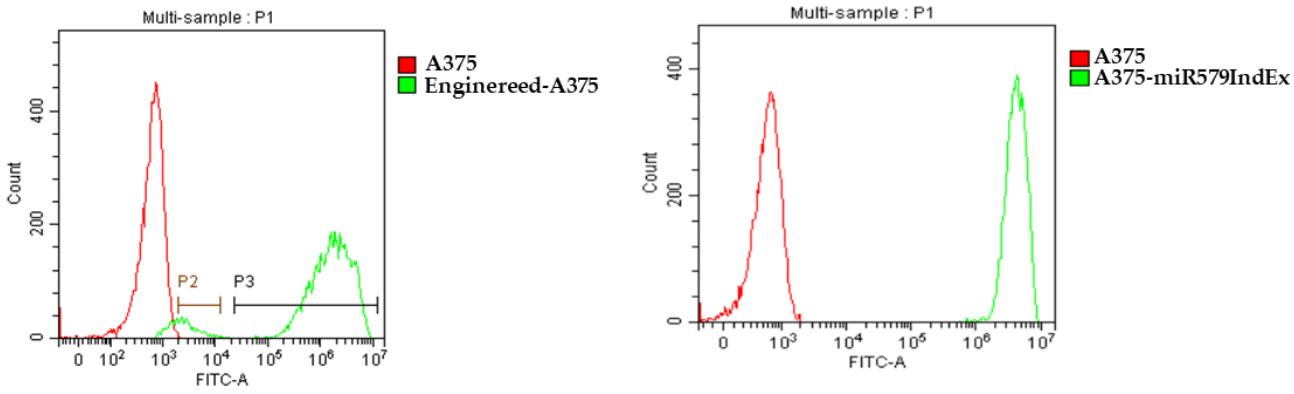

Figure 20. FACS analysis showed differences in GFP expression after (left panel) and before (right panel) limiting dilution method. Clonal population A375-miR579-IndEx homogenously express GFP by FACS analysis(right panel)

The subsequent experiments were carried out using A375-miR-IndEx as model of study.

4.2 Biochemical and functional characterization of the A375-miR-index (clone n°3)

First of all the plasticity of the A375-miR579IndEx cell model has been tested. To this aim, cells were treated with 100 μgr/ml of Cumate for 72 h (see material and methods for details), then cell media was replaced for additional 72 h in the absence of Cumate. RNA was extracted and subjected to Real-Time PCR analysis to measure the expression levels of miR-579-3p. The results (figure 21) show that miR-579-3p expression was strongly upregulated by the presence of Cumate (CUM ON). In contrast, when Cumate was removed from the medium, miR-579-3p levels dramatically decreased (CUM OFF).

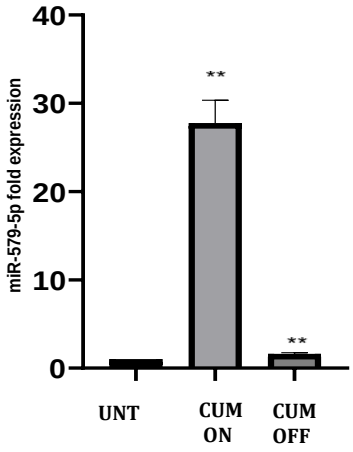

Figure 21. Real-Time PCR on miR-579-3p highlighted the plasticity of this inducible model. The presence of Cumate in culture medium increased the transcription of miR-579-3p (CUM ON) whereas Cumate removal from medium strongly reduced miRNA expression levels (CUM OFF).

It was previously shown that miR-579-3p acts as onco-suppressor miRNA by targeting the 3′ UTR of the BRAF oncogene and by negatively regulating the MAPK-ERK pathway. In agreement with this melanoma cells transiently transfected with a miR-579-3p mimic strongly reduced endogenous BRAF levels (72). To assess whether the same effect is also observed in the "Cumate Switch" Inducible Model, Western Blot analysis was performed with protein extracted from A375-miR579IndEx cells after induction for 72 h with Cumate. The results (figure 22) show both by qualitative and quantitative Western Blot analyses, that the induction of miR-579-3p expression reduced

endogenous BRAF protein levels. In addition, also a strong reduction of ERK 1/2 phosphorylation was observed, underlying that miR-579-3p is able to down-regulate the activation of the MAPK-ERK oncogenic pathway through the inhibition of the BRAF oncoprotein.

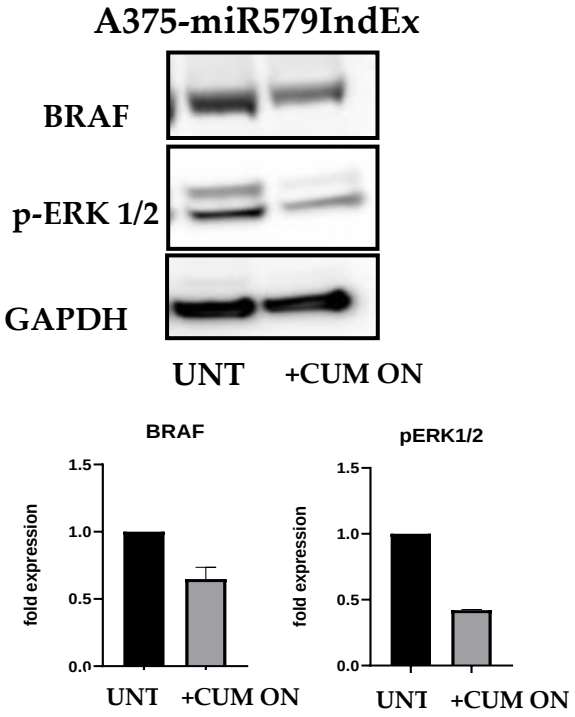

Figure 22. miR-579-3p induction impacts on MAPK-ERK signaling. A375-miR579IndEx cells were treated with Cumate for 72h and then subjected to Western Blot analysis.

miR-579-3p transient overexpression has been previously reported by our group to be able to potentiate the growth inhibitory effects of targeted therapies on BRAF-mutant melanoma cells (72). Therefore, the following experiments were directed to assess whether inducible miR-579-3p upregulation could be able to exert the same effects. To this purpose, clonogenic assays were carried out on A375-miR579IndEx cells treated with Cumate alone, Dabrafenib + trametinib (MAPKi), or their combination. In detail, these experiments were performed measuring the clonogenicity of the cells through Crystal Violet staining after 72 h of exposure to 100 μgr/ml of Cumate alone or in combination with the concentration relative to the IC_{50} of Dabrafenib [2nM] and Trametinib [1nM] (calculated on A375 parental melanoma cell line) (84). Results shown in figure 23 demonstrated that Cumate alone did

not affect cell clonogenicity whereas it was able to strongly potentiate targeted therapies growth inhibitory effects.

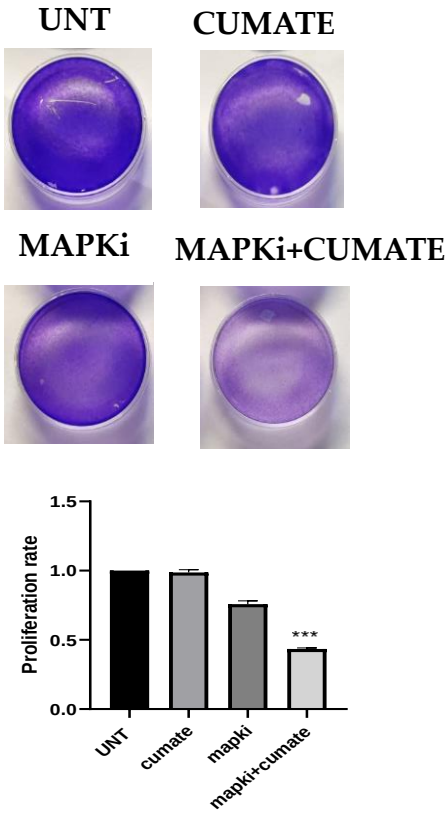

Figure 23. miR-579-3p induction potentiates MAPK inhibitors in short-term condition. A375-miR579IndEx cells were plated in 60mm² dishes and subsequent treated with Cumate, MAPK inhibitors (BRAFi plus MEKi), and combination MAPKi plus Cumate. After 72 h, cell were processed by Cristal Violet assay.

To further investigate the effect of miR-579-3p induction, proliferation assays were carried out on A375-miR579IndEx cells using cell-titer Glo assays. This method measures the number of viable and metabolically active cells based on the quantification of ATP levels. Also in this case, figure 24 A showed that the induction of miR-579-3p alone upon Cumate exposure for 72 h did not affect cell viability.

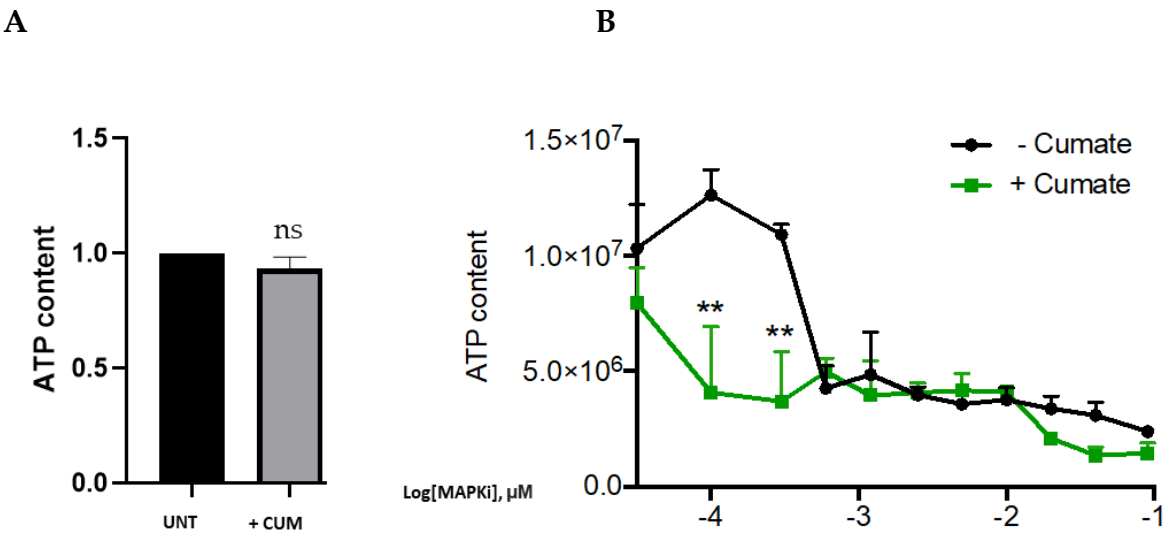

Figure 24. Cell-titer Glo assay shows that miR-579-3p in combination with MAPKi inhibits cell viability. (A) Only miR-579-3p induction not impair cell viability after 72 h of treatment with Cumate. (B) Dose-response curve for evaluating of ATP levels and cell vitality on A375-miRIndEx with MAPK inhibitors alone and in combination with Cumate after 72 h of treatments.

In contrast, when Cumate was added to cell culture in combination with MAPKi, this resulted in a synergistic inhibition of cell growth especially at low drug concentration as shown in the dose response curve (figure 24 B) .

These data taken together show that A375-miR579IndEx cells undergo the desired transcriptionally inducible expression of miR-579-3p and this is resulting in downregulation of MAPK-ERK signaling and reduction of cell growth in synergy with MAPK inhibitors. Hence this is a suitable system for further studies.

4.3 miR-579-3p prevents the onset of resistance to MAPK inhibitors in BRAF-mutated metastatic melanoma

The results of the previous section have allowed to set up the A375-miR579IndEx cell model and demonstrated that the inducible expression of miR-579-3p is able to potentiate MAPK inhibitors in short term clonogenic assays.

The following experiments took advantage of this model to perform different biological long term assays in the presence of either Cumate and/or MAPKi. The goal of these studies were directed to assess whether miR-579-3p inducible expression could be able to hamper the establishment of drug tolerance upon exposure to target therapy. Before using the A375-miR579IndEx cell model the experimental conditions were set up using the relative A375 drug sensitive parental counterpart. To this aim, cells were exposed for one month to the combination of Dabrafenib (as BRAFi) and Trametinib (as MEKi) at the concentration corresponding to the IC_{50}, i.e. 2nM and 1nM of the two drugs, respectively for the following times different time points (3, 6, 12, 21, 30 days) . In order to maintain continuous exposure to the two drugs fresh addition of the two MAPKi was ensured every 3 days. Cells were to two different biological assays, i.e. cell cycle analysis and clonogenic assays.

The results of cell cycle analysis, performed using Flow cytometry are shown in Figure 25 A. Their quantification in Figure 25 B. It is evident that exposure to the combination of the two MAPKi induces a block in the G1 phase until day 12 with complete absence of cells in the S and P2 phases of the cell cycle. Starting at day 21 cell restart cycling again as evident from the presence again of an equivalent number of cells in S and G2 phases at this and at the following time point (30 days) as in untreated samples (figure 25 B). These findings were corroborated also by clonogenic assays, which confirmed a strong reduction of clonogenicity at the initial time points, e.g at 3, 6 and 12 days and a full recovery at the following time points, namely at 21 and 30 days (figure 25 C). Altogether these results confirm that this isogenic melanoma cell population undergoes a rapid adaption to the therapeutic pressure imposed by MAPKi.

A

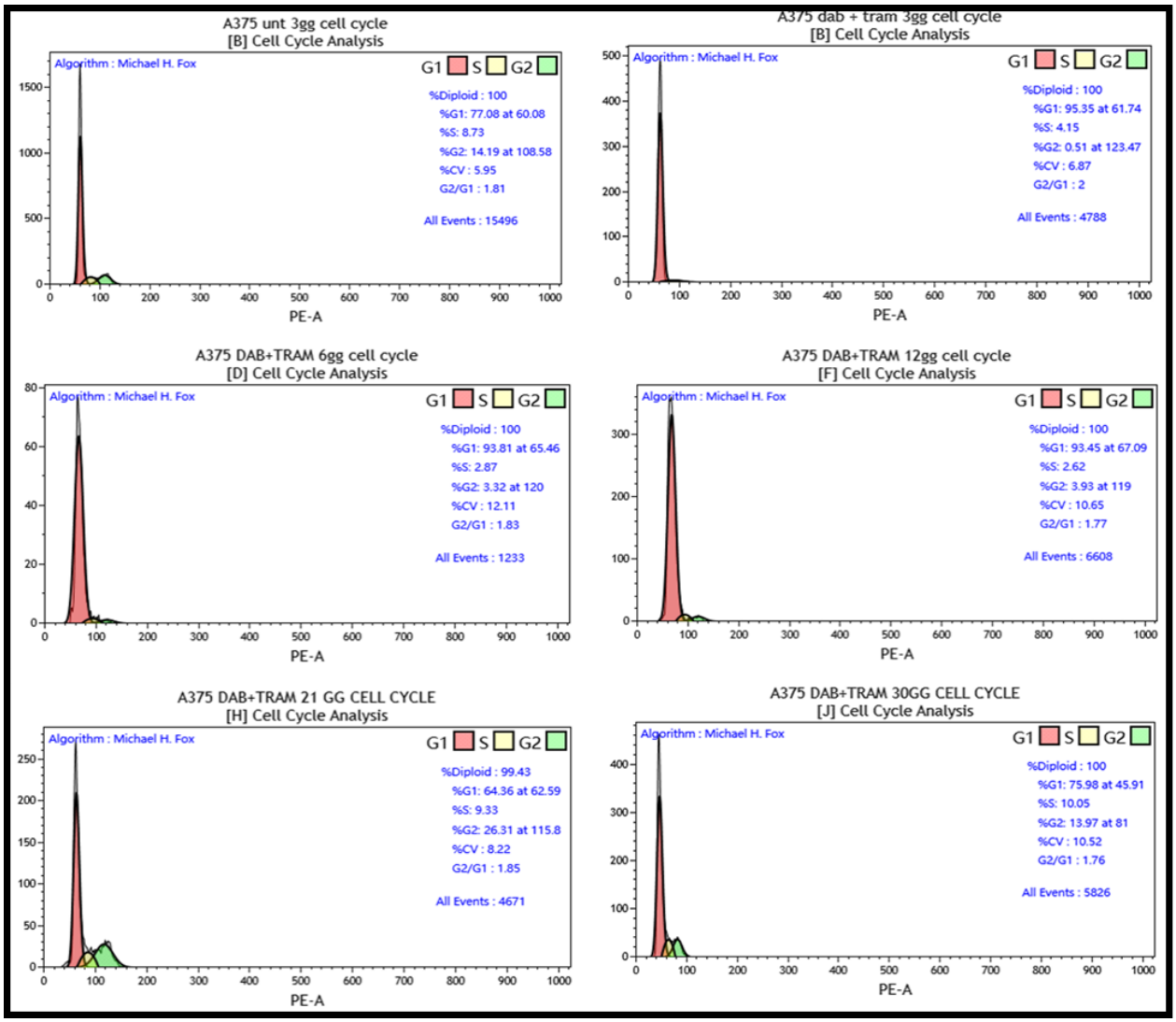
A375 unt 3gg cell cycle
[B] Cell Cycle Analysis
Algorithm : Michael H. Fox
G1 S G2
%Diploid : 100
%G1: 77.08 at 60.08
%S: 8.73
%G2: 14.19 at 108.58
%CV : 5.95
G2/G1 : 1.81
All Events : 15496
PE-A
A375 dab + tram 3gg cell cycle
[B] Cell Cycle Analysis
Algorithm : Michael H. Fox
G1 S G2
%Diploid : 100
%G1: 95.35 at 61.74
%S: 4.15
%G2: 0.51 at 123.47
%CV : 6.87
G2/G1 : 2
All Events : 4788
PE-A
A375 DAB+TRAM 6gg cell cycle
[D] Cell Cycle Analysis
Algorithm : Michael H. Fox
G1 S G2
%Diploid : 100
%G1: 93.81 at 65.46
%S: 2.87
%G2: 3.32 at 120
%CV : 12.11
G2/G1 : 1.83
All Events : 1233
PE-A
A375 DAB+TRAM 12gg cell cycle
[F] Cell Cycle Analysis
Algorithm : Michael H. Fox
G1 S G2
%Diploid : 100
%G1: 93.45 at 67.09
%S: 2.62
%G2: 3.93 at 119
%CV : 10.65
G2/G1 : 1.77
All Events : 6608
PE-A
A375 DAB+TRAM 21 GG CELL CYCLE
[H] Cell Cycle Analysis
Algorithm : Michael H. Fox
G1 S G2
%Diploid : 99.43
%G1: 64.36 at 62.59
%S: 9.33
%G2: 26.31 at 115.8
%CV : 8.22
G2/G1 : 1.85
All Events : 4671
PE-A
A375 DAB+TRAM 30GG CELL CYCLE
[J] Cell Cycle Analysis
Algorithm : Michael H. Fox
G1 S G2
%Diploid : 100
%G1: 75.98 at 45.91
%S: 10.05
%G2: 13.97 at 81
%CV : 10.52
G2/G1 : 1.76
All Events : 5826
PE-A

B

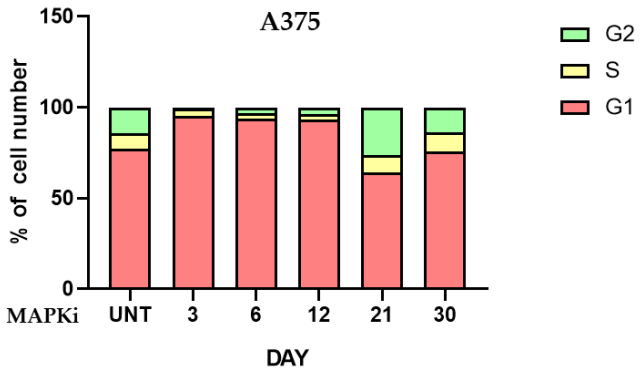
A375
% of cell number
150
100
50
0
MAPKi
UNT
3
6
12
21
30
DAY
G2
S
G1

C

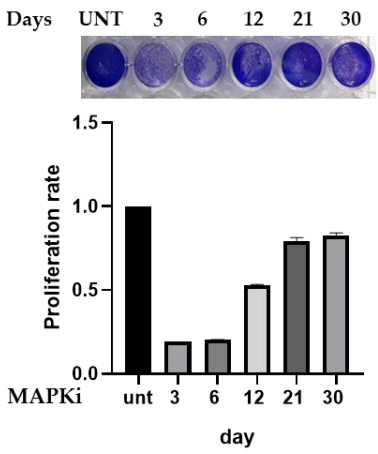
Days
UNT
3
6
12
21
30
Proliferation rate
1.5
1.0
0.5
0.0
MAPKi
unt
3
6
12
21
30
day

Figure 25. Long-term experiment with Dabrafenib (BRAF inhibitor) and Trametinib (MEK inhibitor) on parental A375 $BRAF^{V600E}$ melanoma cell line. Qualitative (A) and quantitative (B) analyses of cell cycle and clonogenic assay by Cristal Violet method (C). Cells were processed after 3, 6, 12, 21 and 30 days of drug-treatments.

The next question was directed to ask whether the constant and inducible expression of miR-579-3p in long term assays could be able to block the onset of drug adaptation. Using the same experimental setting parental A375 andA375-miR579IndEx cells were exposed to Cumate alone, the two MAPKi inhibitors or the combination of MAPKi + Cumate at different time points as shown in the figure 26 below and subjected to quantitative FACS analysis.

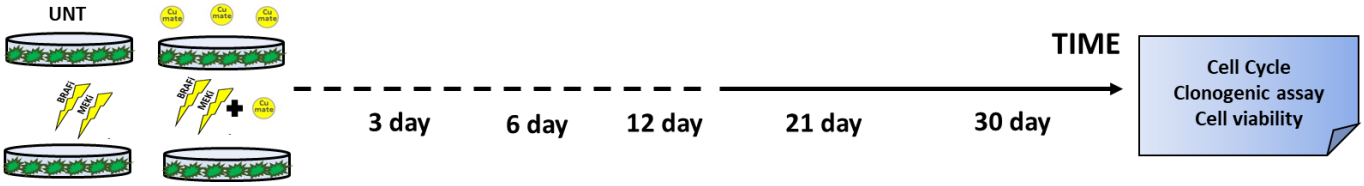

Figure 26. Model of experimental setting for evaluating the impact of miR-579-3p on drug-tolerant phenotype.

The results (figure 27) show that 1) exposure to Cumate alone is unable to affect cell cycle progression. This is in agreement with the results of the proliferation assay shown in the previous section (figure 23 A), 2) exposure to MAPKi blocks melanoma cells in the G1 phase only until day 12 after which they restart growing even in the constant presence of the drug 3) the concomitant treatment with MAPKi + Cumate prolong cell cycle blockade also after day 12 as it can be seen at the 21 day time point. At 30 days it was not possible to carry out cell cycle analysis for this treatment because of the very low amount of remaining living cells.

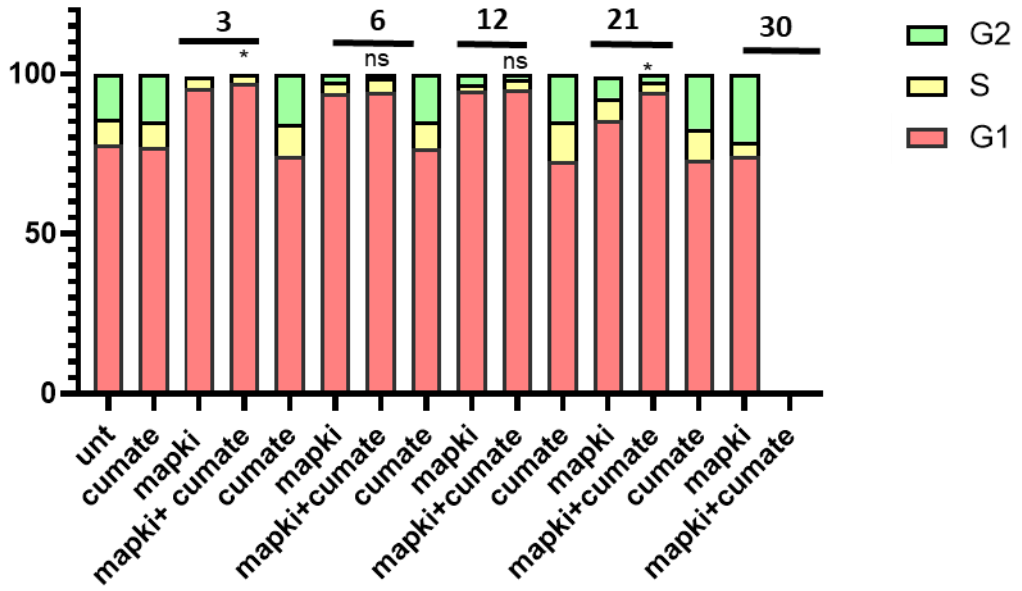

Figure 27. Quantitative evaluation of cell cycle analysis by Flow Cytometry. G1 phase = Red bars. S phase = Yellow Bars. G2 phase = Green Bars. Cell cycles were evaluated at 3, 6, 12, 21, 30 days upon treatments.

Figure 28 showed representative imagines of each treatment with Cumate, MAPKi and MAPKi+Cumate at 30 day from treatments. Pictures highlighted that chronic treatments with MAPKi+Cumate led to a completely cell death compared to MAPKi sole.

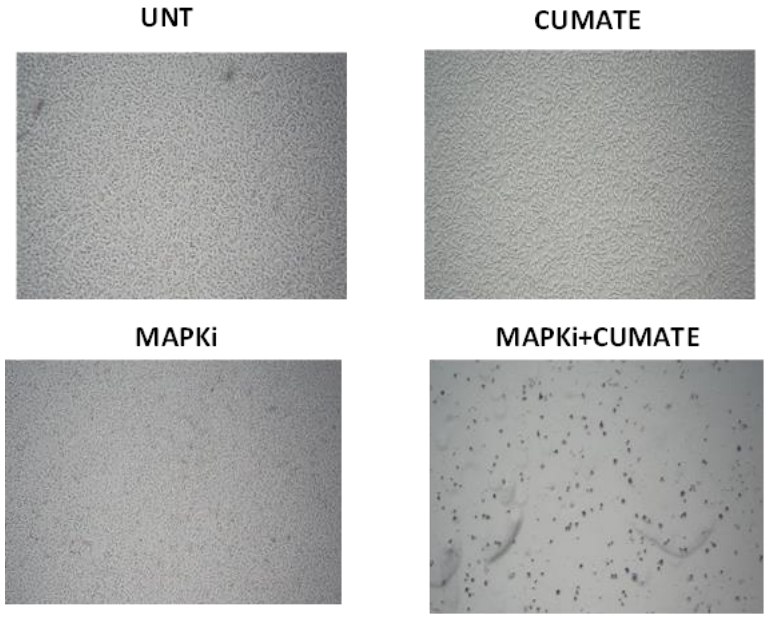

Figure 28. Representative imagines of UNT, Cumate, MAPKi and MAPKi+Cumate experimental conditions at 30 days from treatments. (4X magnification)

In order to measure the pro-apoptotic effect of the various drug treatments the percentage of cells in the Sub-G1 phase was determined by cell cycle analysis . The data were quantified and results are shown in figure 29. It can be appreciated that, in agreement with the previous findings, treatment with the two MAPKi was able to increase only transiently the percentage of cells in Sub-G1 untill day 12. Thereafter, Sub-G1 positive cells dramatically dropped down until the last time point. In contrast, when cells were exposed to the combination of MAPKi + Cumate the increase in Sub-G1 cells remained elevated until day 21, showing a prolongued induction of cell death (figure 29). After the 21 day time point, in these samples it was not possible to determine the percentage of Sub-G1 cells due to the low amount of cells remaining in the wells.

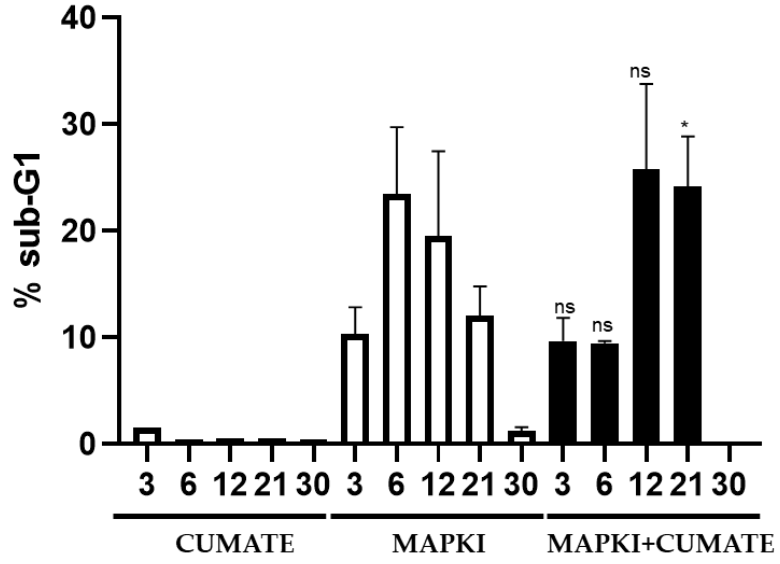

Figure 29. Percentage of sub-G1 (apoptotic cells) in treatments with Cumate, MAPKi and MAPKi+Cumate. Percentage of sub-G1 was evaluated a 3, 6, 12, 21, 30 days from treatments.

These results were confirmed using different biological assays focusing on the two conditions MAPKi vs MAPKi+Cumate treated cells. First of all, we determined the percentage of proliferating cells measuring the ATP content. Results (figure 30) show that 1) 3 days upon drug exposure Cumate was able to potentiate the inhibitory effects of target therapies 2) at days 6 and 12 there were no differences in the amount of proliferating cells between the two experimental conditions (in agreement with FACS analyses) and 3) finally

at days 21 and 30 cell proliferation was vigorous in the presence of the two MAPKi but strongly abated in the presence of the combination of MAPKi+Cumate (figure 30).

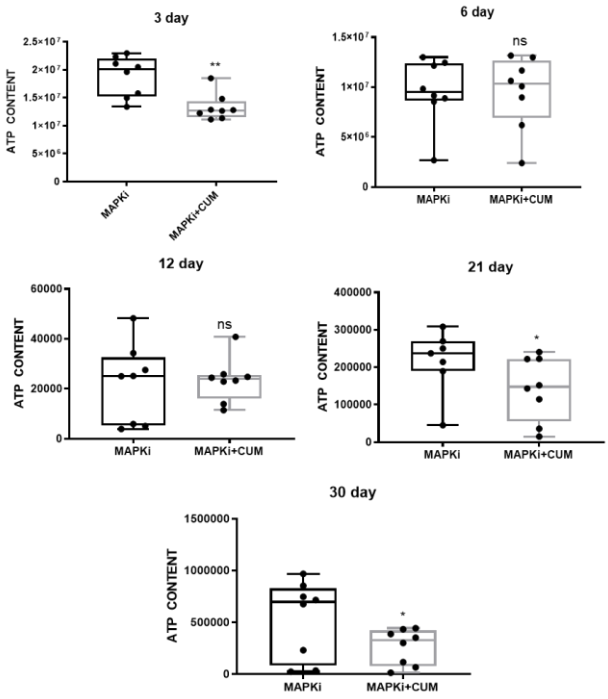

Figure 30. Box-whiskers plots showing ATP content upon treatments with MAPKi and MAPKi+Cumate. Cells were processed by Cell-Titer Glo assay at 3, 6, 12, 21, 30 days from treatments.

These findings were confirmed also by clonogenic assays performed at days 6 and 21 which demonstrated that the co-treatments of MAPKi + Cumate were able to strongly reduce the clonogenic potential of melanoma cells as compared to MAPKi treated cells (figure 31).

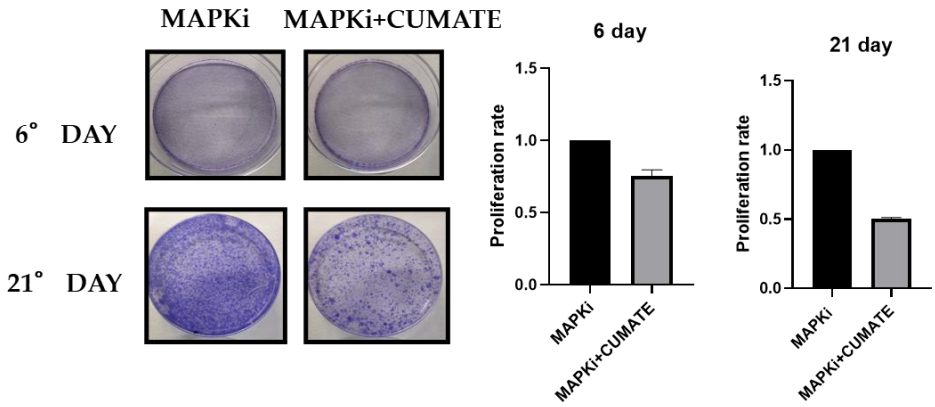

Figure 31. miR-579-3p improve the effects of MAPK inhibitors in long-term condition on proliferation rate. At 6 and 21 days from treatments, MAPKi and MAPKi + Cumate conditions were processed by Crystal Violet method.

Altogether the results of this section has showed that: a) while prolonged induction of mir-579-3p alone is unable to affect melanoma cell behavior; b) prolonged exposure to BRAF and MEK inhibitors only exerts a transient inhibition of the cell cycle and a limited induction of cell death, after which cells adapt to the presence of the drugs and start re-growing; c) combination of MAPKi together with prolonged miR-579-3p expression impairs the establishment of drug adaptation and cells undergo a stable block of proliferation followed by massive cell death.

4.4 Bulk RNA sequencing identifies distinct transcriptomic signatures of A375-miR579IndEx cells treated with MAPKi vs MAPKi+Cumate

Given that inducible miR-579-3p expression impairs the onset of a drug-tolerant phenotype upon exposure to MAPKi, the following step was directed to investigate the molecular basis of this phenomenon at a transcriptional level. To this aim, bulk RNA-Sequencing (RNA-Seq) analysis was performed on A375-miR579IndEx treated with Cumate, MAPKi or their combination according to the schematic representation reported in figure 32 below.

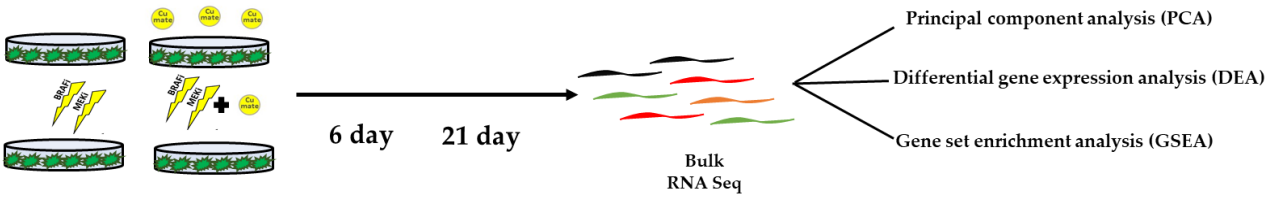

Figure 32. Schematic representation of RNA-Seq workflow. At 6 and 21 days of treatment, total RNA was extracted from 4 experimental conditions (UNT, Cumate, MAPKi and MAPKi+Cumate) and RNA-Seq analysis was carried out. Principal component analysis (PCA) was performed to highlight transcriptomic differences between samples. Differential gene expression analysis (DEA) and Gene Set Enrichment analysis (GSA) allowed to define specific pathways and genes affected by each treatment.

According to the results of the experiments described in the previous sections, these analyses were restricted to two time-points: day 6 and day 21 of consecutive drug-treatments The rationale behind the choice of these time points is the following 1) at day 6, MAPKi are still effective in the inhibition of melanoma cell growth and cell cycle progression at all conditions tested and 2) at day 21, melanoma cells treated with MAPKi, have undergone a clear reactivation of proliferation and cell cycle progression, suggestive of the adoption of a drug adaptive behavior, whereas, melanoma cells co-treated with MAPKi and Cumate (and its related induction of miR-579-3p) still result in complete inhibition of proliferation and cell cycle progression suggestive of a failure to undergo drug adaptation.

To carry out RNA-Seq analyses, total RNA was extracted from samples in triplicate and subjected to library preparation (see materials and methods). Bioinformatics analyses of the results obtained thanks to the collaboration with Bioinformatic Unit of Regina Elena Cancer Institute highlighted substantial transcriptomic differences determined as 1) Principal component analysis (PCA), 2) Differential Gene Expression analysis (DEA) and 3) Gene-set enrichment analysis (GSEA).

Here below is a detailed report of the findings.

Figure 33 shows the result of Principal Component Analysis (PCA), that was performed to cluster the samples based on their global pattern of gene expression. Results show that transcriptomic profiles clearly segregate in three different clusters (UNT/CUMATE, MAPKi, MAPKi+CUMATE), at both time points. Non-treated cells (UNT) and treatment with Cumate showed very high similarity at transcriptomic level and grouped as a single cluster. This was in part expected given that no substantial differences were observed at cell cycle or proliferation levels in Cumate-treated cells as compared to controls as shown in the previous sections. In contrast, MAPKi alone or in combination with miR-579-3p induction were transcriptionally different from UNT/CUMATE and between each other both at days 6 and 21.

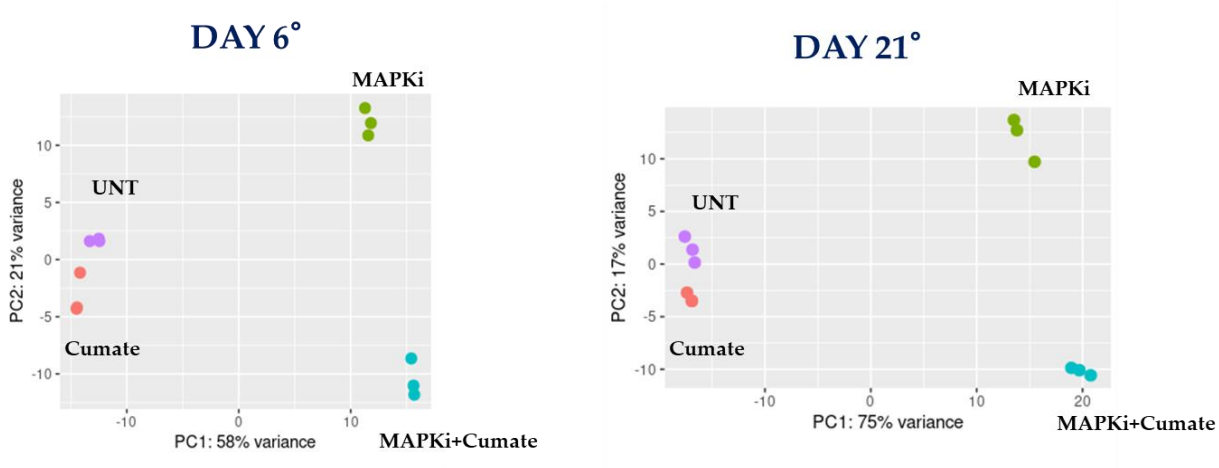

Figure 33. Principal Component Analysis (PCA) performed at 6 day and 21 day on non-treated (UNT) cells (purple dots),

treatment with Cumate (orange plots), treatment with MAPK inhibitors (green plots), treatment with MAPKi + Cumate condition (light blue dots). Each dot corresponds to the number of replicates used for RNA-Seq experiment.

Given that the experimental conditions of MAPKi alone and MAPKi+Cumate were characterized by the highest transcriptomic differences as compared to untreated cells, the following activities were directed to better dissect their RNA-seq profiles through DEGSeq2 differential expression analyses (DEA). Deregulation of gene expression analysis (DEGs) was calculated as at least Log2Fold Change >2 and Log2Fold Change < -2 respectively and adjusted p-value < 0.05.

As shown in the volcano plots at 6st day (figure 34 A), MAPKi-treated cells showed 1,887 Differentially Expressing Genes (DEGs) vs untreated cells, of which 672 downregulated and 1,215 upregulated. Differently, treatment with MAPKi+Cumate showed a higher number of DEGs, namely 2,730, of which 1,229 downregulated and 1,501 upregulated. Moreover, volcano plots at 21st day (figure 34 B), revealed 3,442 DEGs in cells treated only with MAPKi, of which 1,252 downregulated and 2,190 upregulated genes. Treatment with MAPKi+Cumate increased the total number of deregulated genes to 5,118, of which 2,186 downregulated and 2,932 upregulated. Of note, the number of downregulated genes in MAPKi+CUMATE was approximately doubled compared to treatment with MAPK-inhibitors alone, both at day 6 and 21.

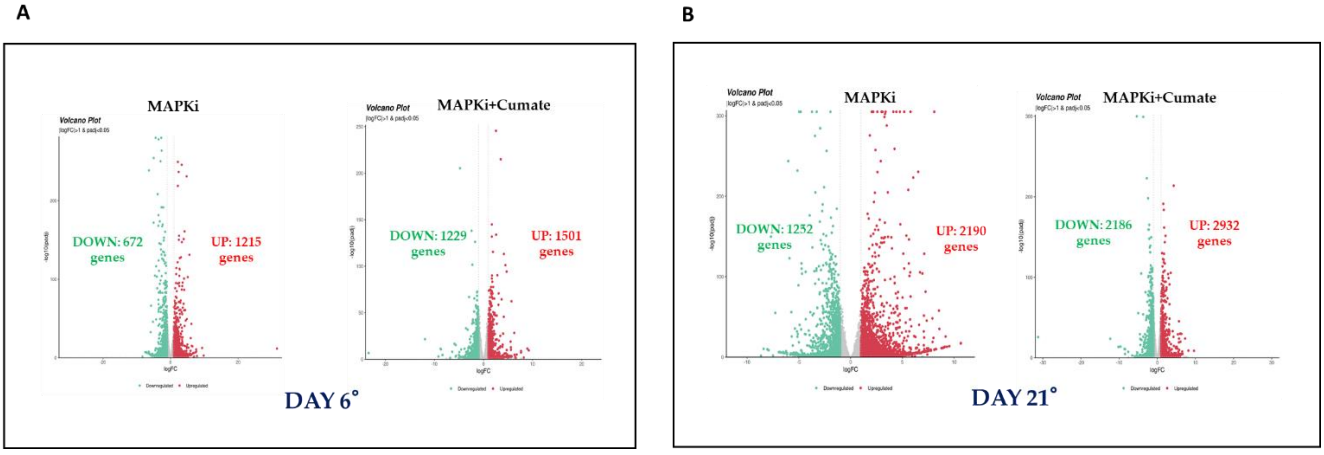

Figure 34. Volcano plots showing the upregulated and downregulated genes resulted from the differential expression analysis performed between treatments with MAPKi and MAPKi+Cumate at 6 day (A) and 21 day (B) compared to non-

treated (UNT) condition. Only genes with Log2Fold Change (FC) >2 or <-2 and adjusted p_val <0.05 were considered significantly upregulated (red dots) or downregulated (green dots).

To identify the molecular pathways affected by DEGs following treatments with MAPKi vs MAPKi+Cumate functional enrichment analyses were performed by grouping these genes into Gene Ontology (GO) categories based on Biological Processes (BP). Figure 35 summarizes GO enrichment analysis of MAPKi treated vs UNT cells at day 6 and 21^{s} of treatment considering the top 20 up- and down-modulated enriched terms.

At day 6, the most up-regulated enriched terms correspond to transcriptomics profiles related to the activation of the interferon gamma signaling pathway. Interestingly, these alterations have been already described to be able to sustain the evolving trajectories of melanoma during the development of therapeutic resistance (90). Furthermore, additional enriched terms include cytokine related signaling pathway and positive regulation of apoptotic processes. The presence of this last BP is in line with the evidence that MAPKi are still active at inducing apoptosis at this time point (figure 35 A) (see previous results of subG1 FACS analyses). Interestingly, also the positive regulation of the MAPK pathway was observed among the enriched terms thus suggesting that reactivation of this signaling pathway already occurs as early sign of adaptation from drug treatment. It has to be taken into account however, that the among the most down-regulated enriched terms are present proliferation and migration related biological processes, this indicating that at this time point cells have not yet developed a fully drug tolerant state (figure 35 B).

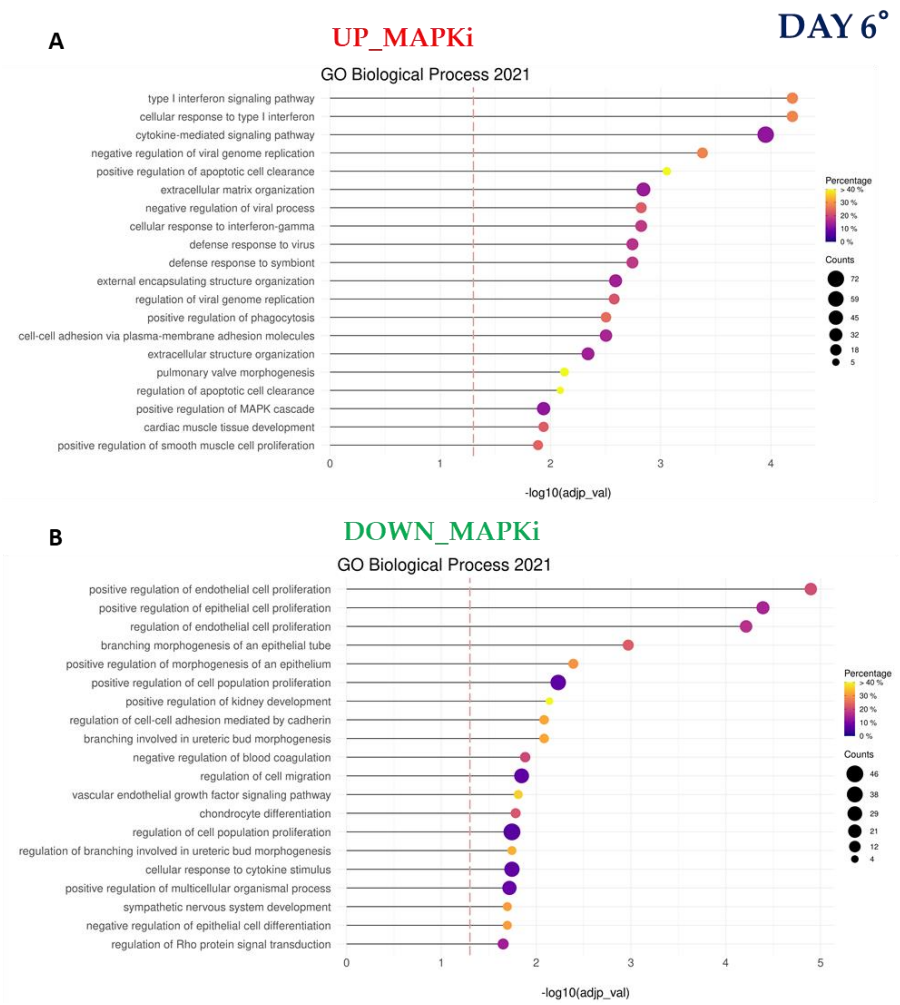

Figure 35. Gene Ontology (GO) analysis on deregulated genes in MAPKi treatment compared to untreated sample at day 6. Terms over red dashed line are considered statistically significant (adjusted p_val < 0.05). (A) Up-regulated enriched terms. (B) Down-regulated enriched terms.

At day 21, Interferon gamma pathway and related pro-inflammatory response were the most up-regulated terms confirming their prominent role in the evolution of drug tolerance upon the exposure to MAPK inhibitors (figure 36 A). Besides them, additional up-regulated enriched terms were related to extracellular matrix organization, positive regulation of MAPK cascade and cell migration. Among down-regulated terms, a high number of down-regulated genes (>40%) are involved in negative regulation of mitotic transition (figure 36 B). Furthermore, we observed an enrichment of terms related to DNA metabolic process, proliferation and G2/M transition (figure 36 B). Of note, the same G2/M transition terms were found more down-regulated in MAPKi+Cumate (figure 38 B) treatments than MAPKi. This aspect will be described below.

Altogether these findings suggest that long-term exposure to MAPKi inhibitors allows to select drug-tolerant cells characterized by re-activation of oncogenic MAPK signaling and migratory phenotype disadvantaging highly proliferative cells.

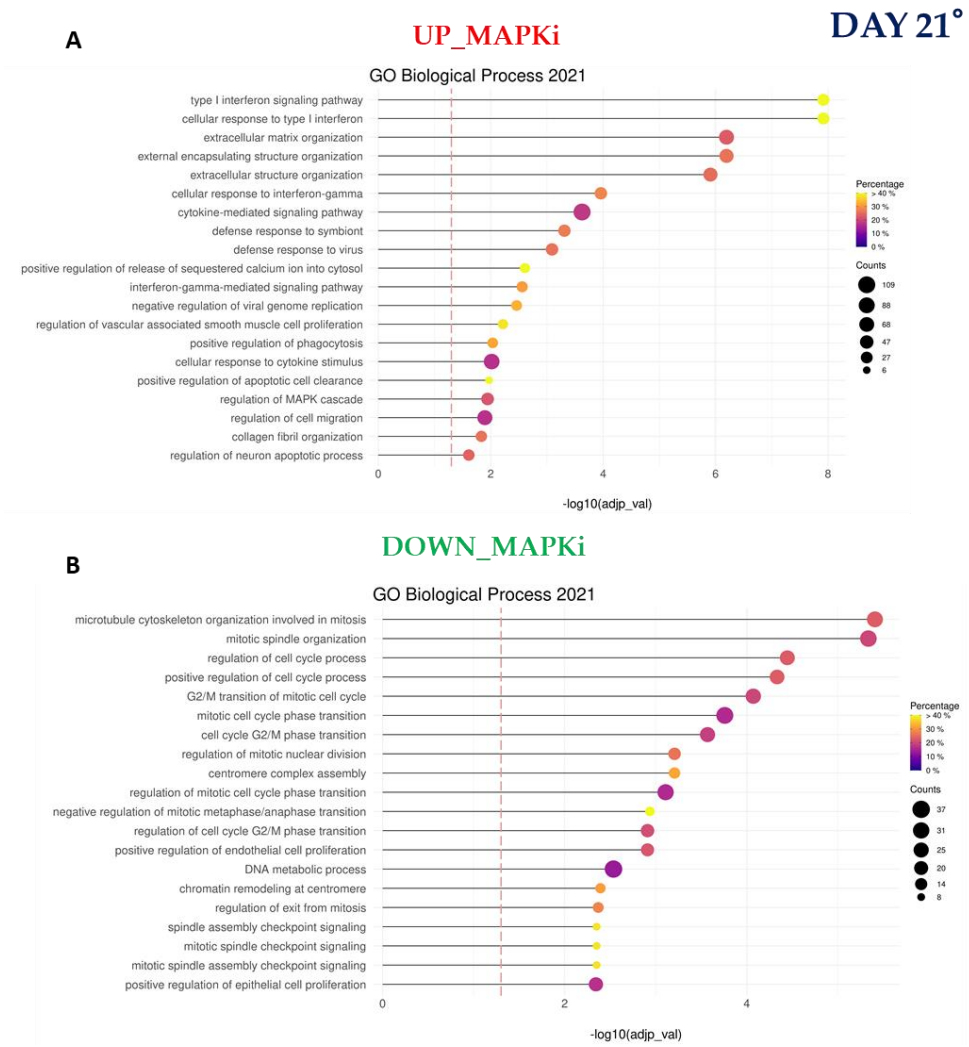

Figure 36. Gene Ontology (GO) analysis on deregulated genes in MAPKi treatment compared to untreated sample at day 21. Terms over red dashed line are considered statistically significant (adjusted p_val < 0.05). (A) Up-regulated enriched terms. (B) Down-regulated enriched terms.

Moving forward, Figure 37 shows GO enrichment analysis of treatments with MAPKi+Cumate vs UNT cells. Again the top 20 enriched up- or down-regulated terms were considered. In summary, at day 6, also in this case up-regulated enriched terms were related to interferon gamma signaling pathway, positive regulation of apoptotic process and pro-inflammatory response (figure 37 A). Interestingly, as compared to the sole MAPKi-treated cells the positive regulation of the MAPK cascade was not present in MAPKi+Cumate

treated cells. This suggests that the early activation of MAPK cascade as drug-adaptive escaping mechanism is counteracted by the constant induction of miR-579-3p expression.

Figure 37 B shows that also down-regulated enriched terms of MAPKi+Cumate treated cells were related to proliferation and cell migration BP as well as those observed in MAPKi sole treated cells (figure 35 B). Interestingly, a well-known drug-adaptive event, namely epithelial to mesenchymal transition, was exclusively down-regulated enriched term in treatments with MAPKi+Cumate as compared to MAPKi alone.

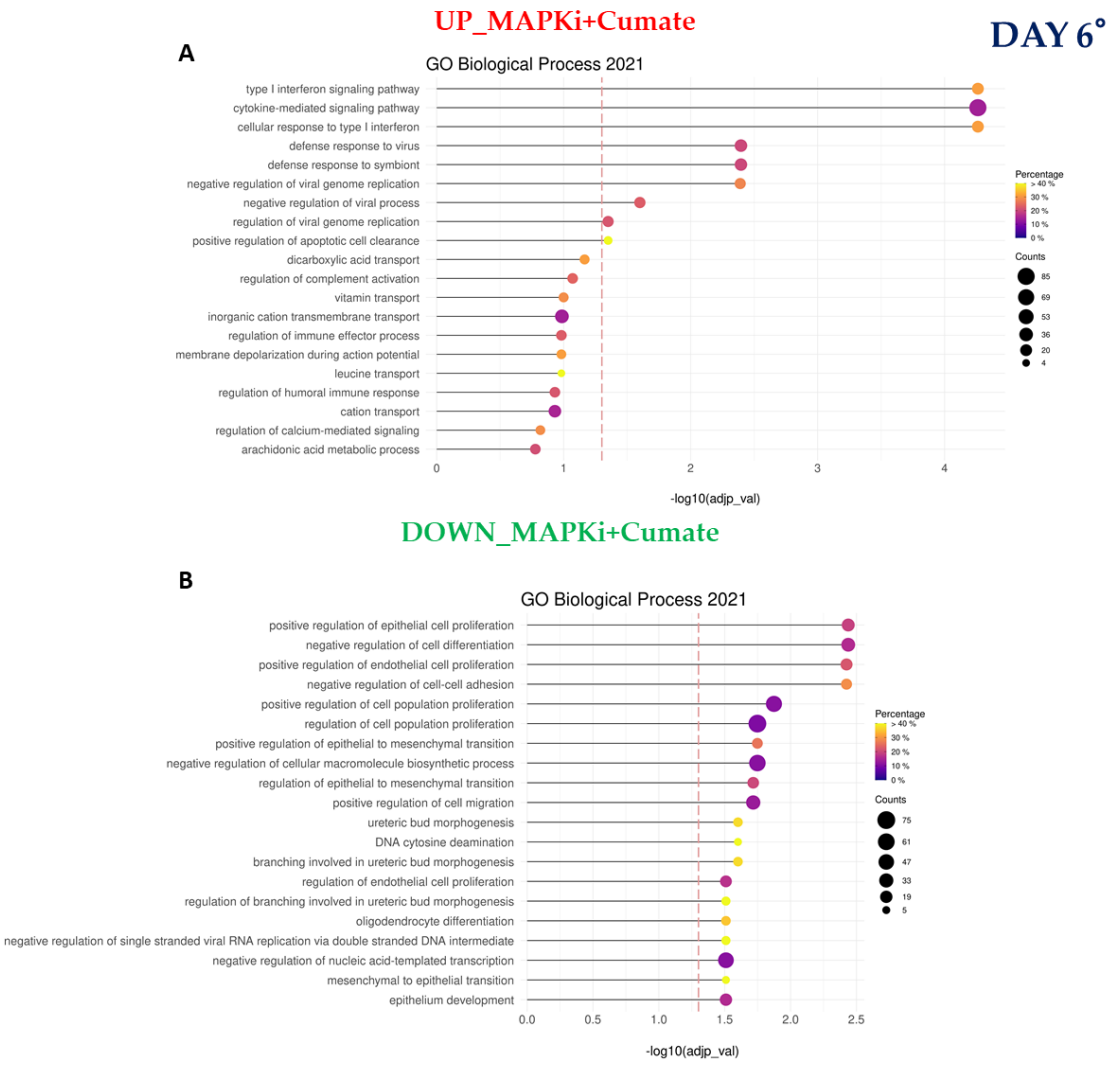

Figure 37. Gene Ontology (GO) analysis on deregulated genes in MAPKi+Cumate treatments compared to untreated sample at 6 day. Terms over red dashed line are considered statistically significant (adjusted p_val < 0.05). (A) Up-regulated enriched terms. (B) Down-regulated enriched terms.

At day 21, the most important finding was the lack of enrichment of MAPK cascade and cell migration terms (figure 38 A). These results suggest that the induction of miR-579-3p blunts the re-activation of MAPK signaling and the switch toward an invasive phenotype which are both well-known mechanisms associated with the development of drug tolerance in melanoma (24, 57-59). Among down-regulated enriched terms, most of them correspond to the transition of cell cycle progression (G2/M). As expected, terms related to G2/M transition are strongly down-regulated in MAPKi+Cumate condition as compared to MAPKi treatment. In fact in the treatment with MAPKi+Cumate, G2/M transition terms showed an enrichment of number genes involved with a better significative p-value (figure 38 B). In line with previous data, this aspect suggests that inducible miR-579-3p is able to keep melanoma cells blocked in cell cycle progression also 21 days upon MAPKi exposure. Furthermore, many down-regulated BPs correspond to pathways involved in mRNA processing (figure 38 B).

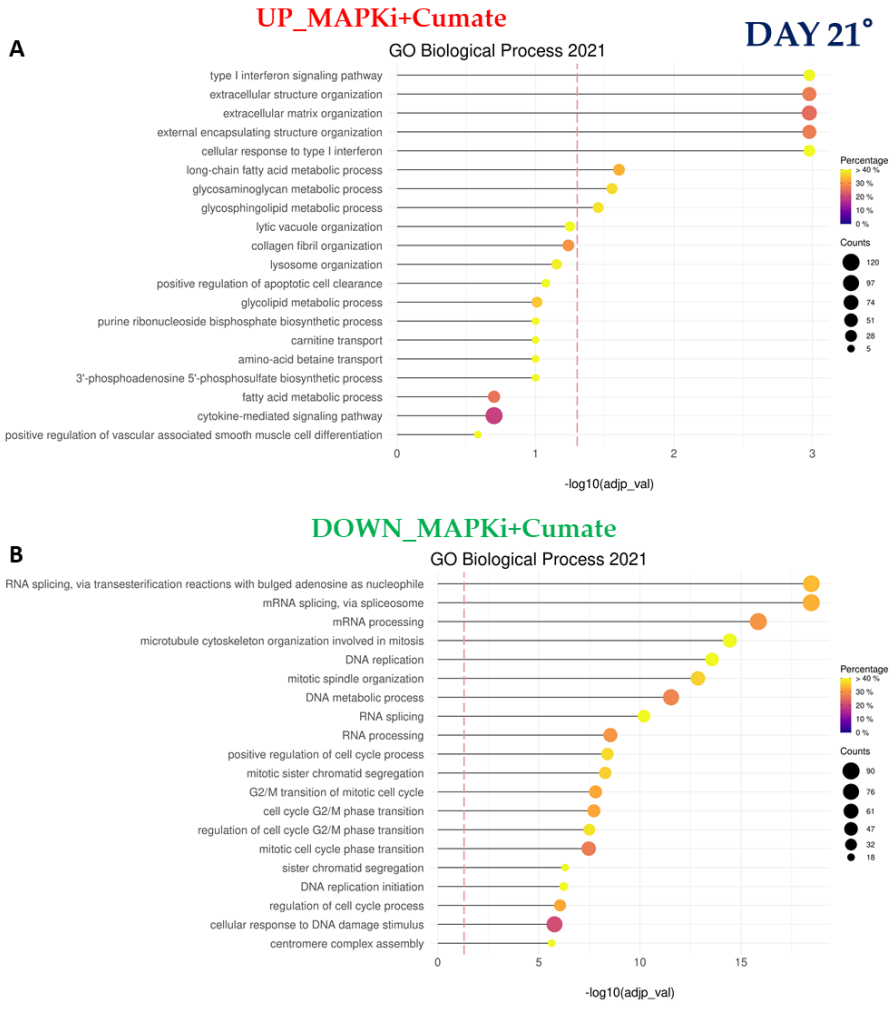

Figure 38. Gene Ontology (GO) analysis on deregulated genes in MAPKi+Cumate treatments compared to untreated sample at 21 day. Terms over red dashed line are considered statistically significant (adjusted p_val < 0.05). (A) Up-regulated enriched terms. (B) Down-regulated enriched terms.

GO analyses were validated using a different bioinformatic algorithm, namely Gene-Set Enrichment analysis (GSEA) again focusing on treatments with MAPKi and MAPKi+Cumate. To specifically identify the molecular pathways affected by miR-579-3p expression, given its known role as oncosuppressor miRNA, we focused on negative enriched pathways derived from GSEA both at day 6 and 21 of treatment. The lost of GSEA-derived terms from MAPKi vs MAPKi+CUMATE treatments were matched, in order to obtain negative enriched pathways peculiar of MAPKi+CUMATE. At day 6 day as shown in figure 39 A, Venn Diagrams revealed that 9 negative enriched pathways were typical of treatments with MAPK inhibitors alone; 9 were in common; 50 were peculiar of MAPKi+Cumate treated cells. The most 20 relevant negative enriched pathways are represented as Bubble plot in figure 39 B. In line with previous data, many down-regulated molecular pathways involve the control of cell cycle progression (M phase, S phase, G1/S transition). Furthermore, the top negative enriched term encompasses the regulation of E2F transcription factor on its molecular targets. This is a well-known oncogene, activator of cell cycle process and proliferation (91). Additional interesting negative enriched pathways were related to oncogenic WNT and MYC signaling, epithelial to mesenchymal transition and invasive Neural-Crest signature. This last signature includes genes such as genes LHX1, ZIC1, BMP4 or NOTCH4.

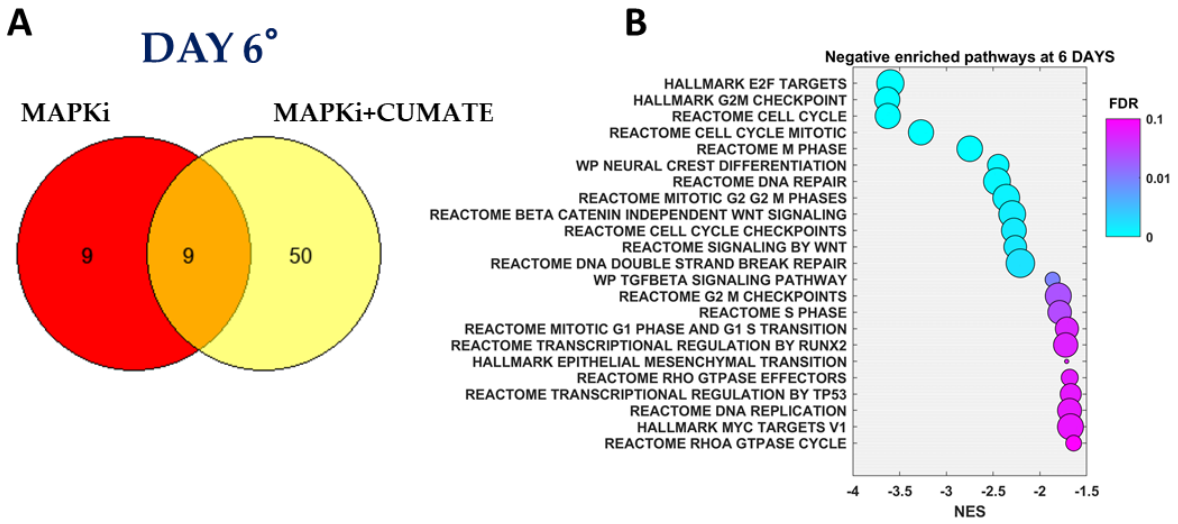

Figure 39. GSEA analysis identifies down-regulated pathways in treatments with MAPKi+Cumate at 6 day. (a) Venn Diagram divides negative enriched terms peculiar of MAPKi and MAPKi+CUMATE treatments. (b) Bubble-plots shows the 20 most relevant negative enriched pathways in MAPKi+CUMATE treatments. Statistically significant enrichments (0.1 <FDR<0) are shown as filled circles.

Using the same approach to identify peculiar negative enriched pathways related to MAPKi+Cumate treatments at 21 day, Venn Diagrams in figure 40 A reveal that 15 pathways were typical of treatments with MAPK inhibitors alone; 58 in common; 115 belong specifically to treatment with MAPKi+Cumate. Again, as observed already at day 6, we observed the negative enrichment of pro-oncogenic signaling such as MYC and TGF-β pathways. Furthermore, additional downregulated terms control cell cycle progression. This is in line with previous long-term experiments and cell-cycle analyses. Finally, negative enriched terms were related also to NOTCH signaling and Neural Crest signature (figure 40 B). Altogether, these findings confirm at the hypothesis that miR-579-3p acts as a potential inhibitor of melanoma cell adaptation to target therapy by acting on a set of key oncogenic pathways.

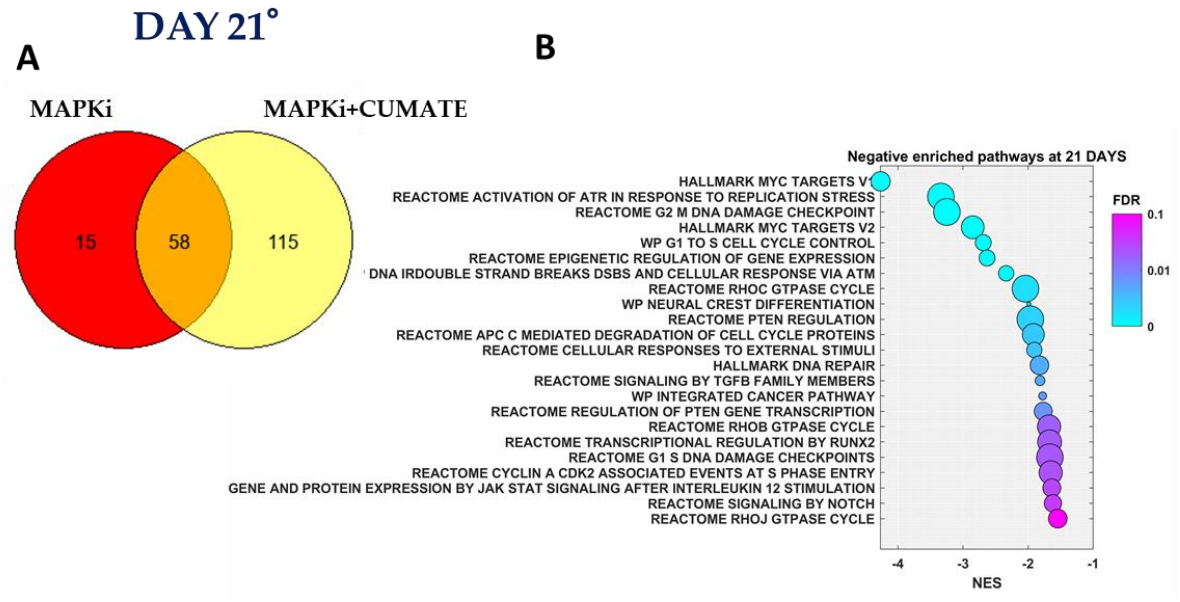

Figure 40. GSEA analysis identifies down-regulated pathways in the treatment of MAPKi+Cumate at day 21. (a) Venn Diagrams divides negative enriched terms peculiar of MAPKi and MAPKi+CUMATE treatments. (b) Bubble-plots shows the 20 most relevant negative enriched pathways in MAPKi+CUMATE treatments. Statistically significant enrichments (0.1 <FDR < 0) are shown as filled circles.

To explain the different number of enriched downregulated pathways in the treatment with MAPKi+Cumate at day 6 and to 21 , the levels of miR-579-3p expression were evaluated by RT-PCR in these experimental conditions. As shown in figure 41, RT-PCR revealed an increased expression of about 20 fold expression of miR-579-3p, at day 6 day (left panel) and 50 fold at day 21(right panel). Higher levels of miR-579-3p upon long exposure to MAPKi+Cumate could explain the higher number of enriched down-regulated pathways at day 21 (115 pathways) as compared to day 6 (50 pathways).

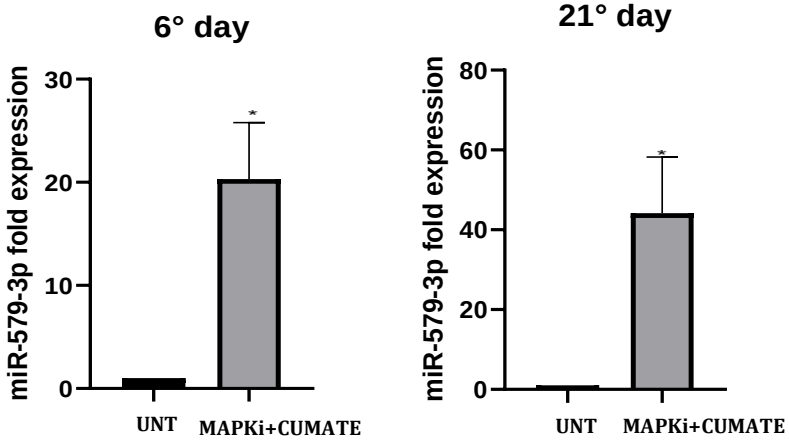

Figure 41. Higher levels of miR-579-3p could be associated to high number of enriched down-regulated pathways. Levels of miR-579-3p were evaluated at day 6 (left panel) and day 21 (right panel) of treatment.

4.5 Definition of a panel of antibodies suitable for the study of melanoma cells by single-cell mass cytometry

To assess the degree of cell heterogeneity in a isogenic cell population and how this is affected by exposure to drugs and/or miR-579-3p , we decided to carry out single-cell mass cytometry (CyTOF) experiments in collaboration with the group of Prof. Cesareni at the University of Tor Vergata (Rome).

Mass cytometry (see introduction, section 4) allows the simultaneous measurement of up to more than 40 cellular parameters (antigens) at single-cell level with over 100 available detection channels. As first step toward this goal we had the necessity to define a customized panel of antibodies capable to characterize the degree of tumor heterogeneity in a population of metastatic melanoma cells such as the A375 cell line. The workflow that was followed is schematically represented in figure 42 below.

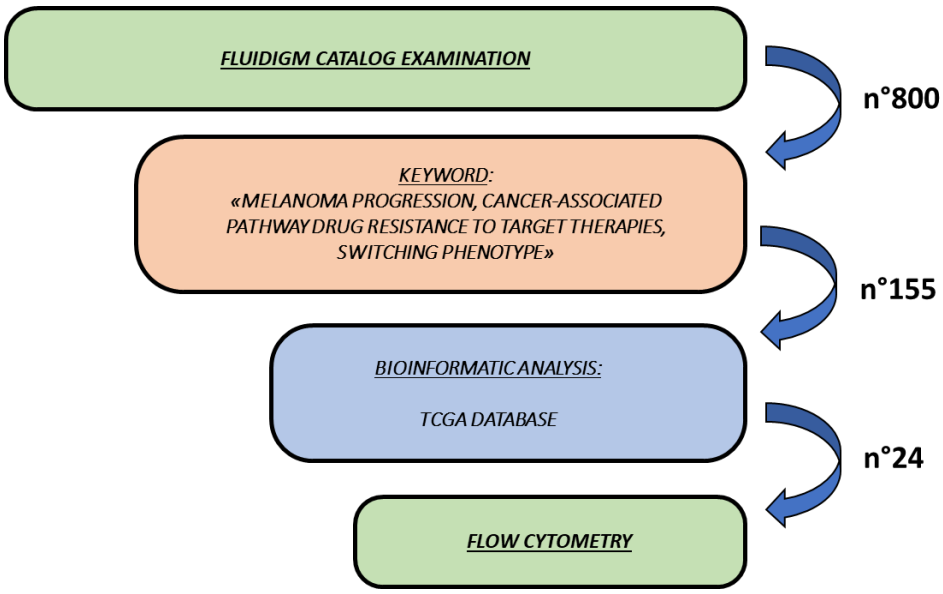

Figure 42. Schematic workflow used for the identification a list of markers for single-cell mass cytometry analyses.

As shown in figure 42, we have undertaken the following steps: 1) we started from the list of 800 human antigens included in the Fluidigm catalog. Fluidigm is the major distributor of antibodies for single-cell mass cytometry; 2) We conducted an extensive bibliographic search using as keywords "melanoma progression", "cancer-associated pathways",

"resistance to target therapy", and "phenotype switching" which allowed us to restrict the list to 155 antigens. 3) In order to prioritize for the most abundantly expressed antigens, we mined TGCA data from 472 cases of Skin Cutaneous Melanoma. 4) This allowed to shortlist 24 antigens whose expression in A375 cells was assessed experimentally by flow cytometry to effectively evaluate presence/absence in our experimental system (data not shown).

This process allowed to define a list of 20 final markers. In detail, the complete list is available in the Table 2 below, in which markers are split into two group, based on their cellular localization: surface (n°12) and intracellular (n°8) antigens.

SURFACE ANTIGENS	**INTRACELLULAR ANTIGENS**
CD63	**p-NFkB**
CD47	**MITF**
CD147 (BSG)	**p-STAT3**
CD90	**p-CREB**
CD271 (NGFR)	**pERK 1/2**
CD273 (PDL-2)	**p-AKT**
CD274 (PDL-1)	**Nestin**
CD56	**β -Catenin**
NOTCH2	
NG2 (HMW-MAA)	

AXL	
MART-1	

Table 2. List of markers for single-cell mass cytometry.

In order to experimentally validate the 20 antibody panel for single-cell mass cytometry (a more detailed description of used antibodies is reported in the in the materials and methods section) we conducted a comparative study on the parental A375 melanoma cell line and its BRAF inhibitor resistant counterpart (A375 R) already available in the laboratory of Prof. Mancini, which was selected by serial passaging of cells at increasing concentrations of dabrafenib over a period of more than two months (73).

We sought to characterize, at a single-cell level, phenotypic changes between parental A375 and A375 R, based on the expression of the panel of previously selected antigens.

Before labeling with antibodies, each sample was barcoded separately with specific Palladium Isotopes (see material and methods). This allowed to simultaneously analyze parental A375 and A375 R cell lines in a single-run experiment on a CyTOF2 mass cytometer. Single-cell data were analyzed by applying t-distributed stochastic neighbor embedding (t-SNE) algorithm in order to plot visual "viSNE" map (92). T-SNE algorithms clustered cells expressing similar levels of antigens used for single-cell mass cytometry experiment on map.

As shown in viSNE map reported in Figure 43, we identified two highly different cell patterns associated with parental A375 (blue cluster) vs A375 R cells (red cluster), respectively.

Our data, in line with previous findings obtained using different single cell approaches (mainly single cell RNA-Seq) by other groups (62,93), revealed that, compared to the resistant counterpart, the parental A375 cells showed a completely different spatial distribution on the viSNE map, thus suggesting a highly divergent phenotypic behavior.

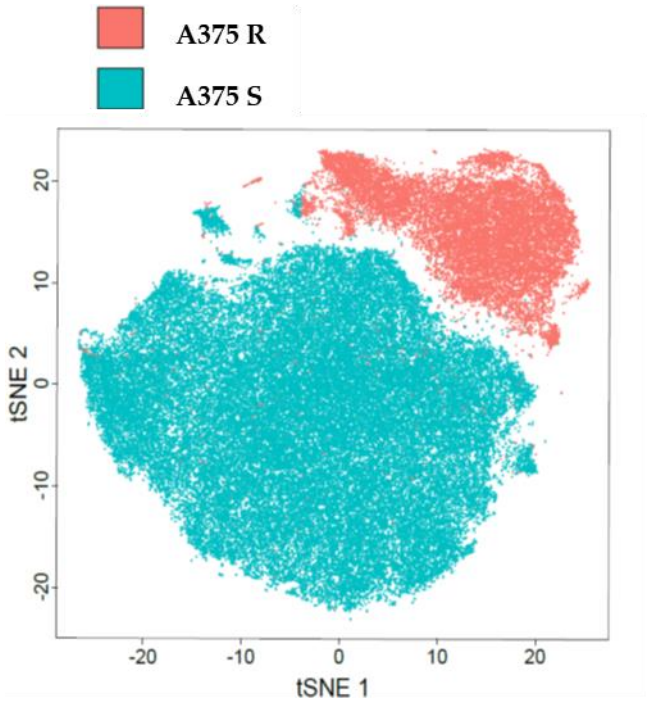

Figure 43. viSNE map shows different spatial distribution between parental A375 (blue cluster) and A375 R (red cluster) cell populations

In order to identify the specific markers that characterize these two different cell populations, we evaluated the expression levels of each given antigen (ranging from blue, low expression, to red, high expression) (figure 44). Our results confirmed the up-regulation of receptor-tyrosine kinase AXL, which is a well-known marker of drug resistance to target therapies, in A375 R compared to parental counterpart (94). Of note, CD47, PDL-1, PDL-2 markers were expressed at higher levels in A375 R cells suggesting the acquisition in cells resistant to target therapies of a phenotype resistant also to immunotherapy (95).

Interestingly, A375 R cells were also characterized by up-regulation of CD147, NOTCH2, NESTIN, CD90 and CD56 antigens suggesting more invasive and migrative phenotype compared to parental A375 (96-99). As expected, CD63 antigen, a negative regulator of epithelial to mesenchymal transition was down-regulated in A375 R compared to the parental counterparts (100). Regarding intracellular antigens, p-ERK 1/2 and p-STAT3 were up-regulated in in A375 R cells suggesting an hyperactivation of MAPK and STAT/JAK pathways in drug-resistance phenotype. β-catenin was highly expressed in parental A375

compared to resistant counterparts. No substantial differences were observed for p-AKT, p-NFkB , MITF and NGFR.

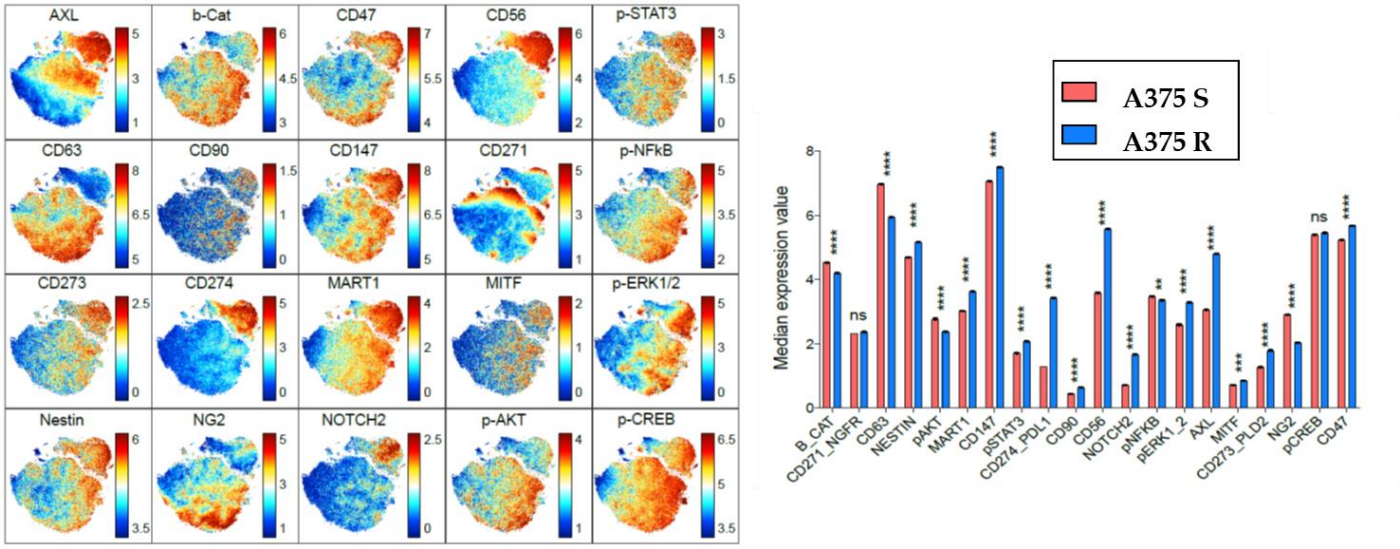

Figure 44. Expression levels of single markers between parental A375 and A375 R. (A) t-SNE map of each antigens. Each event in the figure represents a cell expressing at specific levels the antigens monitored in the experiment. The color scale (from blue to red) represents the level of expression of the selected antigen. (B) Median expression value of each antigens.

Taken together, these data confirmed that the panel of selected antibodies was a suitable tool for the characterization by mass cytometry of the melanoma cell population under examination and encouraged us to use the same panel to monitor shifts in the composition of this cell population in the early phases upon exposure to target therapy alone or in combination with miR-579-3p enforced expression.

4.6 miR-579-3p restrains the degree of tumor heterogeneity imposed by MAPKi treatments.

In the previous section I described the definition of a panel of antibodies suitable for the single-cell analysis of a melanoma cell line by mass cytometry. Interestingly this panel, when used to analyze the different cell composition between parental and drug resistant A375 cells, allowed to identify a complete phenotypic shift between the two different cell populations.

We next investigated the dynamics of cell heterogeneity upon treatments with Cumate, MAPKi and MAPKi+Cumate on A375-miR579IndEx. Our aim was to assess if and how prolonged expression of the onco-suppressive miR-579-3p is able to influence the degree of tumor heterogeneity imposed by MAPKi on this isogenic cell population.

The experimental design was similar to the RNA-Seq experiment described in a previous section (see figure 32). Cells were processed for single-cell mass cytometry analysis at day 6 and 21 of treatments.

As described in the previous section, cells were barcoded and labeled with the panel of 20 antibodies targeting both surface and intracellular antigens and analyzed by CyTOF2. Single-cell data were analyzed by applying t-distributed stochastic neighbor embedding (t-SNE) algorithm. The viSNE maps below was created considering the expression of all 20 antigens (figure 45). Results showed viSNE maps of non-treated cells (UNT) and treated with Cumate, MAPKi and MAPKi+Cumate, at day 6 and 21. Cells with similar pattern of antigens' expression are represented graphically next to each other in the viSNE maps.

At day 6, viSNE maps of MAPKi and MAPKi+Cumate treated cells revealed different spatial distribution of cell populations as compared to UNT (as a control), suggesting the acquisition of distinct molecular patterns upon short exposure to drug treatment (figure 45 A). Importantly, the two conditions MAPKi and MAPKi+Cumate gave rise to a similar spatial distribution of cells which suggests a similar pattern of expression of the antigens tested (figure 45 A). This is in agreement with the previous findings where no differences

were observed at biological levels (i.e. cell cycle and clonogenic assays) comparing treatments with MAPKi alone in combination with Cumate (figure 27, 30, 31). The most likely explanation of this finding is that at this time point corresponding to a short duration of treatment the pattern of gene expression is dominated by the effect of MAPKi which are responsible for initial blockade of cell cycle and of proliferation and survival pathways. Interestingly single cell analysis by mass cytometry revealed also a partial phenotypic shift in the population of cells treated only with Cumate which is suggestive of cell changes also in this cell population which were not revealed by less sensitive analysis such as cell cycle and clonogenic assays and also bulk RNA seq.

The most important changes were observed at day 21 of treatment. ViSNE maps at this time point clearly showed that treatment with MAPKi or MAPKi+Cumate gave rise to a dramatically different spatial distribution of the cell populations (figure 45 B). Specifically, t-SNE map relative to treatments of MAPKi alone, revealed still a high degree of cell heterogeneity characterized by two distinct clusters of cells (circled in red). In contrast, the combination of MAPKi+Cumate exhibited a unique cell population characterized by one main cluster of cells (figure 45 B). This could suggest that chronic exposure to Cumate, which in turn activated miR-579-3p, reduced the degree of heterogeneity imposed by MAPKi. Furthermore, as observed also at day 6, cells treated with the sole Cumate showed a different spatial distribution compared to UNT, suggesting that expression of miR-579-3p, although unable to overtly affect cell cycle as seen in the previous sections, is able to influence the overall patter of expression of the gene panel chosen for this analysis.

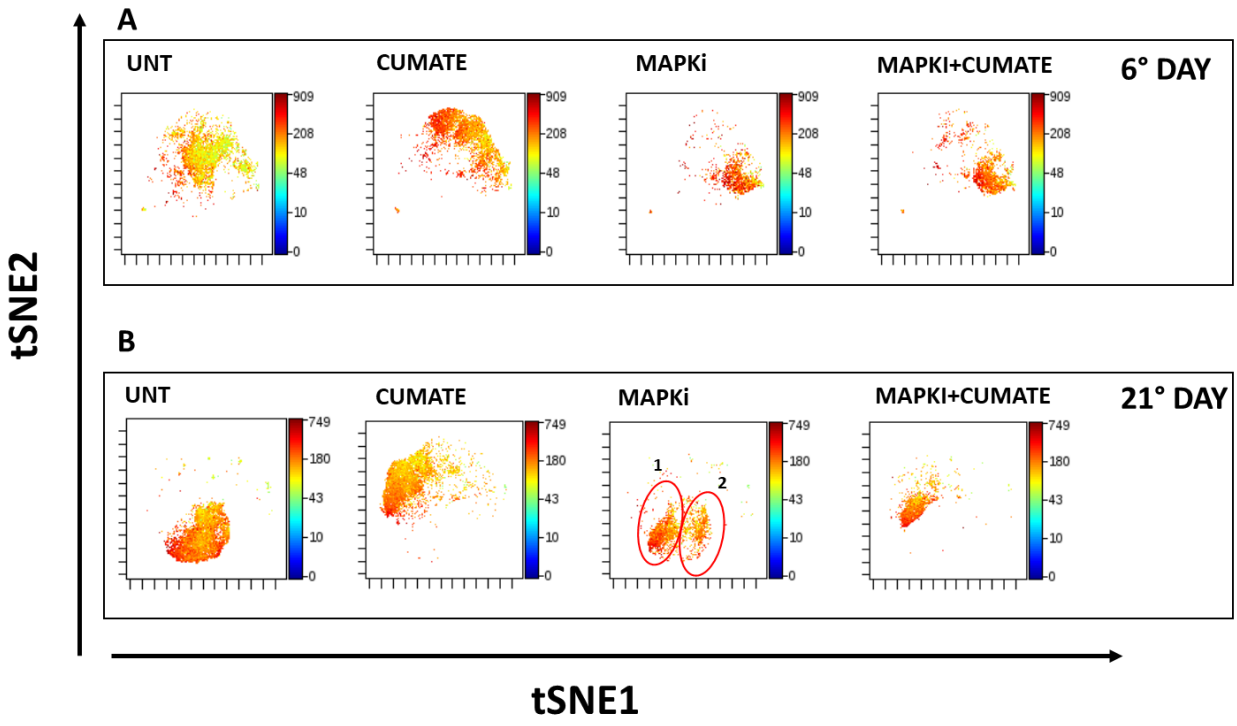

Figure 45. Spatial distribution of A375-miR579IndEx upon treatments with Cumate, MAPKi, MAPKi+Cumate. (A) Representative viSNE maps showing cell heterogeneity at day 6 of treatments (B) Representative viSNE maps showing cell heterogeneity at day 21 of treatment. Each event in the figure represents cell expressing specific levels of 20 antigens used in the experiment. Cells expressing similar levels of the antigens are close in the map.

In order to better interpret our findings we used the list of the 20 markers of the panel to build a protein-protein interaction map using String online database (101). This software allows us to complement available information of Protein-Protein Interaction (PPI) with computational predictions to generate a global network including direct (physical), as well as indirect (functional) interactions. Using a minimum required interaction score (>0.4, medium confidence) we plotted the interactome of the 20 genes, used for mass cytometry analysis, as connected by 70 hedges with a PPI enrichment $p < 1.0 \times 10^{-16}$. The displayed networks available are based on "evidence", as multiple lines where the color indicates the type of interaction. This led to identification of three major clusters (figure 46). On the basis of the genes present in the clusters they were named: 1) Kinase and cancer-related (blue cluster); 2) migration and de-differentiation (red cluster); 3) immune-suppressive and drug-resistance (green cluster). The first cluster includes nearly 50% of the genes (i.e. 9 out 20). Among them, there are ERK 1/2, STAT3, NFkB, AKT kinases as well as cancer-related genes

such as CD147 (BSG) and NOTCH2. Migration-invasive-associated cluster includes genes such as NGFR, CD90, NCAM, NG2. The third cluster encompasses three genes belonging to immune-suppressive microenvironment (i.e. CD273, CD274, CD47) and two genes associated with drug-sensitive and drug-resistance phenotype: MART-1 and AXL respectively.

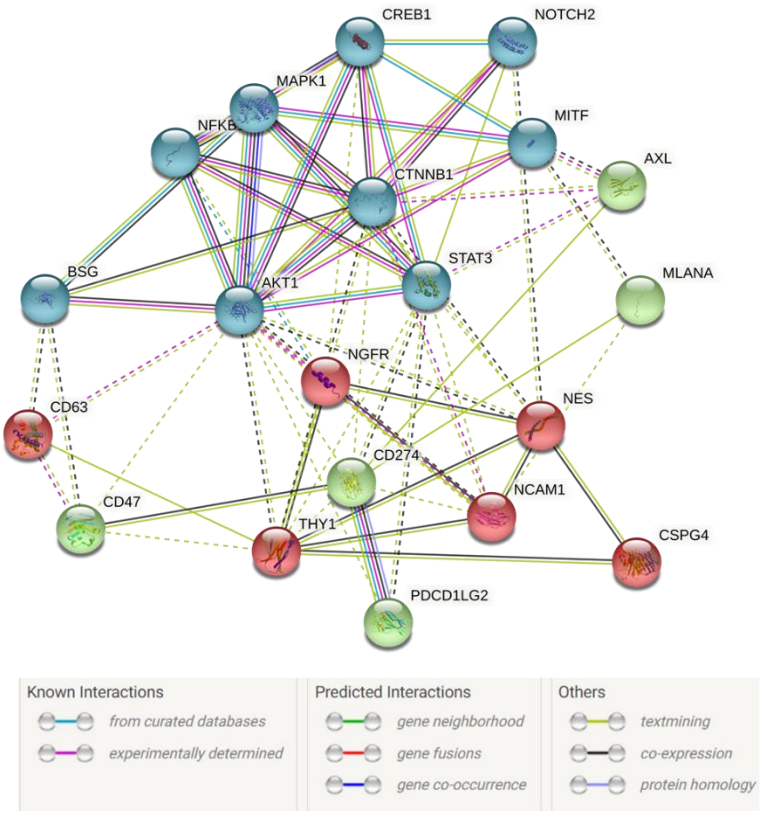

Figure 46. Evidence-based protein-protein interaction (PPI) networks performed using the list of 20 markers used for single-cell mass cytometry experiments. The legends indicate the meaning of the lines. Interaction score applied >0.4 (medium confidence). A total of 70 hedges were obtained with a PPI enrichment $p < 1.0 \times 10{-}16$. https://string-db.org.

Previously shown RNA-Seq data revealed that miR-579-3p is a potential inhibitor of melanoma cell adaptation to therapeutic pressure inhibiting cell migration and invasive phenotypes. For this reason we focused on the signature of genes belonging to migration and invasive cluster (i.e. NGFR, CD63, NESTIN, NCAM, CD90 and CD56) (i.e the red cluster).

To this purpose, we used FlowSOM clustering algorithm that facilitates the analysis of high-dimensional data. Clusters are arranged via a Self-Organizing Map (SOM) (102). The

resulting clustering of the SOM can be visualized in a minimal spanning tree (MST), in which cells are clustered into a hierarchical tree shape for two-dimensional visualization. Each cluster of a FlowSOM tree is graphically represented by a circular node in which the node size symbolizes the frequency of data points within that cluster (number of cells), and the node color shows the signal intensity of a selected marker (intensity of expression level) which could be varied from blue (low expression) to red (high expression) of marker.

At day 6 day, the FlowSOM clustering algorithm revealed that non-treated (UNT) and Cumate-exposed cells do not differ from each other and are characterized by a single albeit slightly extended cluster (figure 47). In contrast, early exposure to MAPKi showed a pattern of cell heterogeneity characterized by two main clusters (cluster n°1 and cluster n°2), (surrounded by red circles in the figure). In addition, also MAPKi treatment in combination with Cumate was characterized by the same specific clusters (red circles). Indeed, in both experimental conditions, MST showed equal: 1) subsets of population density (size of dots); 2) expression of selected markers (NGFR, CD63, NESTIN, NCAM, CD90 and CD56) within each subsets (figure 47). These results suggest that short term exposure to MAPKi alone or in combination with miR-579-3p gives rise to a similar pattern of cell heterogeneity regarding the invasion and migration signature.

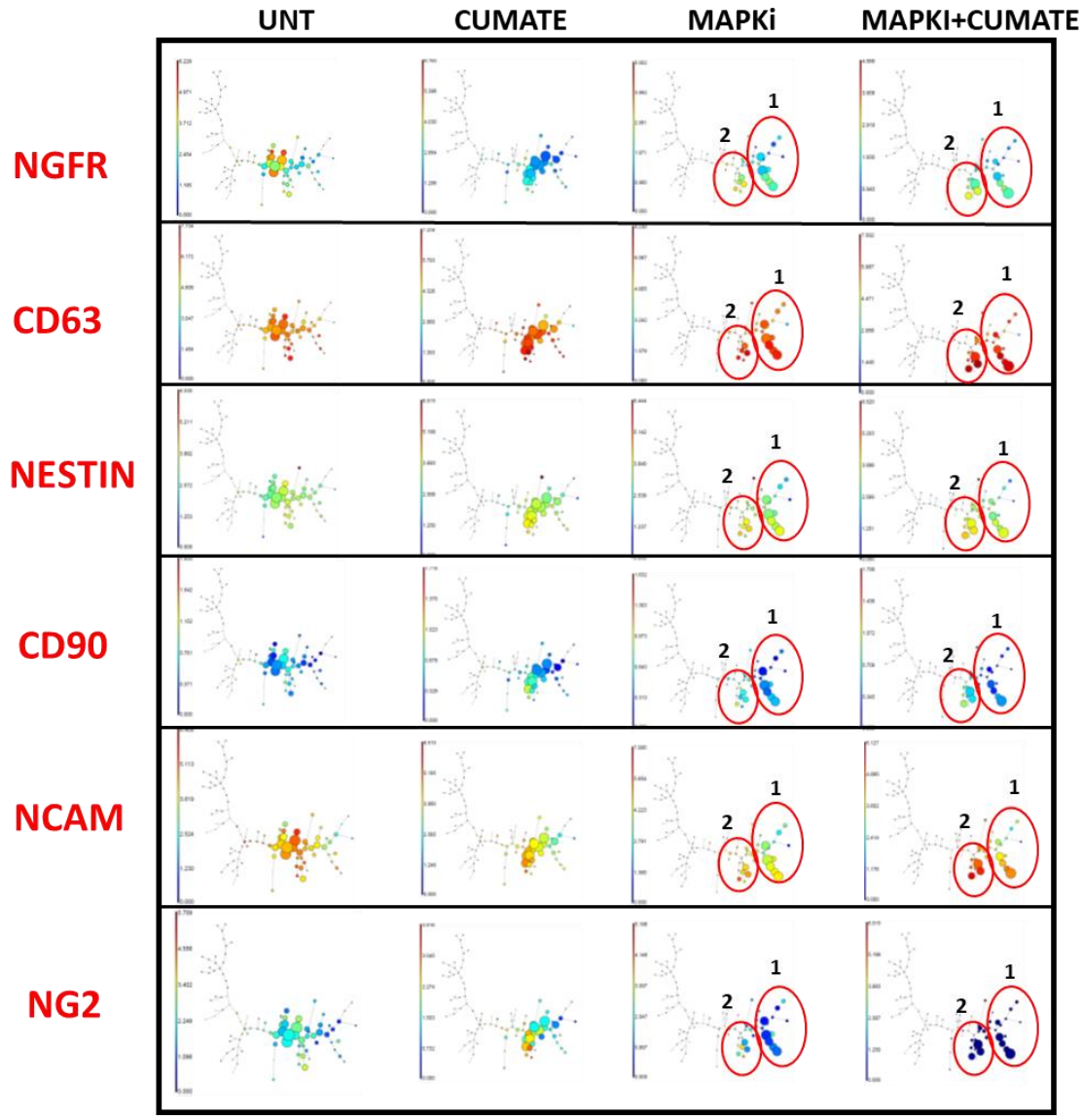

Figure 47. Minimum Spanning Tree (MST) visualizations of mass cytometry analysis of A375-miR579IndEx at day 6 of treatments with Cumate, MAPKi, MAPKi+Cumate. MST panels are colored according to the expression levels of NGFR, CD63, NESTIN, CD90, NCAM, NG2. Colors varies from blue (low expression) to red (high expression) of single antigens.

At day 21, MST, as well as viSNE map, revealed again a single albeit heterogeneous cluster in non-treated condition. Cumate-exposed cells were grouped in a distinct cell cluster confirming previous observations which suggest that prolongued expression of miR-579-3p induces a certain degree of phenotypic changes which are however, insufficient to affect cell proliferation (figure 48). Most importantly, MST visualization of extended treatments with MAPKi alone revealed the re-acquisition of a pattern similar to that of untreated cells, albeit characterized by a higher degree of heterogeneity (see red circles) in genes involved in invasion and migration signatures. Cluster n°1 was characterized by higher expression

levels of NGFR, CD63, NESTIN, NCAM, CD90, CD56 whereas cluster n°2 was characterized by lower levels of selected markers (figure 48). This behavior is strongly suggestive of cells undergoing drug adaptive phenotypic changes.

Finally the most important finding was observed with MST visualization of the day 21 treatment with MAPKi+Cumate. Here cell heterogeneity was strongly restricted to a small and new cell cluster characterized by a rather homogenous expression level of the individual markers (see blue circled area). It is interesting to note that the expression levels of NGFR, CD90, NESTIN and NG2 in this small cell population are lower compared to treatments with MAPKi alone.

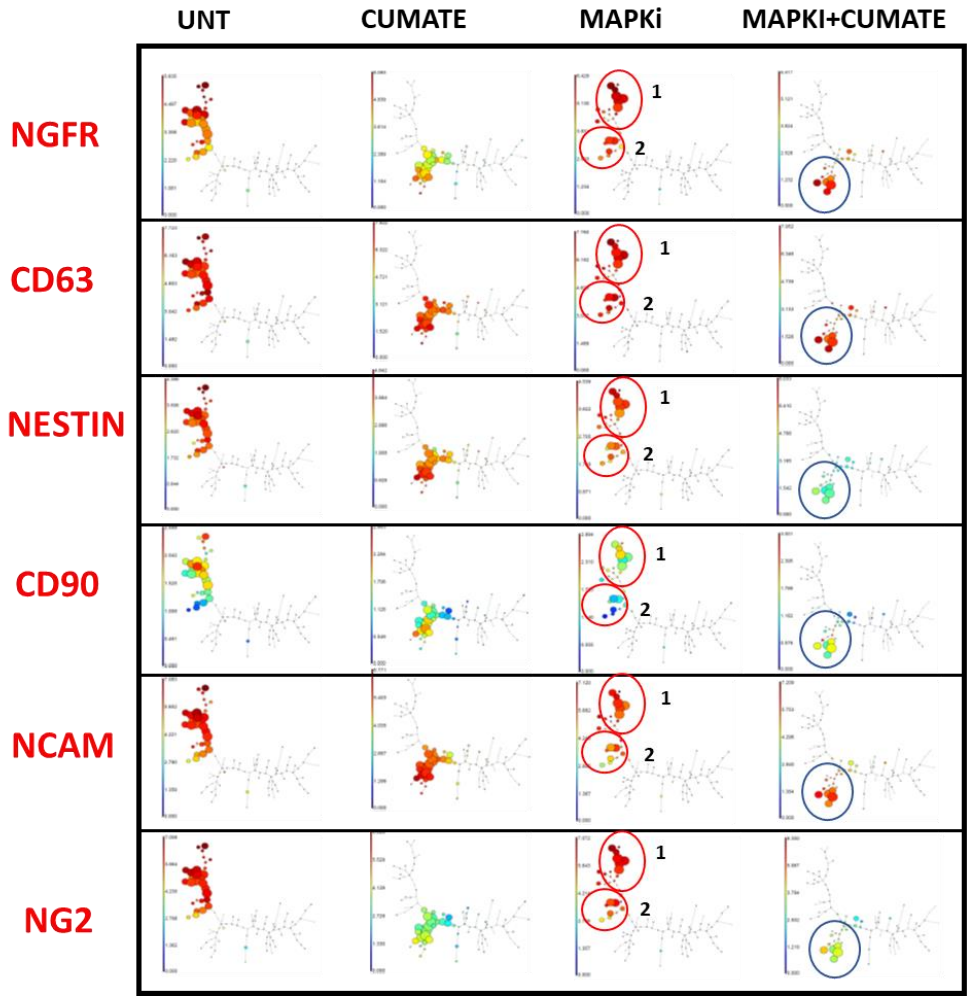

Figure 48. Minimum Spanning Tree (MST) visualizations of mass cytometry analysis of A375-miR579IndEx at day 21 of treatments with Cumate, MAPKi, MAPKi+Cumate. MST panels are colored according to the expression levels of NGFR, CD63, NESTIN, CD90, NCAM, NG2. Colors varies from blue (low expression) to red (high expression) of single antigens.

In summary, using two different bioinformatic approaches (t-SNE and FlowSOM algorithms), the results of this section show that: a) short term exposure to MAPKi and MAPKi+Cumate induces a different degree of cell heterogeneity compared to non-treated and Cumate-exposed cells; b) long term exposure to MAPKi is unable to reduce cell heterogeneity and activated cell migratory and invasive patterns and cells undergo phenotypic changes linked to drug adaptation; c) MAPKi in Cumate strongly restricts heterogeneity linked to the expression of migratory and invasive genes. These data suggest that chronic expression of miR-579-3p restrains the degree of heterogeneity and limits drug adaptive changes

5. DISCUSSION

Therapy of metastatic melanoma has improved dramatically over the last 6-7 years thanks to the development of targeted therapies and immunotherapy with inhibitors of immunological checkpoints. However, drug resistance continues to be a major limitation to the efficacy of these innovative therapies. In the case of target therapies with the combination of BRAF and MEK inhibitors (MAPKi), approximately 20% of patients harboring BRAF mutation do not respond to the first line therapy, whereas roughly 50% of patients undergo only partial responses with recurrent disease more aggressive and incurable. Generally, in melanoma, resistance to MAPKi arises from wide range of secondary mutations which activate bypass proliferation and survival pathways which ultimately lead to disease relapse. This scenario is, however, rendered more complex by the detection of cases where no genetic mutations are found to be responsible for resistance.

In the last few years, intense researches have highlighted the role of non-genetic mechanisms as early adaptive events, responsible for the survival of a small fraction of

tumor cells from which fully resistant tumor can emerge. Among them, our research group has provided robust evidence as to the involvement of a set of microRNAs in non-genetic resistance to target therapy. Among them, the newly discovered miR-579-3p.

miR-579-3p acts as onco-suppressor whose down-regulation is linked to the progression of metastatic melanoma, but also as a factor contributing to the development of drug resistance. My PhD work was addressed to determine the effects of miR-579-3p during the evolution of MAPKi resistance in melanoma. For this purpose, a BRAF-mutated melanoma cell line, namely A375, was engineered to bear an inducible GFP-tagged reporter construct to switch on/off miR-579-3p expression levels at our convenience. Making use of this tool I observed that: a) the inducible expression of miR-579-3p negatively impacts on MAPK-ERK signaling and this in turn reduces cell growth in synergy with MAPK inhibitors, in short-term treatments; b) combination of MAPKi together with miR-579-3p expression impairs the establishment of drug adaptation and cells are characterized by inducing a stable block of proliferation.

A drug-adaptative state has been previously associated to a "switching phenotype" model, which is linked to intratumor heterogeneity (58). Several studies have revealed that drug-adaptation is fueled by transcriptionally distinct cell populations that emerge over time (57-59). Selective pressure by MAPKi leads to an initial phase of populations showing increased melanocytic differentiation (MITF ^{high}), followed by continuous dedifferentiation and invasive phenotype with the appearance of cells with a slow-cycling neural-crest-like state that express NGFR (NGFR ^{high}) (65). The recent application of high-throughput single-cell techniques has revealed a higher degree of transcriptional heterogeneity providing new evidences about the activation of survival mechanisms able to counteract drug-treatment. For example, single cell RNA-Seq studies demonstrated that upon the exposure of MAPKi, different subpopulations tend to take different transcriptional trajectories to develop drug tolerance (83). We postulated that these transcriptional trajectories are influenced by microRNAs such as miR-579-3p. Hence, a substantial effort of my PhD work has been directed to investigate the main transcriptional pathways modulated by miR-579-3p

involved in the establishment of drug-adaptation, and whether inducible expression of miR-579-3p is able to affect the degree of intratumor heterogeneity linked to drug adaptation.

In collaboration with the Bioinformatic Unit of Regina Elena Cancer Institute (Rome), our transcriptomic analysis on bulk population revealed that drug-adaptation is characterized by the reactivation of MAPK signaling. This is consistent with extensive literature documenting a key role of MAPK pathway reactivation upon BRAF inhibition in melanoma (24). Furthermore, also the emergence of an invasive phenotype occurs upon the exposure to MAPKi with a concurrent reduction of highly proliferative cells. Interestingly, the induction of miR-579-3p blunts the re-activation of MAPK signaling and the switch of toward a migrative state. In addition, invasive the "Neural-Crest" signature appeared down-regulated upon long-term induction of miR-579-3p. These results were also corroborated by single-cell analysis. In collaboration with the Department of Biology, University of "Tor Vergata" (Rome), I exploited the resolution power of mass cytometry. Mass cytometry is a multi-parametric technology, which enables the study of heterogeneous populations with higher resolution than flow cytometry. To this end, we assembled a panel of 20 metal-tagged antibodies and characterized, at the single-cell level, the dynamics of cell heterogeneity upon treatments with MAPKi alone and in combination with the expression of miR-579-3p. Our results strongly suggest that miR-579-3p restrains, in a system represented by a isogenic cell population of metastatic melanoma cells, the degree of temporal heterogeneity triggered by the selective pressure imposed by MAPKi. In particular, miR-579-3p negatively impacts on the expression of genes associated with invasion and this is accompanied by a reduction of cell heterogeneity.

These results suggest a therapeutic possibility may encompass the use of miRNAs to hit pathways responsible for drug tolerance in order to improve the efficacy of target therapy for metastatic melanoma through a significant reduction of degree of cell heterogeneity.

It will be important in the future to investigate in detail the mechanisms responsible for the regulation of miR-579-3p expression and how these are affected during melanoma

progression and development of drug adaptation. A possible role could be played by the microphthalmia-associated transcription factor (MITF), a known master regulator of melanocyte development. Our research group has observed (unpublished data) that MITF transcription factor is a positive regulator of miR-579-3p since it has two functional binding sites within its promoter, which is shared with Zinc Finger Recombinase, ZFR. We observed a positive correlation between miR-579-3p and MITF expression levels whereas an inverse correlation was observed with MAPK activation levels. For example, BRAF-mutated melanoma cell lines with low MITF/miR-579-3p were characterized by high levels of p-ERK and *vice versa*. Of note, it is well-known that BRAF-V600 signaling exerts a post-translational regulation on MITF levels through its phosphorylation and proteasomal degradation. These evidences may led to hypothesize a feedback regulatory circuit linking MAPK signaling, MITF and miR-579-3p. It is possible to speculate, therefore, that during the establishment of a drug-adaptive state, re-activation of MAPK signaling exerts a negative regulation on MITF levels, which in turn down-regulates the expression of miR-579-3p. Further studies are required to confirm this model.

Finally, our research group, supervised by Prof. Mancini in collaboration with Prof. Ciliberto, have started to explore the therapeutic potential of two other onco-suppressive miRNAs, namely miR-204-5p and miR-199b-5p using a well-characterized delivery approach consisting in the formulation of microRNAs into lipid nanoparticles (LNPs) (84). LNPs loaded with miR-204-5p and miR-199b-5p are able to potentiate the combination of MAPK inhibitors, resulting in a reduction of tumor growth. Based on the results obtained by my PhD work, it is conceivable to formulate new LNPs, containing miR-204-5p, miR-199b-5p and miR-579-3p, in order to hit simultaneously multiple oncogenic signaling and to exert most powerful inhibition of melanoma cell growth.

6. BIBLIOGRAPHY

1. Liu Y, Sheikh MS. Melanoma: Molecular Pathogenesis and Therapeutic Management. Mol Cell Pharmacol. 2014;6(3):228. PMID: 25745537; PMCID: PMC4346328.

2. Ali Z, Yousaf N, Larkin J. Melanoma epidemiology, biology and prognosis. EJC Suppl. 2013 Sep;11(2):81-91. doi: 10.1016/j.ejcsup.2013.07.012. PMID: 26217116; PMCID: PMC4041476.

3. Adameyko I, Lallemend F, Aquino JB, Pereira JA, Topilko P, Müller T, Fritz N, Beljajeva A, Mochii M, Liste I, Usoskin D, Suter U, Birchmeier C, Ernfors P. Schwann cell precursors from nerve innervation are a cellular origin of melanocytes in skin. Cell. 2009 Oct 16;139(2):366-79. doi: 10.1016/j.cell.2009.07.049. PMID: 19837037.

4. Mort RL, Jackson IJ, Patton EE. The melanocyte lineage in development and disease. Development. 2015 Feb 15;142(4):620-32. doi: 10.1242/dev.106567. Erratum in: Development. 2015 Apr 1;142(7):1387. PMID: 25670789; PMCID: PMC4325379.

5. Sung H, Ferlay J, Siegel RL, Laversanne M, Soerjomataram I, Jemal A, Bray F. Global Cancer Statistics 2020: GLOBOCAN Estimates of Incidence and Mortality Worldwide for 36 Cancers in 185 Countries. CA Cancer J Clin. 2021 May;71(3):209-249. doi: 10.3322/caac.21660. Epub 2021 Feb 4. PMID: 33538338.

6. Memon A, Bannister P, Rogers I, Sundin J, Al-Ayadhy B, James PW, McNally RJQ. Changing epidemiology and age-specific incidence of cutaneous malignant melanoma in England: An analysis of the national cancer registration data by age, gender and anatomical site, 1981-2018. Lancet Reg Health Eur. 2021 Jan 6;2:100024. doi: 10.1016/j.lanepe.2021.100024. PMID: 34557790; PMCID: PMC8454583.

7. Bray F, Ferlay J, Soerjomataram I, Siegel RL, Torre LA, Jemal A. Global cancer statistics 2018: GLOBOCAN estimates of incidence and mortality worldwide for 36 cancers in 185 countries. CA Cancer J Clin. 2018 Nov;68(6):394-424. doi: 10.3322/caac.21492. Epub 2018 Sep 12. Erratum in: CA Cancer J Clin. 2020 Jul;70(4):313. PMID: 30207593.

8. https://ecis.jrc.ec.europa.eu/

9. Gandini S, Autier P, Boniol M. Reviews on sun exposure and artificial light and melanoma. Prog Biophys Mol Biol. 2011 Dec;107(3):362-6. doi: 10.1016/j.pbiomolbio.2011.09.011. Epub 2011 Sep 19. PMID: 21958910.

10. Boniol M, Autier P, Boyle P, Gandini S. Cutaneous melanoma attributable to sunbed use: systematic review and meta-analysis. BMJ. 2012 Jul 24;345:e4757. doi: 10.1136/bmj.e4757. PMID: 22833605; PMCID: PMC3404185.

11. Berwick M, Erdei E, Hay J. Melanoma epidemiology and public health. Dermatol Clin. 2009 Apr;27(2):205-14, viii. doi: 10.1016/j.det.2008.12.002. PMID: 19254665; PMCID: PMC3595561.

12. van der Leest RJ, Flohil SC, Arends LR, de Vries E, Nijsten T. Risk of subsequent cutaneous malignancy in patients with prior melanoma: a systematic review and meta-analysis. J Eur Acad Dermatol Venereol. 2015 Jun;29(6):1053-62. doi: 10.1111/jdv.12887. Epub 2014 Dec 10. PMID: 25491923.

13. Alexandrov LB, Nik-Zainal S, Wedge DC, Aparicio SA, Behjati S, Biankin AV, Bignell GR, Bolli N, Borg A, Børresen-Dale AL, Boyault S, Burkhardt B, Butler AP, Caldas C, Davies HR, Desmedt C, Eils R, Eyfjörd JE, Foekens JA, Greaves M, Hosoda F, Hutter B, Ilicic T, Imbeaud S, Imielinski M, Jäger N, Jones DT, Jones D, Knappskog S, Kool M, Lakhani SR, López-Otín C, Martin S, Munshi NC, Nakamura H, Northcott PA, Pajic M, Papaemmanuil E, Paradiso A, Pearson JV, Puente XS, Raine K, Ramakrishna M, Richardson AL, Richter J, Rosenstiel P, Schlesner M, Schumacher TN, Span PN, Teague JW, Totoki Y, Tutt AN, Valdés-Mas R, van Buuren MM, van 't Veer L, Vincent-Salomon A, Waddell N, Yates LR; Australian Pancreatic Cancer Genome Initiative; ICGC Breast Cancer Consortium; ICGC MMML-Seq Consortium; ICGC PedBrain, Zucman-Rossi J, Futreal PA, McDermott U, Lichter P, Meyerson M, Grimmond SM, Siebert R, Campo E, Shibata T, Pfister SM, Campbell PJ, Stratton MR. Signatures of mutational processes in human cancer. Nature. 2013 Aug 22;500(7463):415-21. doi: 10.1038/nature12477. Epub 2013 Aug 14. Erratum in: Nature. 2013

Oct 10;502(7470):258. Imielinsk, Marcin [corrected to Imielinski, Marcin]. PMID: 23945592; PMCID: PMC3776390.

14. Lawrence MS, Stojanov P, Polak P, Kryukov GV, Cibulskis K, Sivachenko A, Carter SL, Stewart C, Mermel CH, Roberts SA, Kiezun A, Hammerman PS, McKenna A, Drier Y, Zou L, Ramos AH, Pugh TJ, Stransky N, Helman E, Kim J, Sougnez C, Ambrogio L, Nickerson E, Shefler E, Cortés ML, Auclair D, Saksena G, Voet D, Noble M, DiCara D, Lin P, Lichtenstein L, Heiman DI, Fennell T, Imielinski M, Hernandez B, Hodis E, Baca S, Dulak AM, Lohr J, Landau DA, Wu CJ, Melendez-Zajgla J, Hidalgo-Miranda A, Koren A, McCarroll SA, Mora J, Crompton B, Onofrio R, Parkin M, Winckler W, Ardlie K, Gabriel SB, Roberts CWM, Biegel JA, Stegmaier K, Bass AJ, Garraway LA, Meyerson M, Golub TR, Gordenin DA, Sunyaev S, Lander ES, Getz G. Mutational heterogeneity in cancer and the search for new cancer-associated genes. Nature. 2013 Jul 11;499(7457):214-218. doi: 10.1038/nature12213. Epub 2013 Jun 16. PMID: 23770567; PMCID: PMC3919509.

15. Shain AH, Bastian BC. From melanocytes to melanomas. Nat Rev Cancer. 2016 Jun;16(6):345-58. doi: 10.1038/nrc.2016.37. Epub 2016 Apr 29. Erratum in: Nat Rev Cancer. 2020 Jun;20(6):355. PMID: 27125352.

16. Vogelstein B, Kinzler KW. The Path to Cancer --Three Strikes and You're Out. N Engl J Med. 2015 Nov 12;373(20):1895-8. doi: 10.1056/NEJMp1508811. PMID: 26559569.

17. Shain AH, Yeh I, Kovalyshyn I, Sriharan A, Talevich E, Gagnon A, Dummer R, North J, Pincus L, Ruben B, Rickaby W, D'Arrigo C, Robson A, Bastian BC. The Genetic Evolution of Melanoma from Precursor Lesions. N Engl J Med. 2015 Nov 12;373(20):1926-36. doi: 10.1056/NEJMoa1502583. PMID: 26559571.

18. Cancer Genome Atlas Network. Genomic Classification of Cutaneous Melanoma. Cell. 2015 Jun 18;161(7):1681-96. doi: 10.1016/j.cell.2015.05.044. PMID: 26091043; PMCID: PMC4580370.

19. Cohn-Cedermark G, Rutqvist LE, Andersson R, Breivald M, Ingvar C, Johansson H, Jönsson PE, Krysander L, Lindholm C, Ringborg U. Long term results of a randomized

study by the Swedish Melanoma Study Group on 2-cm versus 5-cm resection margins for patients with cutaneous melanoma with a tumor thickness of 0.8-2.0 mm. Cancer. 2000 Oct 1;89(7):1495-501. PMID: 11013363.

20. Thomas JM, Newton-Bishop J, A'Hern R, Coombes G, Timmons M, Evans J, Cook M, Theaker J, Fallowfield M, O'Neill T, Ruka W, Bliss JM; United Kingdom Melanoma Study Group; British Association of Plastic Surgeons; Scottish Cancer Therapy Network. Excision margins in high-risk malignant melanoma. N Engl J Med. 2004 Feb 19;350(8):757-66. doi: 10.1056/NEJMoa030681. PMID: 14973217.

21. Hayes AJ, Maynard L, Coombes G, Newton-Bishop J, Timmons M, Cook M, Theaker J, Bliss JM, Thomas JM; UK Melanoma Study Group; British Association of Plastic; Reconstructive and Aesthetic Surgeons, and the Scottish Cancer Therapy Network. Wide versus narrow excision margins for high-risk, primary cutaneous melanomas: long-term follow-up of survival in a randomised trial. Lancet Oncol. 2016 Feb;17(2):184-192. doi: 10.1016/S1470-2045(15)00482-9. Epub 2016 Jan 12. PMID: 26790922; PMCID: PMC4737890.

22. Tang T, Eldabaje R, Yang L. Current Status of Biological Therapies for the Treatment of Metastatic Melanoma. Anticancer Res. 2016 Jul;36(7):3229-41. PMID: 27354579.

23. Millet A, Martin AR, Ronco C, Rocchi S, Benhida R. Metastatic Melanoma: Insights Into the Evolution of the Treatments and Future Challenges. Med Res Rev. 2017 Jan;37(1):98-148. doi: 10.1002/med.21404. Epub 2016 Aug 29. PMID: 27569556.

24. Gerosa L, Chidley C, Fröhlich F, Sanchez G, Lim SK, Muhlich J, Chen JY, Vallabhaneni S, Baker GJ, Schapiro D, Atanasova MI, Chylek LA, Shi T, Yi L, Nicora CD, Claas A, Ng TSC, Kohler RH, Lauffenburger DA, Weissleder R, Miller MA, Qian WJ, Wiley HS, Sorger PK. Receptor-Driven ERK Pulses Reconfigure MAPK Signaling and Enable Persistence of Drug-Adapted BRAF-Mutant Melanoma Cells. Cell Syst. 2020 Nov 18;11(5):478-494.e9. doi: 10.1016/j.cels.2020.10.002. Epub 2020 Oct 27. PMID: 33113355; PMCID: PMC8009031.

25. Ascierto PA, Kirkwood JM, Grob JJ, Simeone E, Grimaldi AM, Maio M, Palmieri G, Testori A, Marincola FM, Mozzillo N. The role of BRAF V600 mutation in melanoma. J

Transl Med. 2012 Jul 9;10:85. doi: 10.1186/1479-5876-10-85. PMID: 22554099; PMCID: PMC3391993.

26. Cheng L, Lopez-Beltran A, Massari F, MacLennan GT, Montironi R. Molecular testing for BRAF mutations to inform melanoma treatment decisions: a move toward precision medicine. Mod Pathol. 2018 Jan;31(1):24-38. doi: 10.1038/modpathol.2017.104. Epub 2017 Nov 17. PMID: 29148538; PMCID: PMC5758899.

27. Yang H, Higgins B, Kolinsky K, Packman K, Go Z, Iyer R, Kolis S, Zhao S, Lee R, Grippo JF, Schostack K, Simcox ME, Heimbrook D, Bollag G, Su F. RG7204 (PLX4032), a selective BRAFV600E inhibitor, displays potent antitumor activity in preclinical melanoma models. Cancer Res. 2010 Jul 1;70(13):5518-27. doi: 10.1158/0008-5472.CAN-10-0646. Epub 2010 Jun 15. Erratum in: Cancer Res. 2010 Nov 15;70(22):9527. PMID: 20551065.

28. Sosman JA, Kim KB, Schuchter L, Gonzalez R, Pavlick AC, Weber JS, McArthur GA, Hutson TE, Moschos SJ, Flaherty KT, Hersey P, Kefford R, Lawrence D, Puzanov I, Lewis KD, Amaravadi RK, Chmielowski B, Lawrence HJ, Shyr Y, Ye F, Li J, Nolop KB, Lee RJ, Joe AK, Ribas A. Survival in BRAF V600-mutant advanced melanoma treated with vemurafenib. N Engl J Med. 2012 Feb 23;366(8):707-14. doi: 10.1056/NEJMoa1112302. PMID: 22356324; PMCID: PMC3724515.

29. Trinh VA, Davis JE, Anderson JE, Kim KB. Dabrafenib therapy for advanced melanoma. Ann Pharmacother. 2014 Apr;48(4):519-29. doi: 10.1177/1060028013513009. Epub 2013 Nov 20. PMID: 24259661.

30. Li Z, Jiang K, Zhu X, Lin G, Song F, Zhao Y, Piao Y, Liu J, Cheng W, Bi X, Gong P, Song Z, Meng S. Encorafenib (LGX818), a potent BRAF inhibitor, induces senescence accompanied by autophagy in BRAFV600E melanoma cells. Cancer Lett. 2016 Jan 28;370(2):332-44. doi: 10.1016/j.canlet.2015.11.015. Epub 2015 Nov 14. PMID: 26586345.

31. Rizos H, Menzies AM, Pupo GM, Carlino MS, Fung C, Hyman J, Haydu LE, Mijatov B, Becker TM, Boyd SC, Howle J, Saw R, Thompson JF, Kefford RF, Scolyer RA, Long GV. BRAF inhibitor resistance mechanisms in metastatic melanoma: spectrum and clinical

impact. Clin Cancer Res. 2014 Apr 1;20(7):1965-77. doi: 10.1158/1078-0432.CCR-13-3122. Epub 2014 Jan 24. PMID: 24463458.

32. Johnson DB, Menzies AM, Zimmer L, Eroglu Z, Ye F, Zhao S, Rizos H, Sucker A, Scolyer RA, Gutzmer R, Gogas H, Kefford RF, Thompson JF, Becker JC, Berking C, Egberts F, Loquai C, Goldinger SM, Pupo GM, Hugo W, Kong X, Garraway LA, Sosman JA, Ribas A, Lo RS, Long GV, Schadendorf D. Acquired BRAF inhibitor resistance: A multicenter meta-analysis of the spectrum and frequencies, clinical behaviour, and phenotypic associations of resistance mechanisms. Eur J Cancer. 2015 Dec;51(18):2792-9. doi: 10.1016/j.ejca.2015.08.022. Epub 2015 Nov 19. PMID: 26608120; PMCID: PMC4666799.

33. Manzano JL, Layos L, Bugés C, de Los Llanos Gil M, Vila L, Martínez-Balibrea E, Martínez-Cardús A. Resistant mechanisms to BRAF inhibitors in melanoma. Ann Transl Med. 2016 Jun;4(12):237. doi: 10.21037/atm.2016.06.07. PMID: 27429963; PMCID: PMC4930524.

34. Flaherty KT, Puzanov I, Kim KB, Ribas A, McArthur GA, Sosman JA, O'Dwyer PJ, Lee RJ, Grippo JF, Nolop K, Chapman PB. Inhibition of mutated, activated BRAF in metastatic melanoma. N Engl J Med. 2010 Aug 26;363(9):809-19. doi: 10.1056/NEJMoa1002011. PMID: 20818844; PMCID: PMC3724529.

35. Ascierto PA, McArthur GA, Dréno B, Atkinson V, Liszkay G, Di Giacomo AM, Mandalà M, Demidov L, Stroyakovskiy D, Thomas L, de la Cruz-Merino L, Dutriaux C, Garbe C, Yan Y, Wongchenko M, Chang I, Hsu JJ, Koralek DO, Rooney I, Ribas A, Larkin J. Cobimetinib combined with vemurafenib in advanced BRAF(V600)-mutant melanoma (coBRIM): updated efficacy results from a randomised, double-blind, phase 3 trial. Lancet Oncol. 2016 Sep;17(9):1248-60. doi: 10.1016/S1470-2045(16)30122-X. Epub 2016 Jul 30. PMID: 27480103.

36. Long GV, Flaherty KT, Stroyakovskiy D, Gogas H, Levchenko E, de Braud F, Larkin J, Garbe C, Jouary T, Hauschild A, Chiarion-Sileni V, Lebbe C, Mandalà M, Millward M, Arance A, Bondarenko I, Haanen JBAG, Hansson J, Utikal J, Ferraresi V, Mohr P, Probachai V, Schadendorf D, Nathan P, Robert C, Ribas A, Davies MA, Lane SR, Legos JJ, Mookerjee

B, Grob JJ. Dabrafenib plus trametinib versus dabrafenib monotherapy in patients with metastatic BRAF V600E/K-mutant melanoma: long-term survival and safety analysis of a phase 3 study. Ann Oncol. 2017 Jul 1;28(7):1631-1639. doi: 10.1093/annonc/mdx176. Erratum in: Ann Oncol. 2019 Nov 1;30(11):1848. PMID: 28475671; PMCID: PMC5834102.

37. Ascierto PA, Dummer R, Gogas HJ, Flaherty KT, Arance A, Mandala M, Liszkay G, Garbe C, Schadendorf D, Krajsova I, Gutzmer R, de Groot JWB, Loquai C, Gollerkeri A, Pickard MD, Robert C. Update on tolerability and overall survival in COLUMBUS: landmark analysis of a randomised phase 3 trial of encorafenib plus binimetinib vs vemurafenib or encorafenib in patients with BRAF V600-mutant melanoma. Eur J Cancer. 2020 Feb;126:33-44. doi: 10.1016/j.ejca.2019.11.016. Epub 2020 Jan 2. PMID: 31901705.

38. . Dummer R, Schadendorf D, Ascierto PA, Arance A, Dutriaux C, Di Giacomo AM, Rutkowski P, Del Vecchio M, Gutzmer R, Mandala M, Thomas L, Demidov L, Garbe C, Hogg D, Liszkay G, Queirolo P, Wasserman E, Ford J, Weill M, Sirulnik LA, Jehl V, Bozón V, Long GV, Flaherty K. Binimetinib versus dacarbazine in patients with advanced NRAS-mutant melanoma (NEMO): a multicentre, open-label, randomised, phase 3 trial. Lancet Oncol. 2017 Apr;18(4):435-445. doi: 10.1016/S1470-2045(17)30180-8. Epub 2017 Mar 9. PMID: 28284557.

39. Pardoll DM. The blockade of immune checkpoints in cancer immunotherapy. Nat Rev Cancer. 2012 Mar 22;12(4):252-64. doi: 10.1038/nrc3239. PMID: 22437870; PMCID: PMC4856023.

40. Tran E, Turcotte S, Gros A, Robbins PF, Lu YC, Dudley ME, Wunderlich JR, Somerville RP, Hogan K, Hinrichs CS, Parkhurst MR, Yang JC, Rosenberg SA. Cancer immunotherapy based on mutation-specific CD4+ T cells in a patient with epithelial cancer. Science. 2014 May 9;344(6184):641-5. doi: 10.1126/science.1251102. PMID: 24812403; PMCID: PMC6686185.

41. Lee JH, Shklovskaya E, Lim SY, Carlino MS, Menzies AM, Stewart A, Pedersen B, Irvine M, Alavi S, Yang JYH, Strbenac D, Saw RPM, Thompson JF, Wilmott JS, Scolyer RA, Long GV, Kefford RF, Rizos H. Transcriptional downregulation of MHC class I and melanoma de- differentiation in resistance to PD-1 inhibition. Nat Commun. 2020 Apr 20;11(1):1897. doi: 10.1038/s41467-020-15726-7. PMID: 32312968; PMCID: PMC7171183.

42. Mandalà M, Merelli B, Massi D. PD-L1 in melanoma: facts and myths. Melanoma Manag. 2016 Sep;3(3):187-194. doi: 10.2217/mmt-2016-0013. Epub 2016 Aug 22. PMID: 30190888; PMCID: PMC6096437.

43. Pistillo MP, Carosio R, Grillo F, Fontana V, Mastracci L, Morabito A, Banelli B, Tanda E, Cecchi F, Dozin B, Gualco M, Salvi S, Spagnolo F, Poggi A, Queirolo P. Phenotypic characterization of tumor CTLA-4 expression in melanoma tissues and its possible role in clinical response to Ipilimumab. Clin Immunol. 2020 Jun;215:108428. doi: 10.1016/j.clim.2020.108428. Epub 2020 Apr 25. PMID: 32344017.

44. Kythreotou A, Siddique A, Mauri FA, Bower M, Pinato DJ. PD-L1. J Clin Pathol. 2018 Mar;71(3):189-194. doi: 10.1136/jclinpath-2017-204853. Epub 2017 Nov 2. PMID: 29097600.

45. Hodi FS, O'Day SJ, McDermott DF, Weber RW, Sosman JA, Haanen JB, Gonzalez R, Robert C, Schadendorf D, Hassel JC, Akerley W, van den Eertwegh AJ, Lutzky J, Lorigan P, Vaubel JM, Linette GP, Hogg D, Ottensmeier CH, Lebbé C, Peschel C, Quirt I, Clark JI, Wolchok JD, Weber JS, Tian J, Yellin MJ, Nichol GM, Hoos A, Urba WJ. Improved survival with ipilimumab in patients with metastatic melanoma. N Engl J Med. 2010 Aug 19;363(8):711-23. doi: 10.1056/NEJMoa1003466. Epub 2010 Jun 5. Erratum in: N Engl J Med. 2010 Sep 23;363(13):1290. PMID: 20525992; PMCID: PMC3549297.

46. Regan MM, Mantia CM, Werner L, Tarhini AA, Larkin J, Stephen Hodi F, Wolchok J, Postow MA, Stwalley B, Moshyk A, Ritchings C, Re S, van Dijck W, McDermott DF, Atkins MB. Treatment-free survival over extended follow-up of patients with advanced melanoma treated with immune checkpoint inhibitors in CheckMate 067. J Immunother Cancer. 2021 Nov;9(11):e003743. doi: 10.1136/jitc-2021-003743. PMID: 34799400; PMCID: PMC8606772.

47. Subbiah V, Baik C, Kirkwood JM. Clinical Development of BRAF plus MEK Inhibitor Combinations. Trends Cancer. 2020 Sep;6(9):797-810. doi: 10.1016/j.trecan.2020.05.009. Epub 2020 Jun 13. PMID: 32540454.

48. Rizos H, Menzies AM, Pupo GM, Carlino MS, Fung C, Hyman J, Haydu LE, Mijatov B, Becker TM, Boyd SC, Howle J, Saw R, Thompson JF, Kefford RF, Scolyer RA, Long GV. BRAF inhibitor resistance mechanisms in metastatic melanoma: spectrum and clinical impact. Clin Cancer Res. 2014 Apr 1;20(7):1965-77. doi: 10.1158/1078-0432.CCR-13-3122. Epub 2014 Jan 24. PMID: 24463458.

49. Poulikakos PI, Persaud Y, Janakiraman M, Kong X, Ng C, Moriceau G, Shi H, Atefi M, Titz B, Gabay MT, Salton M, Dahlman KB, Tadi M, Wargo JA, Flaherty KT, Kelley MC, Misteli T, Chapman PB, Sosman JA, Graeber TG, Ribas A, Lo RS, Rosen N, Solit DB. RAF inhibitor resistance is mediated by dimerization of aberrantly spliced BRAF(V600E). Nature. 2011 Nov 23;480(7377):387-90. doi: 10.1038/nature10662. PMID: 22113612; PMCID: PMC3266695.

50. Shi H, Moriceau G, Kong X, Lee MK, Lee H, Koya RC, Ng C, Chodon T, Scolyer RA, Dahlman KB, Sosman JA, Kefford RF, Long GV, Nelson SF, Ribas A, Lo RS. Melanoma whole-exome sequencing identifies (V600E)B-RAF amplification-mediated acquired B-RAF inhibitor resistance. Nat Commun. 2012 Mar 6;3:724. doi: 10.1038/ncomms1727. PMID: 22395615; PMCID: PMC3530385.

51. Flaherty KT. BRAF inhibitors and melanoma. Cancer J. 2011 Nov-Dec;17(6):505-11. doi: 10.1097/PPO.0b013e31823e5357. PMID: 22157295.

52. Shi H, Hugo W, Kong X, Hong A, Koya RC, Moriceau G, Chodon T, Guo R, Johnson DB, Dahlman KB, Kelley MC, Kefford RF, Chmielowski B, Glaspy JA, Sosman JA, van Baren N, Long GV, Ribas A, Lo RS. Acquired resistance and clonal evolution in melanoma during BRAF inhibitor therapy. Cancer Discov. 2014 Jan;4(1):80-93. doi: 10.1158/2159-8290.CD-13-0642. Epub 2013 Nov 21. PMID: 24265155; PMCID: PMC3936420.

53. Kozar I, Margue C, Rothengatter S, Haan C, Kreis S. Many ways to resistance: How melanoma cells evade targeted therapies. Biochim Biophys Acta Rev Cancer. 2019 Apr;1871(2):313-322. doi: 10.1016/j.bbcan.2019.02.002. Epub 2019 Feb 15. PMID: 30776401.

54. Ruggiero CF, Malpicci D, Fattore L, Madonna G, Vanella V, Mallardo D, Liguoro D, Salvati V, Capone M, Bedogni B, Ascierto PA, Mancini R, Ciliberto G. ErbB3 Phosphorylation as Central Event in Adaptive Resistance to Targeted Therapy in Metastatic Melanoma: Early Detection in CTCs during Therapy and Insights into Regulation by Autocrine Neuregulin. Cancers (Basel). 2019 Sep 25;11(10):1425. doi: 10.3390/cancers11101425. PMID: 31557826; PMCID: PMC6826737.

55. De Conti G, Dias MH, Bernards R. Fighting Drug Resistance through the Targeting of Drug-Tolerant Persister Cells. Cancers (Basel). 2021 Mar 5;13(5):1118. doi: 10.3390/cancers13051118. PMID: 33807785; PMCID: PMC7961328.

56. Trotta AP, Gelles JD, Serasinghe MN, Loi P, Arbiser JL, Chipuk JE. Disruption of mitochondrial electron transport chain function potentiates the pro-apoptotic effects of MAPK inhibition. J Biol Chem. 2017 Jul 14;292(28):11727-11739. doi: 10.1074/jbc.M117.786442. Epub 2017 May 25. PMID: 28546431; PMCID: PMC5512068.

57. Roesch A, Fukunaga-Kalabis M, Schmidt EC, Zabierowski SE, Brafford PA, Vultur A, Basu D, Gimotty P, Vogt T, Herlyn M. A temporarily distinct subpopulation of slow-cycling melanoma cells is required for continuous tumor growth. Cell. 2010 May 14;141(4):583-94. doi: 10.1016/j.cell.2010.04.020. PMID: 20478252; PMCID: PMC2882693.

58. Arozarena I, Wellbrock C. Phenotype plasticity as enabler of melanoma progression and therapy resistance. Nat Rev Cancer. 2019 Jul;19(7):377-391. doi: 10.1038/s41568-019-0154-4. Epub 2019 Jun 17. PMID: 31209265.

59. Rambow F, Marine JC, Goding CR. Melanoma plasticity and phenotypic diversity: therapeutic barriers and opportunities. Genes Dev. 2019 Oct 1;33(19-20):1295-1318. doi: 10.1101/gad.329771.119. PMID: 31575676; PMCID: PMC6771388.

60. Hoek KS, Schlegel NC, Brafford P, Sucker A, Ugurel S, Kumar R, Weber BL, Nathanson KL, Phillips DJ, Herlyn M, Schadendorf D, Dummer R. Metastatic potential of melanomas defined by specific gene expression profiles with no BRAF signature. Pigment Cell Res. 2006 Aug;19(4):290-302. doi: 10.1111/j.1600-0749.2006.00322.x. PMID: 16827748.

61. Widmer DS, Cheng PF, Eichhoff OM, Belloni BC, Zipser MC, Schlegel NC, Javelaud D, Mauviel A, Dummer R, Hoek KS. Systematic classification of melanoma cells by phenotype-specific gene expression mapping. Pigment Cell Melanoma Res. 2012 May;25(3):343-53. doi: 10.1111/j.1755-148X.2012.00986.x. Epub 2012 Mar 2. PMID: 22336146.

62. Tirosh I, Izar B, Prakadan SM, Wadsworth MH 2nd, Treacy D, Trombetta JJ, Rotem A, Rodman C, Lian C, Murphy G, Fallahi-Sichani M, Dutton-Regester K, Lin JR, Cohen O, Shah P, Lu D, Genshaft AS, Hughes TK, Ziegler CG, Kazer SW, Gaillard A, Kolb KE, Villani AC, Johannessen CM, Andreev AY, Van Allen EM, Bertagnolli M, Sorger PK, Sullivan RJ, Flaherty KT, Frederick DT, Jané-Valbuena J, Yoon CH, Rozenblatt-Rosen O, Shalek AK, Regev A, Garraway LA. Dissecting the multicellular ecosystem of metastatic melanoma by single-cell RNA-seq. Science. 2016 Apr 8;352(6282):189-96. doi: 10.1126/science.aad0501. PMID: 27124452; PMCID: PMC4944528.

63. Smalley I, Kim E, Li J, Spence P, Wyatt CJ, Eroglu Z, Sondak VK, Messina JL, Babacan NA, Maria-Engler SS, De Armas L, Williams SL, Gatenby RA, Chen YA, Anderson ARA, Smalley KSM. Leveraging transcriptional dynamics to improve BRAF inhibitor responses in melanoma. EBioMedicine. 2019 Oct;48:178-190. doi: 10.1016/j.ebiom.2019.09.023. Epub 2019 Oct 5. PMID: 31594749; PMCID: PMC6838387.

64. Boiko AD, Razorenova OV, van de Rijn M, Swetter SM, Johnson DL, Ly DP, Butler PD, Yang GP, Joshua B, Kaplan MJ, Longaker MT, Weissman IL. Human melanoma-initiating cells express neural crest nerve growth factor receptor CD271. Nature. 2010 Jul 1;466(7302):133-7. doi: 10.1038/nature09161. Erratum in: Nature. 2011 Feb 17;470(7334):424. PMID: 20596026; PMCID: PMC2898751.

65. Restivo G, Diener J, Cheng PF, Kiowski G, Bonalli M, Biedermann T, Reichmann E, Levesque MP, Dummer R, Sommer L. low neurotrophin receptor CD271 regulates phenotype switching in melanoma. Nat Commun. 2017 Dec 7;8(1):1988. doi: 10.1038/s41467-017-01573-6. Erratum in: Nat Commun. 2018 Jan 22;9(1):314. PMID: 29215016; PMCID: PMC5719420.

66. Sun V, Zhou WB, Majid S, Kashani-Sabet M, Dar AA. MicroRNA-mediated regulation of melanoma. Br J Dermatol. 2014 Aug;171(2):234-41. doi: 10.1111/bjd.12989. Epub 2014 Jul 26. PMID: 24665835.

67. Griffiths-Jones S, Grocock RJ, van Dongen S, Bateman A, Enright AJ. miRBase: microRNA sequences, targets and gene nomenclature. Nucleic Acids Res. 2006 Jan 1;34(Database issue):D140-4. doi: 10.1093/nar/gkj112. PMID: 16381832; PMCID: PMC1347474.

68. Ha M, Kim VN. Regulation of microRNA biogenesis. Nat Rev Mol Cell Biol. 2014 Aug;15(8):509-24. doi: 10.1038/nrm3838. Epub 2014 Jul 16. PMID: 25027649.

69. Cai X, et al. 2004. Human microRNAs are processed from capped, polyadenylated transcripts that can also function as mRNAs, in RNA, vol. 10, nº 12, Dicembre, pp. 1957–66, DOI:10.1261/rna.7135204, PMC 1370684, PMID 15525708

70. Acunzo M, Romano G, Wernicke D, Croce CM. MicroRNA and cancer--a brief overview. Adv Biol Regul. 2015 Jan;57:1-9. doi: 10.1016/j.jbior.2014.09.013. Epub 2014 Sep 28. Erratum in: Adv Biol Regul. 2015 May;58:53. PMID: 25294678.

71. Fattore L, Costantini S, Malpicci D, Ruggiero CF, Ascierto PA, Croce CM, Mancini R, Ciliberto G. MicroRNAs in melanoma development and resistance to target therapy. Oncotarget. 2017 Mar 28;8(13):22262-22278. doi: 10.18632/oncotarget.14763. PMID: 28118616; PMCID: PMC5400662.

72. Fattore L, Mancini R, Acunzo M, Romano G, Laganà A, Pisanu ME, Malpicci D, Madonna G, Mallardo D, Capone M, Fulciniti F, Mazzucchelli L, Botti G, Croce CM, Ascierto PA, Ciliberto G. miR-579-3p controls melanoma progression and resistance to target therapy. Proc Natl Acad Sci U S A. 2016 Aug 23;113(34):E5005-13. doi: 10.1073/pnas.1607753113. Epub 2016 Aug 8. PMID: 27503895; PMCID: PMC5003278.

73. Fattore L, Ruggiero CF, Pisanu ME, Liguoro D, Cerri A, Costantini S, Capone F, Acunzo M, Romano G, Nigita G, Mallardo D, Ragone C, Carriero MV, Budillon A, Botti G, Ascierto PA, Mancini R, Ciliberto G. Reprogramming miRNAs global expression orchestrates development of drug resistance in BRAF mutated melanoma. Cell Death Differ. 2019 Jul;26(7):1267-1282. doi: 10.1038/s41418-018-0205-5. Epub 2018 Sep 25. PMID: 30254376; PMCID: PMC6748102.

74. Sanna A, Harbst K, Johansson I, Christensen G, Lauss M, Mitra S, Rosengren F, Häkkinen J, Vallon-Christersson J, Olsson H, Ingvar Å, Isaksson K, Ingvar C, Nielsen K, Jönsson G. Tumor genetic heterogeneity analysis of chronic sun-damaged melanoma. Pigment Cell Melanoma Res. 2020 May;33(3):480-489. doi: 10.1111/pcmr.12851. Epub 2019 Dec 23. Erratum in: Pigment Cell Melanoma Res. 2021 Jan;34(1):144. PMID: 31811783; PMCID: PMC7217060.

75. Rabbie R, Ansari-Pour N, Cast O, Lau D, Scott F, Welsh SJ, Parkinson C, Khoja L, Moore L, Tullett M, Wong K, Ferreira I, Gómez JMM, Levesque M, Gallagher FA, Jiménez-Sánchez A, Riva L, Miller ML, Allinson K, Campbell PJ, Corrie P, Wedge DC, Adams DJ. Multi-site clonality analysis uncovers pervasive heterogeneity across melanoma metastases. Nat Commun. 2020 Aug 27;11(1):4306. doi: 10.1038/s41467-020-18060-0. PMID: 32855398; PMCID: PMC7453196.

76. Diener J, Baggiolini A, Pernebrink M, Dalcher D, Lerra L, Cheng PF, Varum S, Häusel J, Stierli S, Treier M, Studer L, Basler K, Levesque MP, Dummer R, Santoro R, Cantù C, Sommer L. Epigenetic control of melanoma cell invasiveness by the stem cell factor SALL4. Nat Commun. 2021 Aug 20;12(1):5056. doi: 10.1038/s41467-021-25326-8. PMID: 34417458; PMCID: PMC8379183.

77. Guo M, Peng Y, Gao A, Du C, Herman JG. Epigenetic heterogeneity in cancer. Biomark Res. 2019 Oct 31;7:23. doi: 10.1186/s40364-019-0174-y. PMID: 31695915; PMCID: PMC6824025.

78. Ahmed F, Haass NK. Microenvironment-Driven Dynamic Heterogeneity and Phenotypic Plasticity as a Mechanism of Melanoma Therapy Resistance. Front Oncol. 2018 May 24;8:173. doi: 10.3389/fonc.2018.00173. PMID: 29881716; PMCID: PMC5976798.

79. Grzywa TM, Paskal W, Włodarski PK. Intratumor and Intertumor Heterogeneity in Melanoma. Transl Oncol. 2017 Dec;10(6):956-975. doi: 10.1016/j.tranon.2017.09.007. Epub 2017 Oct 24. PMID: 29078205; PMCID: PMC5671412.

80. Dagogo-Jack I, Shaw AT. Tumour heterogeneity and resistance to cancer therapies. Nat Rev Clin Oncol. 2018 Feb;15(2):81-94. doi: 10.1038/nrclinonc.2017.166. Epub 2017 Nov 8. PMID: 29115304.

81. Fattore L, Ruggiero CF, Liguoro D, Mancini R, Ciliberto G. Single cell analysis to dissect molecular heterogeneity and disease evolution in metastatic melanoma. Cell Death Dis. 2019 Oct 31;10(11):827. doi: 10.1038/s41419-019-2048-5. PMID: 31672982; PMCID: PMC6823362.

82. Schoof EM, Furtwängler B, Üresin N, Rapin N, Savickas S, Gentil C, Lechman E, Keller UAD, Dick JE, Porse BT. Quantitative single-cell proteomics as a tool to characterize cellular hierarchies. Nat Commun. 2021 Jun 7;12(1):3341. doi: 10.1038/s41467-021-23667-y. PMID: 34099695; PMCID: PMC8185083.

83. Su Y, Ko ME, Cheng H, Zhu R, Xue M, Wang J, Lee JW, Frankiw L, Xu A, Wong S, Robert L, Takata K, Yuan D, Lu Y, Huang S, Ribas A, Levine R, Nolan GP, Wei W, Plevritis SK, Li G, Baltimore D, Heath JR. Multi-omic single-cell snapshots reveal multiple independent trajectories to drug tolerance in a melanoma cell line. Nat Commun. 2020 May 11;11(1):2345. doi: 10.1038/s41467-020-15956-9. PMID: 32393797; PMCID: PMC7214418.

84. Fattore L, Campani V, Ruggiero CF, Salvati V, Liguoro D, Scotti L, Botti G, Ascierto PA, Mancini R, De Rosa G, Ciliberto G. In Vitro Biophysical and Biological Characterization of Lipid Nanoparticles Co-Encapsulating Oncosuppressors miR-199b-5p and miR-204-5p as Potentiators of Target Therapy in Metastatic Melanoma. Int J Mol Sci. 2020 Mar 12;21(6):1930. doi: 10.3390/ijms21061930. PMID: 32178301; PMCID: PMC7139872.

85. Mullick A, Xu Y, Warren R, Koutroumanis M, Guilbault C, Broussau S, Malenfant F, Bourget L, Lamoureux L, Lo R, Caron AW, Pilotte A, Massie B. The cumate gene-switch: a system for regulated expression in mammalian cells. BMC Biotechnol. 2006 Nov 3;6:43. doi: 10.1186/1472-6750-6-43. PMID: 17083727; PMCID: PMC1654148.

86. Ewels PA, Peltzer A, Fillinger S, Patel H, Alneberg J, Wilm A, Garcia MU, Di Tommaso P, Nahnsen S. The nf-core framework for community-curated bioinformatics pipelines. Nat Biotechnol. 2020 Mar;38(3):276-278. doi: 10.1038/s41587-020-0439-x. PMID: 32055031.

87. Huang DW, Sherman BT, Tan Q, Collins JR, Alvord WG, Roayaei J, Stephens R, Baseler MW, Lane HC, Lempicki RA. The DAVID Gene Functional Classification Tool: a novel biological module-centric algorithm to functionally analyze large gene lists. Genome Biol. 2007;8(9):R183. doi: 10.1186/gb-2007-8-9-r183. PMID: 17784955; PMCID: PMC2375021.

88. Chen TJ, Kotecha N. Cytobank: providing an analytics platform for community cytometry data analysis and collaboration. Curr Top Microbiol Immunol. 2014;377:127-57. doi: 10.1007/82_2014_364. PMID: 24590675.

89. Caputo E, Maiorana L, Vasta V, Pezzino FM, Sunkara S, Wynne K, Elia G, Marincola FM, McCubrey JA, Libra M, Travali S, Kane M. Characterization of human melanoma cell lines and melanocytes by proteome analysis. Cell Cycle. 2011 Sep 1;10(17):2924-36. doi: 10.4161/cc.10.17.17068. Epub 2011 Sep 1. PMID: 21857157; PMCID: PMC5479465.

90. Bai X, Fisher DE, Flaherty KT. Cell-state dynamics and therapeutic resistance in melanoma from the perspective of MITF and IFNγ pathways. Nat Rev Clin Oncol. 2019 Sep;16(9):549-562. doi: 10.1038/s41571-019-0204-6. PMID: 30967646; PMCID: PMC7185899

91. White JR, Thompson DT, Koch KE, Kiriazov BS, Beck AC, van der Heide DM, Grimm BG, Kulak MV, Weigel RJ. AP-2α-Mediated Activation of E2F and EZH2 Drives Melanoma Metastasis. Cancer Res. 2021 Sep 1;81(17):4455-4470. doi: 10.1158/0008-5472.CAN-21-0772. Epub 2021 Jul 1. PMID: 34210752; PMCID: PMC8416798.

92. Chen H, Lau MC, Wong MT, Newell EW, Poidinger M, Chen J. Cytofkit: A Bioconductor Package for an Integrated Mass Cytometry Data Analysis Pipeline. PLoS Comput Biol. 2016

Sep 23;12(9):e1005112. doi: 10.1371/journal.pcbi.1005112. PMID: 27662185; PMCID: PMC5035035.

93. Rambow F, Rogiers A, Marin-Bejar O, Aibar S, Femel J, Dewaele M, Karras P, Brown D, Chang YH, Debiec-Rychter M, Adriaens C, Radaelli E, Wolter P, Bechter O, Dummer R, Levesque M, Piris A, Frederick DT, Boland G, Flaherty KT, van den Oord J, Voet T, Aerts S, Lund AW, Marine JC. Toward Minimal Residual Disease-Directed Therapy in Melanoma. Cell. 2018 Aug 9;174(4):843-855.e19. doi: 10.1016/j.cell.2018.06.025. Epub 2018 Jul 12. PMID: 30017245.

94. Zuo Q, Liu J, Huang L, Qin Y, Hawley T, Seo C, Merlino G, Yu Y. AXL/AKT axis mediated-resistance to BRAF inhibitor depends on PTEN status in melanoma. Oncogene. 2018 Jun;37(24):3275-3289. doi: 10.1038/s41388-018-0205-4. Epub 2018 Mar 19. PMID: 29551771; PMCID: PMC6508599.

95. Hugo W, Zaretsky JM, Sun L, Song C, Moreno BH, Hu-Lieskovan S, Berent-Maoz B, Pang J, Chmielowski B, Cherry G, Seja E, Lomeli S, Kong X, Kelley MC, Sosman JA, Johnson DB, Ribas A, Lo RS. Genomic and Transcriptomic Features of Response to Anti-PD-1 Therapy in Metastatic Melanoma. Cell. 2016 Mar 24;165(1):35-44. doi: 10.1016/j.cell.2016.02.065. Epub 2016 Mar 17. Erratum in: Cell. 2017 Jan 26;168(3):542. PMID: 26997480; PMCID: PMC4808437.

96. Kanekura T, Chen X. CD147/basigin promotes progression of malignant melanoma and other cancers. J Dermatol Sci. 2010 Mar;57(3):149-54. doi: 10.1016/j.jdermsci.2009.12.008. Epub 2010 Jan 8. PMID: 20060267.

97. Keyghobadi F, Mehdipour M, Nekoukar V, Firouzi J, Kheimeh A, Nobakht Lahrood F, Azimian Zavareh V, Azimi M, Mohammadi M, Sodeifi N, Ebrahimi M. Long-Term Inhibition of Notch in A-375 Melanoma Cells Enhances Tumor Growth Through the

Enhancement of *AXIN1, CSNK2A3*, and *CEBPA2* as Intermediate Genes in Wnt and Notch Pathways. Front Oncol. 2020 Jun 30;10:531. doi: 10.3389/fonc.2020.00531. PMID: 32695658; PMCID: PMC7338939.

98. Lee CW, Zhan Q, Lezcano C, Frank MH, Huang J, Larson AR, Lin JY, Wan MT, Lin PI, Ma J, Kleffel S, Schatton T, Lian CG, Murphy GF. Nestin depletion induces melanoma matrix metalloproteinases and invasion. Lab Invest. 2014 Dec;94(12):1382-95. doi: 10.1038/labinvest.2014.130. Epub 2014 Nov 3. PMID: 25365206; PMCID: PMC4419570.

99. Shi Y, Liu R, Zhang S, Xia YY, Yang HJ, Guo K, Zeng Q, Feng ZW. Neural cell adhesion molecule potentiates invasion and metastasis of melanoma cells through CAMP-dependent protein kinase and phosphatidylinositol 3-kinase pathways. Int J Biochem Cell Biol. 2011 Apr;43(4):682-90. doi: 10.1016/j.biocel.2011.01.016. Epub 2011 Jan 26. PMID: 21277992.

100. Lupia A, Peppicelli S, Witort E, Bianchini F, Carloni V, Pimpinelli N, Urso C, Borgognoni L, Capaccioli S, Calorini L, Lulli M. CD63 tetraspanin is a negative driver of epithelial-to-mesenchymal transition in human melanoma cells. J Invest Dermatol. 2014 Dec;134(12):2947-2956. doi: 10.1038/jid.2014.258. Epub 2014 Jun 18. PMID: 24940653.

101. von Mering C, Huynen M, Jaeggi D, Schmidt S, Bork P, Snel B. STRING: a database of predicted functional associations between proteins. Nucleic Acids Res. 2003 Jan 1;31(1):258-61. doi: 10.1093/nar/gkg034. PMID: 12519996; PMCID: PMC165481.

102. Van Gassen S, Callebaut B, Van Helden MJ, Lambrecht BN, Demeester P, Dhaene T, Saeys Y. FlowSOM: Using self-organizing maps for visualization and interpretation of cytometry data. Cytometry A. 2015 Jul;87(7):636-45. doi: 10.1002/cyto.a.22625. Epub 2015 Jan 8. PMID: 25573116.

105.

7. PUBLICATIONS

1. Fattore L, Ruggiero CF, Pisanu ME, **Liguoro D**, Cerri A, Costantini S, Capone F, Acunzo M, Romano G, Nigita G, Mallardo D, Ragone C, Carriero MV, Budillon A, Botti G, Ascierto PA, Mancini R, Ciliberto G. Reprogramming miRNAs global expression orchestrates development of drug resistance in BRAF mutated melanoma. Cell Death Differ. 2019 Jul;26(7):1267-1282. doi: 10.1038/s41418-018-0205-5. Epub 2018 Sep 25. PMID: 30254376; PMCID: PMC6748102.
2. Ruggiero CF, Malpicci D, Fattore L, Madonna G, Vanella V, Mallardo D, **Liguoro D**, Salvati V, Capone M, Bedogni B, Ascierto PA, Mancini R, Ciliberto G. ErbB3 Phosphorylation as Central Event in Adaptive Resistance to Targeted Therapy in Metastatic Melanoma: Early Detection in CTCs during Therapy and Insights into Regulation by Autocrine Neuregulin. Cancers (Basel). 2019 Sep 25;11(10):1425. doi: 10.3390/cancers11101425. PMID: 31557826; PMCID: PMC6826737.
3. Fattore L, Ruggiero CF, **Liguoro D**, Mancini R, Ciliberto G. Single cell analysis to dissect molecular heterogeneity and disease evolution in metastatic melanoma. Cell Death Dis. 2019 Oct 31;10(11):827. doi: 10.1038/s41419-019-2048-5. PMID: 31672982; PMCID: PMC6823362.
4. Fattore L, Campani V, Ruggiero CF, Salvati V, **Liguoro D**, Scotti L, Botti G, Ascierto PA, Mancini R, De Rosa G, Ciliberto G. In Vitro Biophysical and Biological Characterization of Lipid Nanoparticles Co-Encapsulating Oncosuppressors miR-199b-5p and miR-204-5p as Potentiators of Target Therapy in Metastatic Melanoma. Int J Mol Sci. 2020 Mar 12;21(6):1930. doi: 10.3390/ijms21061930. PMID: 32178301; PMCID: PMC7139872.
5. **Liguoro D**, Fattore L, Mancini R, Ciliberto G. Drug tolerance to target therapy in melanoma revealed at single cell level: What next? Biochim Biophys Acta Rev Cancer. 2020 Dec;1874(2):188440. doi: 10.1016/j.bbcan.2020.188440. Epub 2020 Sep 29. PMID: 33007433.

6. Fattore L, Ruggiero CF, **Liguoro D**, Castaldo V, Catizone A, Ciliberto G, Mancini R. The Promise of Liquid Biopsy to Predict Response to Immunotherapy in Metastatic Melanoma. Front Oncol. 2021 Mar 18;11:645069. doi: 10.3389/fonc.2021.645069. PMID: 33816298; PMCID: PMC8013996.
7. Minini M, Senni A, He X, Proietti S, **Liguoro D**, Catizone A, Giuliani A, Mancini R, Fuso A, Cucina A, Cao Y, Bizzarri M. miR-125a-5p impairs the metastatic potential in breast cancer via IP_6K1 targeting. Cancer Lett. 2021 Nov 1;520:48-56. doi: 10.1016/j.canlet.2021.07.001. Epub 2021 Jul 3. PMID: 34229060.